

UNIVERSITY OF TWENTE

FACULTY OF ENGINEERING TECHNOLOGY

Design And Analysis of An In-flight Anti-icing System For An Airplane Wing

Authors

Monique LAMERS
Sameer NIZAMUDEEN
Kelvin JARAMILLO
Timo NIEUWERF
Niek REULING
Jesper KUSSENDRAGER
David CARRERA ROBLES
Kevin CACARIN CUMBAL

February 5, 2021

Contents

1	Introduction	4
2	Literature Study and Problem Definition	5
2.1	Icing	5
2.1.1	Icing Types	5
2.1.2	Conditions	6
2.1.3	Aerodynamic Effects	8
2.2	Possible anti-icing systems	11
2.2.1	What is Anti-icing and Deicing?	11
2.2.2	Pneumatic Boots	11
2.2.3	Electric Boots	13
2.2.4	Weeping Wings	13
2.2.5	Electro Impulse	14
2.2.6	Thermal Heat	15
2.2.7	Icephobic surfaces	16
2.3	FAA Requirements	17
2.3.1	Relevant requirements	18
2.3.2	Maximum Atmospheric Icing Conditions	19
2.3.3	Compliance of Boeing 737 MAX To The Icing Conditions	22
2.4	Problem Identification	22
2.4.1	Bleed air Ice Protection System	23
2.4.2	Fluid based Ice Protection System	23
2.4.3	Pneumatic boots	23
2.4.4	EESS (Electro-Expulsive Separation System)	24
2.4.5	EIDI (Electro-Impulse Deicing)	24
3	External Flows and Heat Exchange	25
3.1	Trajectories of Droplets	25
3.1.1	Derivation of Potential Flow	25
3.1.2	Plotting The Velocity Field	26
3.1.3	Plotting Trajectories of Droplets	27
3.2	Mass and energy balance	30
3.2.1	Assumptions	31
3.2.2	Mass balance	31
3.2.3	Energy Balance	32
3.2.4	Local Heat Transfer	35
3.3	Simulations using 2DFOIL-ICE	39

3.3.1	Tests	39
3.3.2	Comparing the 2DFOIL-ICE simulations to the cylinder simulations	39
3.3.3	Keeping the wing ice free using 2DFOIL-ICE	44
4	Internal Flows and Heat exchange	46
4.1	Introduction	46
4.2	Electric Heating Mats	47
4.2.1	Over Wing Wall Thickness	47
4.2.2	Along The Wing	49
4.2.3	Conclusion	50
4.3	Heating through radiation and free convection	50
4.3.1	Radiation	50
4.3.2	Free convection	52
4.4	Forced convection	53
4.5	Impinging Jets	56
4.6	Conclusion	59
5	Design of An Anti-icing System	60
5.1	Temperature difference along the wing	60
5.2	Choice of Anti-icing - Impinging Jets	60
5.2.1	Nusselt Number For Impinging Jets	61
5.2.2	Optimization along y-direction	62
5.2.3	Optimization along x-direction	64
5.2.4	Final Layout of Nozzles And Mass Flow	64
5.2.5	Conclusion	66
5.3	Ice-phobic Anti-icing System	66
5.3.1	Comparison to Ice-adhesion strength	68
6	Ethics in Engineering	70
6.1	Step 1: Ethical Risk Sweeping	70
6.2	Step 2: Ethical Pre-mortems and Post-mortems	71
6.2.1	Post-Mortems	71
6.2.2	Pre-Mortems	72
6.3	Step 3: Expanding the Ethical Circle	72
6.4	Step 4: Case-based Analysis	74
6.4.1	Similar cases	74
6.4.2	Parallels and differences	74
6.4.3	Evaluate choices and outcomes in the cases	75
6.4.4	Parallel risks, opportunities, solutions	75
6.4.5	Concluded	76
6.5	Step 5: Remembering the Ethical Benefits of Creative Work	76
6.5.1	Why an anti-icing system and for what good ends?	76
6.5.2	Would society/customers be better off with this technique? Is this product a new thing to sell?	76
6.5.3	Is the ethical benefit at the centre of the work and thinking of the company?	77
6.5.4	What were they willing to sacrifice to make sure the system worked right?	77
6.6	Step 6: Think About the Terrible People	77

6.6.1	Who will want to abuse, steal, misinterpret, hack, destroy, or weaponize what we built?	77
6.6.2	Who will use it with alarming stupidity/irrationality?	78
6.6.3	What rewards/incentives/openings have our design inadvertently created for those people?	78
6.6.4	How can we remove those rewards/incentives?	78
6.7	Step 7: Closing the Loop: Ethical Feedback and Iteration	78
6.7.1	Remember That Ethical Design/Engineering Is Never a Finished Task	78
6.7.2	Identify Feedback Channels that Will Deliver Reliable Data on Ethical Impact	79
6.7.3	Integrate the Process w/Quality Management User Support; Make it Standard	79
6.7.4	Develop Formal Procedures and Chains of Responsibility for Ethical Iteration	79
7	Conclusion	80
8	Appendix	81
8.1	FAA maximum icing atmospheric conditions.	81
8.1.1	Continuous Icing Maximum:	81
8.1.2	Intermittent Icing Maximum:	84
8.1.3	Supercooled large drop icing conditions	87
8.2	Derivations to calculate the heat transfer coefficient	93
8.2.1	Derivation of the velocity boundary layer	93
8.2.2	Derivation of the local heat transfer coefficient	95
8.3	2DFOIL-ICE tests	97
8.3.1	Test 1: low, cold, wet (fog)	97
8.3.2	Test 2: slightly higher, cold, wet	97
8.3.3	Test 3: low, medium warm, wet	98
8.3.4	Test 4: high, cold, dry (clouds do not allow rainy weather at this altitude)	98
8.3.5	Test 5: high, warm, dry	99
8.3.6	Test 6: low, warm, dry	99
8.3.7	Test 7: low, warm, wet	100
8.3.8	Test 8: freezing rain (low, wet, big droplets, cold)	100
8.3.9	Test 9: freezing drizzle (low, wet, still big droplets, cold)	101
Bibliography		102

Chapter 1

Introduction

The airplane industry is one of the fastest growing industries of the world. Because of this planes have to fly in all weather types and to all corners of the world. When the air is cold, ice will form on the plane's wing and this can cause dangerous situations. In this report, a safe and reliable anti-icing system for the wing will be designed so that planes can fly in common, but hazardous environments. First, a literature study will be conducted to see what information there currently is on the types of weather, anti-icing systems, regulations and what kind of problems will be faced. Second, the air flow will be calculated and simulated around the wing to see how much ice will accumulate on the wing. The mass and energy balance will be calculated to calculate the amount of heat needed to keep the wing ice free. Third, the internal flow will be calculated to know how the heat will be divided within the wing itself using data from the external flow. There will also be looked at several ways to heat up the wing. Forth, a design will be made for an anti icing system using all previous knowledge from earlier chapters. Fifth, an ethical study will be conducted to know the ethical impact of the anti-icing system that is designed to ensure the design process is moral and ethical, so no person can get harmed. The conclusion summarizes and discusses the results found in this report.

Chapter 2

Literature Study and Problem Definition

This chapter shows results of research done in the different types of icing accretion, the conditions in which those happens and the effect of them in the aerodynamics of aircrafts. Also, the different types of anti-icing systems are presented together with their working principles and their advantages and disadvantages. Furthermore, relevant regulation for the FAA (Federal Aviation Administration) related to icing accretion are listed for commercial aircrafts, these considering the maximum atmospheric conditions stated in the e-CFR(electronic Code of Federal Regulations). To conclude, the current problems with anti-icing systems are identified and explained.

2.1 Icing

Super-cooled water droplets are droplets that did not freeze yet, even though the outside temperature is below zero degrees Celsius. On impact, the droplets freeze due to a nucleation process. In an experimental study [1] it appeared that the shape as well as the temperature of the surface on which the droplets impact, affect the freezing process and shape of the ice beads. In another study, it was found that the supercooling degree of the water also influences the nucleation and growth processes of icing [2]. This means that the conditions for icing depend on the weather and the droplets as well as the aircraft itself. The water droplets impact and then ice crystals coat the wing of the plane. This causes the wing's shape to change, depending on the type of icing. When the shape changes, the performance of the wing can decrease. Icing accumulates on all exposed surfaces; it does not only appear on the plane's wings but also on sensors or the engines.

2.1.1 Icing Types

Several types of icing exist. Each type has a different appearance but also in structure. The structures depend on the weather conditions as well as some aircraft-specific factors.

Rime Ice Rime ice forms when water droplets freeze instantly when coming into contact with the impact surface. It appears with a spearhead-shape on the leading edge of the wing. The accretion looks relatively streamlined, like the wings, but have a greater surface roughness. This type of ice accretion is brittle and has a low density. In the quick freezing process of the droplets, some air is captured between droplets. These air pockets lower the density and toughness of the ice [3]. The water droplets stay at the leading edge of the wing due to low temperatures, low speeds, low liquid water content in the clouds or a combination of these factors. Usually, the ambient temperature lies

below -10°C [3]. Increasing these factors give another type of ice: clear or glaze ice. The clouds in which this icing can frequently occur are stratiform clouds [4].

Clear or Glaze Ice Glaze or clear ice that forms when a water droplet hits an airfoil and freezes on the airfoil. It does not freeze instantly like rime ice. Glaze ice forms when the temperatures are relatively high but water still freezes, -10-0 °C [5]. Because glaze ice does not freeze instantly the ice will form further on the airfoil. This has significantly more impact on the aerodynamic flow. The ice is clear because it has no impurities like air because it has time to settle and freeze. This type of icing is observed in stratiform clouds (less frequently) as well as in cumuliform clouds [3][4].

Mixed Ice This type of ice accretion is a mix of rime and clear ice. It occurs at transition points or combinations of the conditions of the above mentioned types of icing. Intermediate or mixed ice occurs as well due to a droplet distribution in the clouds. Not all droplet sizes are the same and clouds differ in their liquid water contents (LWC)[3]. This icing type forms at -20 to -10 degrees Celsius [6] in cumuliform clouds [4].

Supercooled Large Droplets In this case, the large droplets can not freeze quick enough to stay at the stagnation point of the wing. The droplets run back and freeze further along the wing than rime or clear ice. This causes the ice to accrete as a ridge on the wing [7]. Usually, these droplets have a median volumetric diameter larger than 50 µm [3] and are often referred to as freezing drizzle or freezing rain, depending on their diameters.

2.1.2 Conditions

The parameters that influence icing can be split up in roughly two parts. The weather conditions in which the aircraft fly can cause icing, but there are some aircraft-specific factors as well that can worsen icing processes.

Meteorological-specific factors:

Outside or ambient air temperature

Below -40°C, water supercooled water droplets will freeze to ice crystals [3][6]. When lowering the temperature, the number of water droplets decrease and ice crystals increase. In icing processes, supercooled water droplets are important and crystals do not pose a big problem. This means that the likelihood of icing occurs around -2 to -10°C [6]. Approaching a temperature of 0°C can increase runback on the wing, after which the droplets freeze further downstream [3][6].

Droplet diameter

Since clouds contain droplets with different diameters, the median volumetric diameter (MVD) is used to express the range of droplets diameters. The diameter range of the important droplets in clouds lies approximately between 15 and 40 or 50 µm [3][6]. The minimum in this range is for the small droplets that follow the airflow around the wing instead of impacting onto the wing [3][6][8]. This means that larger droplets can cause more ice accretion on the leading edge of the wing. Freezing drizzle contains SLD with diameters starting from the upper limit, 40 or 50 µm. Freezing rain contains SLD with

Cloud conditions	Droplet diameter D (micrometer)
General	$14 < D < 40$
Freezing drizzle	$40 < D < 400$
Freezing rain	$400 < D$

Table 2.1

droplets diameters greater than $400 \mu\text{m}$ [6]. These conditions are summarized in Table 2.1.

Liquid water content

The liquid, in this case supercooled, water content (LWC) is the amount of water that an aircraft can meet when flying through a cloud. Therefore, the cloud's LWC can be used as a measure for aircraft icing severity. This parameter is strongly dictated by the cloud types and influences the icing type and rate.

Cloud types [4]

Cloud types are described based on their appearance and characteristics. Their names are derived from the Latin language.

- Stratus or strato-: these clouds look smooth, flat and spread-out;
- Cumulus or cumulo-: the clouds look puffy and heaped-up;
- Cirrus or cirro-: a curly, wispy type of cloud;
- Nimbus or nimbo-: rain-bearing clouds;
- Alto: these clouds are considered at mid level, even though it means “high” in Latin.

The clouds that cause main hazards of icing are stratiform and cumuliform clouds.

Stratiform clouds at high level contain ice crystals. This does not contribute to airframe icing. However, the crystals can form a problem for engine icing. In the mid-level, stratiform clouds contain solid as well as liquid water content. At low level, the clouds have a high LWC. With decreasing temperature, the LWC and droplet diameter increase. Icing related to these clouds is called “continuous icing” (CM)[3][4]. Cumuliform clouds tend to develop in a vertical direction. Increasing cloud height gives also an increase in droplet diameter and LWC. The exposure duration is usually short, so the icing related to these clouds is known as “intermittent icing” (IM)[3][4].

Airplane-specific factors

Altitude

At high altitudes, above 7 km, icing phenomena are rare and referred to as light icing [3][4]. Between approximately 1 km and 1.5 km icing occurs the most frequently [8].

Airspeed

As the airspeed increases, the intercepted mass of water increases as well [6][8]. The aerodynamic heating increases too; this can cause the structural icing to melt. At higher altitudes, the conditions are harsher, thus the required airspeed needs to be higher to melt the ice. At 6 km, airspeeds from

475 knots cause water to not freeze anymore. An airspeed of 580 knots is sufficient to eliminate icing completely[3][6].

Angle of attack

The exposed surface area depends amongst others on the angle of attack. This gives changes to the catching efficiency, ice shapes and locations of the ice accumulation, for example[6].

Encounter duration

How long an aircraft is in a cloud and collects supercooled water droplets, is dependent on the size of the cloud and its horizontal extent. Guidelines are that an aircraft should be able to withstand 45 minutes in continuous icing conditions[3].

Maximum ceiling

The maximum ceiling of an aircraft indicated the maximum altitude that an aircraft can reach. If an aircraft is able to reach altitudes above critical icing-altitudes, ice accumulation will mostly take place in ascending and descending moments and not during cruising[3].

Leading edge radius

The collection efficiency on a wing decreases as the radius of the leading edge increases. The wing will collect more droplets if the leading edge radius is smaller[3][6]. The radius indicates the wing's ability to deflect the droplet's paths[3].

Thickness-to-chord ratio

This ratio compares the wing's thickness its chord or characteristic length. This also relates to the same effects as the leading edge radius has. When the RTC increases, the wing seems to become blunter. Though this deflects the particle paths better, the total water impingement increases. It depends on the conditions and the aircraft which effect dominates[3].

Surface characteristics

The surface temperature of the aircraft has to be below freezing point to encounter ice accumulation or airframe icing. The colder the surface that the droplet impacts, the faster it freezes. It is more likely that rime ice is formed on a cold surface temperature[3][6].

The catching efficiency depends on the shape of the wing as well as its surface roughness. A rough surface provides more catching area for the droplets to freeze on, increasing aircraft icing.

2.1.3 Aerodynamic Effects

When ice forms on airfoils the ice does not form the same. Ice forms different shapes and sizes on airfoils. These geometries have different aerodynamic effects on the airfoil. There are four different geometries of ice that form; streamwise, spanwise-ridge, horn and roughness [5][7] as seen in figures 2.1 and 2.2.

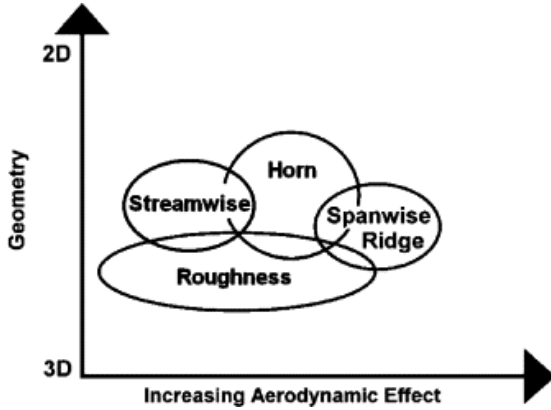


Figure 2.1: Aerodynamic effect due to geometry of ice [5]

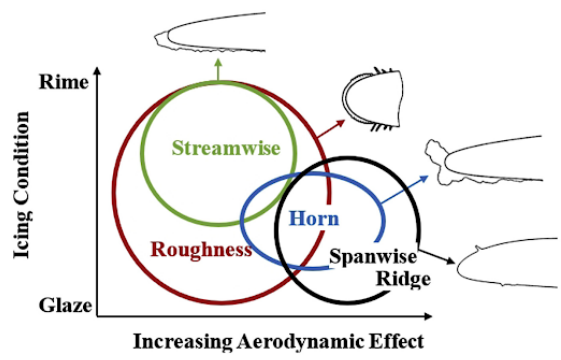


Figure 2.2: Aerodynamic effect due to ice type [7]

Roughness

In the initial stages of ice formation rough ice is formed, all the ice is rough but this is how it is named because it is a rough area on the wing and seen first. Roughness is made of three areas [7]; smooth part in the front, rough part further from the tip and behind that is the feather part as seen in figure 2.3. These areas evolve in both rime and glaze ice conditions [7]. But depending on the conditions the roughness will evolve into the other ice forming effects. Roughness itself does not change the aerodynamics much but if it develops into a further stage it can significantly effect the aerodynamics.

Streamwise Ice

Streamwise ice has the least impact on the aerodynamics of the aerofoil. This is because it is made of mostly rime ice and therefore freezes on impact. Because it freezes on impact the ice will take shape of the existing aerodynamics on the front of the aerofoil. However the ice is not smooth so the aerodynamics will change a little [7]. It usually only occurs when the angle of attack is high [5].

Spanwise-ridge Ice

Spanwise-ridge ice forms at the further up on the aerofoil; 5-20% of the chord of the aerofoil, as seen in figure 2.4. Spanwise-ridge ice is associated with SLD-ice and faulty anti-ice systems. It is made of mostly glaze ice and it has a big impact on the aerodynamics of the aerofoil [7]. It forms very rough ice that hinders the flow of air around the thickest point of the aerofoil [5]. Due to the hinder the pressure gradient changes dramatically and the air behind the ice will turn turbulent as seen in figure 2.5.

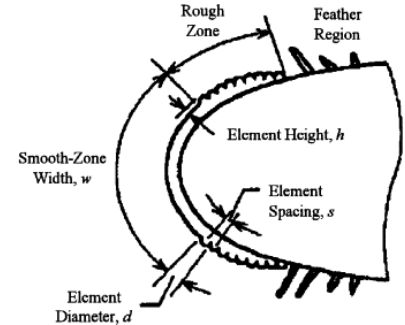


Figure 2.3: A cross section of the roughness effect [5]

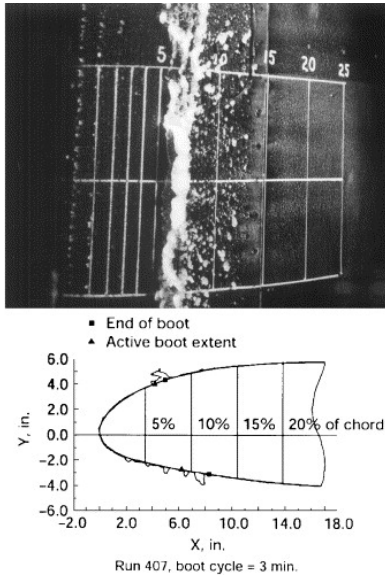


Figure 2.4: A cross section and top view photo of spanwise-ridge ice [7]

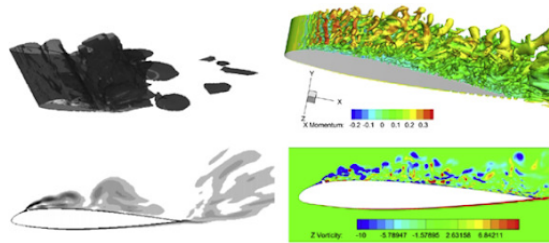


Figure 2.5: Turbulent air because of spanwise-ridge ice [7]

Horn Ice

Horn ice like the name suggests one or two horns that form on the front of the aerofoil as seen in figure 2.6. The ice is mostly glaze ice. Research shows it is usually one "horn". Horn ice is the most commonly experienced ice and researched. Ice forms at the front tip of the aerofoil but commonly some feather ice will form further on the aerofoil as well [7]. Horn has a smaller impact than spanwise-ridge ice on the aerodynamics of the aerofoil, but it does have a large impact as seen in figure 2.7. The ice has less of an impact on the aerodynamics because the ice forms on the front so the air stays laminar but a "bubble" will evolve behind the horn that will cause drag [5].

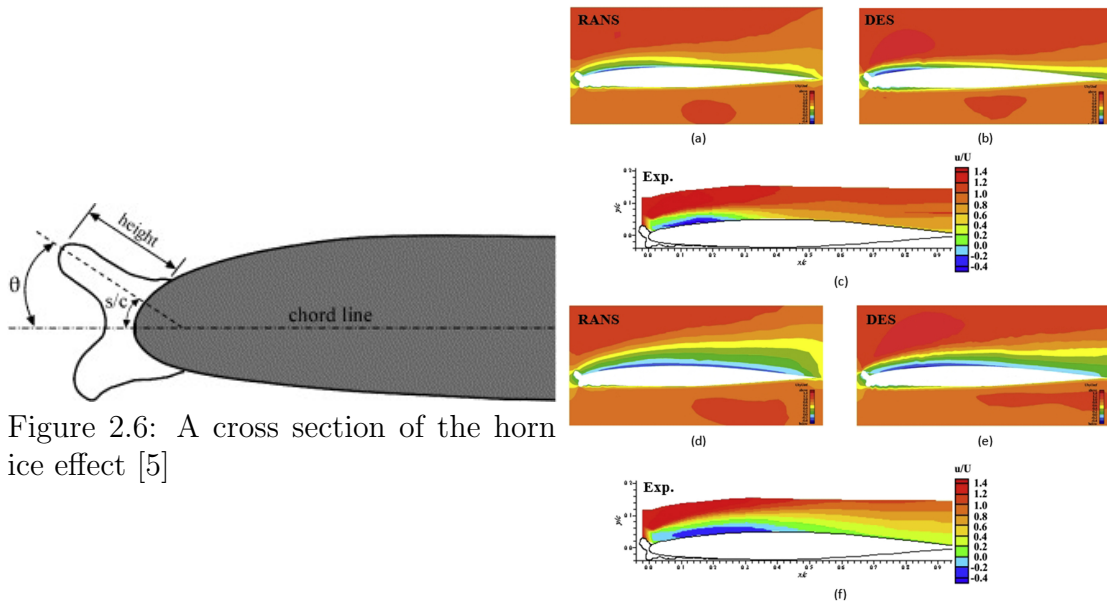


Figure 2.6: A cross section of the horn ice effect [5]

Figure 2.7: The aerodynamic effect of the horn ice effect [7]

2.2 Possible anti-icing systems

2.2.1 What is Anti-icing and Deicing?

Equipment specific designed to remove or prevent ice from forming, this research is specially focused on anti-ice systems for the wing of an airplane. These technologies are classified as anti-icing or de-icing [9]. Anti-icing technology prevents icing. Therefore, these technology is turned on long before the ice conditions, while de-icing removes the ice formed on the wing's surface [10].

2.2.2 Pneumatic Boots

The pneumatic boot system was developed by B.F. Goodrich Company in 1930. The system breaks the ice formed on the wing using air pressure. The wing's surface has inflatable tubes. The tubes are inflated and deflated to crack the ice and eliminate ice accretion [12]. During the inflation of the tubes, shear stress causes the separation of the ice from the wing. The aerodynamic forces transport the broken ice out of the turbines to prevent incidents during the flight [13]. The whole system can be operated manually by the crew, or could work in diverse cycles with the help of an icing sensor that will actuate the system when needed. The pneumatic boot system is frequently used in general aviation (GA).

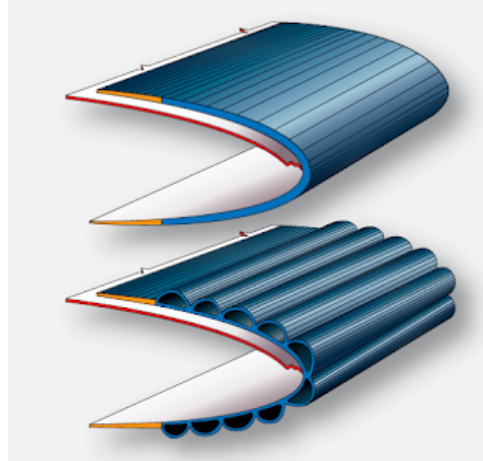


Figure 2.8: Pneumatic system [11]

Working Principle

In figure 2.8, a basic pneumatic boot system in a two-engine GA aircraft is shown. The basic working principle is that the air pressure mainly is produced by a pump that is powered by the engine of the aircraft or directly fed by bleed air. The airflow goes to a pressure regulator and finally to a valve to obtain the exact pressure needed to expand the boots at the surface to eliminate the accumulated ice [11]. Generally, in a GA aircraft, the air is pressurized to 17 psi in tubes. After that, the valves open to allow the deflation of the tubes and re-circulation of the air. The boots are inflated in a symmetrical way to maintain the control in the flight during the de-icing [13].

Material

Pneumatic de-icing boots are made from smooth polyurethane that enhances the performance during extreme conditions. Polyurethane improves resistance to rain erosion, sand abrasion and UV or ozone damage [14]. The diameter of the tubes was reduced to allow quicker rates of inflation and deflation, leading better removal of ice [12]. The outside part, which is in contact with some substance and chemical is covered by conductive neoprene to prevent the quick deterioration. The neoprene also provides a conductive surface to dissipate static electricity charges. Otherwise, the accumulated static electricity will interfere with the radio frequency and some equipment of the aeroplane [12].

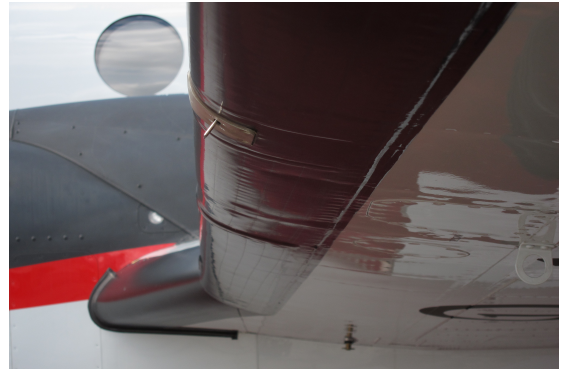


Figure 2.9: Material [14]

Advantages

- **Low weight;** A lightweight system is necessary to avoid excessive fuel consumption. The total weight of the system is just 50 pounds for two-engine aircraft [12].
- **Low power requirements;** The power comes from the engine. Less power to de-icing systems means saving fuel. A maximum of one amp of electrical current is required for six seconds at 28 VDC to cycle the inflation valve solenoids [12].
- **Low cost;** The boot de-icing system in the long term will result inexpensive compared with other systems even when the maintenance and replacement cost is considered [12].
- **Proven Technology;** The present de-icing system has been present for a long time in medium-sized and long planes. This guarantees the quality and the efficiency of the product [12].

Drawbacks

- **Regular Maintenance;** Like any mechanical system, it needs a constant inspection to prevents possible damages in a short time [12].
- **UV Deterioration;** Despite coatings on the wing, UV rays reduce the service life [12].

2.2.3 Electric Boots

Electrical boots follow the principle of pneumatic boots, however, the main variation is the actuation. In this case, the activation is made possible by a magnetic field.

Working Principle

The system electric boots also known as Electro-Expulsive Separation System (EESS) consist of ice sensor, indicator and controllers[13]. When current is passing through both conductors, a magnetic field is created. This produces the repulsive force necessary to break the ice on the surface of the wing [9].The exterior part of the boot will be the same material, polyetherane. The figure 2.10 visualises this working principle.

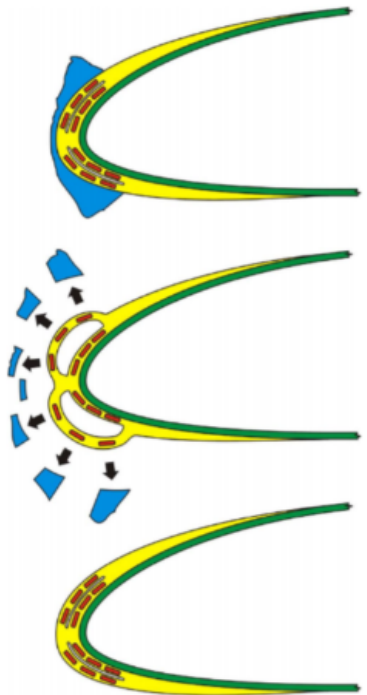


Figure 2.10: Electric boot [9]

2.2.4 Weeping Wings

This system is designed to be anti-icing but is also capable of de-icing. A fluid is released on the airplane's wings. The fluid chemically breaks the bond between ice and frame, allowing the system to shed any accumulated ice and prevent any ice build-up thereafter [15].

Working Principle

The basic concept of the system consists of a porous surface on the wing, in which the fluid can circulate during the flight. The fluid that de-ice the surface is ethylene glycol [15]. The fluid is delivered by reservoirs, which are provided at each leading edges. The fluid is mixed with the supercooled water during the flight. This reaction avoids the formation of ice. Finally the aerodynamical forces carry out the mixture without adhering it to the aircraft [13].

Advantages

- The system can be used as de-icing as well as anti-icing [13];
- The reliability of the system and fluid run back [15];
- The flow of the fluid gives better protection than another system [16];
- Low power demand [15].



Figure 2.11: Weeping Wings[15]

Drawbacks

- The limited space in the reservoir to provide the fluid on the wings, results in limited time against the ice formation. In most cases, the time of endurance of the fluids is about 3 hours. However, it can vary depending on the class of fluid used. [16]

Fluid

A liquid pump and tank that hold ethylene glycol, were installed in the fuselage of the airplane or in each leading edges [13]. The overall weight of the system is neglectable, compared to the size of the airplane. Improvements in the leading-edge weep system include the use of sintered stainless steel fabrics and titanium laser-drilled skins. The latter option has thousands of tiny holes to provide better distribution of the fluid on the wing [16]. The weeping wing system is shown in the figure 2.12

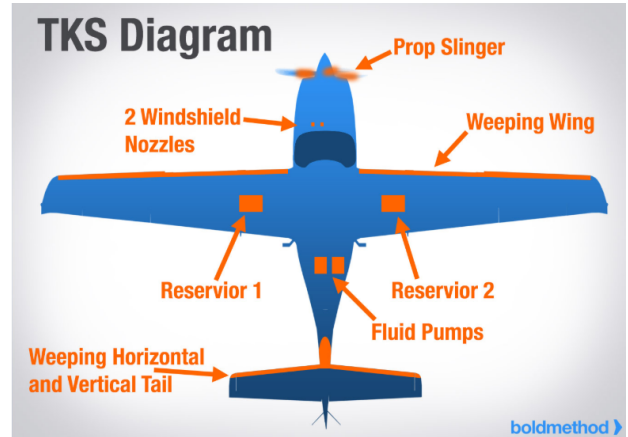


Figure 2.12: Weeping Wings

2.2.5 Electro Impulse

Electro Impulse Deicing (EIDI)

This anti-icing system was suggested in 1937 and was further developed by the renowned agency called National Aeronautics and Space Administration (NASA-Lewis) and different participating industries [17]. The purpose of this development was improving and verifying that it has a low energy consumption and is a highly efficient de-icing method.

Working principle (EIDI)

An electromagnetic coil, made of copper, is placed behind a certain wing surface, with some space separating the coil and the surface, to induce enough Eddy current (loops of electrical current) in the metal surface [9]. The resulting fields and the metal skin create a high magnitude force. Nevertheless, this force duration is extremely short[17]. Moreover, it can only be induced after a certain time. This is because capacitors must be recharged by such a high electrical energy used, but still have low energy consumption [9]. The electro- impulse de-icing system is shown in Figure 2.13.

This method can become autonomous with the simple implementation of ice accumulation sensors, that determine the exact moment that the ice has reached the required thickness to run the anti-icing system [17]. The minimum ice thickness is 0.5" or 12,7cm for a proper operation of this technology [9].

In some aircrafts, the system changes slightly due to the thin metal skin, which is less than the required. Doublers show in Figure 2.14 are implemented with larger dimensions than the coils [17].

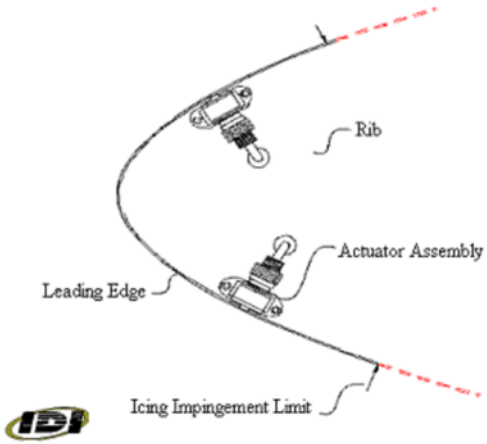


Figure 2.13: EIDI

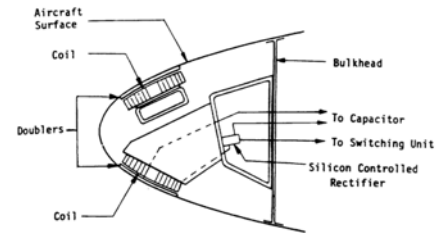


Fig. 1-1 Impulse Coils in a Leading Edge
2

Figure 2.14: EIDI (Doublers)

These doublers will help the thin layer of metal to withstand the eddy currents and make a correct operation of the anti-icing system [17].

2.2.6 Thermal Heat

Bleed air

Bleed air comes from the engine compressor, which significantly increases the air pressure and therefore the temperature. Hot temperature is considered between 200 to 250 degrees Celsius with a pressure of approximately 40 PSI[10]. This bleed air is used for several functions such as: pressurisation, air conditioning, water system pressurization, wing and engine anti-icing systems and more functions[10].

To direct the air though the airplane, ducts are used. These ducts are connected to valves, whose purpose is to control the flow of the bleed air as shown in Figure 2.15. Pressure sensors are implemented behind the valves to keep track of the information[11]. This information is used for the Control System (computer) to remain the icing condition stable during the entire flight time.

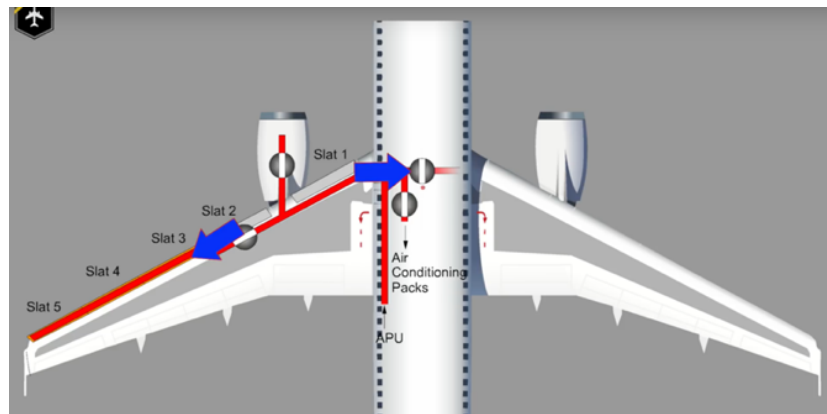


Figure 2.15: Bleed air system [10]

When the hot air is guided along the wing, telescopic pipes into a piccolo tube are used to distribute the air through little holes[11], warming up the slat, Figure 2.16. The air that increases the slat

temperature goes out through the small black holes.

This bleed air system does not cover the entire wing, in Figure 2.17 slot three, four and five use the bleed air system[10]. The inboard slat one and two does not need an anti-icing system because this section is less prone for ice accumulation for aerodynamic reasons [13].



Figure 2.16: Bleed air system [13]



Figure 2.17: Bleed air system [13]

Advantages

This is an efficient method as long as the engine is working. Bleed air from the turbine has enough temperature to prevent ice from forming[10].

Disadvantages

If the cooling system does not turn on in time, a high percentage of runback occurs, damaging the aircraft[11].

2.2.7 Icephobic surfaces

Icephobic surfaces follow the principle of wetting, which is the ability of a liquid to keep contact with solid surfaces [18]. The wetting can be categorized using droplet shape by contact angle measurement. The force balance between adhesive and cohesive forces gives the following main cases:

- **Hydrophilicity;** when water spreads out on the surface and low water wettability (angles smaller than 90°)[18].
- **Hydrophobicity;** when water beads up on the surface (angles bigger than 90°) [18]
- **Superhydrophobicity;** water contact angles greater than 150°. [19]

Super Hydrophobic Surfaces

The principles of ultra-water repellency are based on the roughness of a flat hydrophobic surface with a low surface energy. Real surfaces are rough and many measurements changes because they are non-ideal[20]. Therefore, states of the surfaces are classified in three classes: Wenzel, Cassie and Cassie-Baxter. Two surfaces states are relevant to get a highly improved hydrophobic surface.

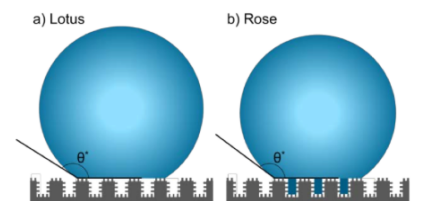


Figure 2.18: Lotus and Rose [18]

The Cassie-Baxter class is a rough hydrophobic surfaced with concave sites where air is trapped, while the liquid in Wenzel state fill these cavities. Cassie-Baxter and Wenzel states are enhanced to reach a new state where the contact area between the water and solid is significantly reduced even in convex and concave sites (Wenzel state)[21]. The way to enhance these state surfaces is by adding proper nano-properties. Cassie-Baxter reach Lotus State, while Wenzel reach the Rose Petal State, represented in Figure 2.18.

Aircrafts application

Superhydrophobic principle is the technology that has been applied in the industry to prevent the formation of the ice. However, there is little research about the efficiency of the superhydrophobic principle under real conditions[19]. Tests have been done in different situations to analyse the behaviour of the coatings and avoid the ice accumulation. Many projects have been created, of the most important “PHOBIC2ICE” in order to avoid the adhesion of ice in different parts of the plane[20]. As a result of the performed test we conclude the efficiency of the superhydrophobic surfaces is reduced with the rise of diameter of the water droplets or the water content inside of the drop due to the higher attractive forces and the moment present in the drop[19]. Recently the super-hydrophobic coatings are still in development or are used in combination with other well known anti-icing technology to increase its efficiency and lifetime of the airplane[19][20].

2.3 FAA Requirements

For this section, the requirements imposed by the FAA (Federal Administration Aviation) are asked to be presented for the aircraft Boeing 737 MAX. Through this research, the limits at which the aircraft fails due to icing accretion can be found. With the knowledge of these limits, effective anti-icing mechanisms can be designed and normative flight condition can be set.

The requirements found are in the e-CFR (Electronic Code of Federal Regulations) [22]. This represents the general, permanent regulation and rules, published in the federal register established by the federal government of the United States, which is composed of 50 entities, one of them being the FAA (Federal Administration Aviation). The FAA is focused in regulation for Aeronautics and Space.

In the official site of FAA, there are requirements for different types of aircrafts available on the market today, but not one specifically for each model of aircraft. Hence, the requirements presented in this section are generalized for aircrafts in the category of transport airplanes (which includes the Boeing 737 MAX). For this paper, the regulation related to icing of the wings is needed, and this information can be found in the e-CFR Chapter 1, title 14 (Aeronautics and Space), subchapter C (Aircrafts) Part 25. Within this part, attention was paid to the subparts and appendices that relate to flying under icing conditions.

2.3.1 Relevant requirements

Subpart F- Equipment- Ice protection

For aircrafts to be certified to fly under icing conditions, it must be demonstrated that the plane operates safely in continuous and intermittent maximum icing conditions.

- Ice protection systems must be analyzed and tested to demonstrate that it can operate during the various atmospheric conditions. These tests must be carried on of the protection system as a whole and to individual components in the system.
- A mechanism must be configured so that the crew notices when the ice protection system is not working properly.
- Methods to detect ice must be provided, it may be automatic, visual clues or atmospheric conditions clues.
- It must be clearly demonstrated that the ice protection system can operate continuously, also that it can cycle automatically or give clues to do it manually, depending on the needs documented in the Airplane manual.

Subpart F- Equipment- Supercooled large icing conditions

- For airplanes with a maximum weight of less than 60 000 pounds (27 216 Kg), it must be demonstrated that it can fly safely under conditions where supercooled droplets sizes are greater than 100 micrometers (large droplets), in accordance with the section of "Supercooled Large Drop Icing Conditions". Also:
 - The aircraft must have means to detect when it is flying under icing conditions described in the section "Supercooled Large Drop Icing Conditions", and be able to operate safely;
 - The aircraft must have means to detect when the icing conditions exceed the "Supercooled Large Drop Icing Conditions", and be able to operate safely while exiting those conditions.
- To show compliance with the point above the airplane and components must be analyzed and tested under similar conditions explained in the section "Supercooled Large Drop Icing Conditions". The analysis and tests can be carried with one or more method(s) below:
 - Laboratory dry ice or simulated dry ice, to test components or models of components and to taste that airplane or a model of the plane;
 - Flight tests under simulated and natural icing conditions;
 - Flight tests with simulated ice shapes.
- The aircraft must show reversible flight controls.
 - If imbalances due to accretion or aerodynamic forces make changes to the control system of the airplane, they must be able to be read in the deck control. Then the pilot must be able to operate these controls manually with his own effort.

2.3.2 Maximum Atmospheric Icing Conditions

MED between 2microns to 50 microns

There are three types of atmospheric icing conditions that an aircraft must show to be able to operate in accordance with the FAA.

The first two icing conditions focuses in the aircraft after take off, therefore the causes for accretion are related to the types of clouds the aircraft is going through. The first type is called stratiform cloud characterized by long length, which can cause continuous accretion. The second type is cumuliform clouds characterized by short length that causes intermittent icing conditions. The third icing is referenced to conditions during take off.

The FAA bases regulation for commercial aircrafts on these three atmospheric icing conditions, which will be explained more in detail below.

Continuous Icing (Stratiform):

This icing condition is characterized because of long horizontal clouds that causes continuous accretion, the atmospheric conditions are:

- Altitude range: sea level up to 22,000 ft;
- Air masses: stable;
- Temperature range: -30° C to 0°C;
- High risk temperature: -20°C to 0°C;
- Medium risk temperature: below -20°C;
- and Low: below -30°C.

Taken from [23].

With these conditions now the maximum accretion intensity condition can be set by the variables of the cloud liquid water content, the mean effective diameter droplets, the ambient temperature and the interrelation of them, as seen in Figure 8.1 in Appendix 8.1. Furthermore, the limits with respect to altitude and temperature are found in Figure 8.2. And the comparison of Figure 8.1 and 8.2 in Appendix 8.1, can show the relation of altitude with liquid water content.

The distance of measurements that was used to set the limits above is the standard 17.4 nautical miles. Because there is a relation between cloud length and its liquid water content, if another length of cloud is found apart from 17.4 nautical miles, the water content in it can be calculated from the liquid water content in Figure 8.1 multiplied by the factor in Figure 8.3 in Appendix 8.1.

Intermittent Icing (Cumuliform Clouds):

This icing condition is characterized because of shorter horizontal clouds length that causes intermittent accretion, the atmospheric conditions are:

- Altitude range: 4000 ft up to 22000 ft, and possibly up to 30000ft;
- Air masses: unstable;
- Temperature range: -30° C to 0°C, possibly from -40°C;
- High risk temperature: -20°C to -3.3°C;
- Medium risk temperature: below -20;
- and Low risk: below -30.

Taken from [23].

With these conditions now the maximum accretion intensity condition can be set by the variables of the cloud liquid water content, the mean effective diameter droplets, the ambient temperature and the interrelation of them, as seen in Figures 8.4 in Appendix 8.1. Furthermore, the limits with respect to altitude and temperature are found in Figure 8.5 in Appendix 8.1. The comparison of Figure 8.4 and 8.5 can show the relation of altitude with liquid water content.

The distance of measurements that was used to set the limits above, is the standard 2.6 nautical miles. Because there is a relation between cloud length and its liquid water content, if another length of cloud is found apart from 2.6 nautical miles, the water content in it can be calculated from the liquid water content in Figure 8.4 multiplied by the factor in Figure 8.6 in Appendix 8.1.

Maximum Take Off Atmospheric Icing Conditions

- Liquid water content: 0.35 g/m³;
- Mean effective drop diameter 20 micrometers;
- Temperature: -9°C;
- Altitude: up to 1500ft.

Taken from [23].

Supercooled large drop icing conditions, MED above 40/50 microns

Supercooled large drop icing conditions are defined as conditions which:

- the drop median volume diameter (MVD) is less than or greater than 40 µm [the maximum mean effective drop diameter (MED) for continuous maximum icing];
- consist of freezing drizzle and freezing rain occurring in and/or below stratiform clouds.

Freezing Drizzle

The characteristics of freezing drizzle are as follows:

- maximum drop diameters from 100µm to 500µm;
- pressure altitude range: 0 to 22,000 feet MSL;

- maximum vertical extent: 12,000 feet;
- horizontal extent: Standard distance of 17.4 nautical miles;
- total liquid water content;
- drop diameter distribution according to Figure 8.7;
- and an altitude and temperature envelope according to Figure 8.8;

From Figure 8.7 in Appendix 8.1 it can be read that for $MVD < 40\mu m$, roughly only 10% of the drops have a diameter greater than $100\mu m$ and contribute to freezing drizzle. For $MVD > 40\mu m$, about 50% of the drops have a diameter greater than $100\mu m$ and a maximum drop diameter of around $500\mu m$. Hence, they also contribute to freezing drizzle.

Figure 8.8 in Appendix 8.1 gives an overview of the ambient conditions in which freezing drizzle occurs. At 12 kft the ambient temperature is 0 degrees and reaches a temperature of -25 degrees at an altitude of 22 kft. Above 22 kft it can be assumed that water no longer exists in liquid form but more as a solid. This means it is not going to stick to the wings and freeze.

Freezing Rain

The characteristics of freezing rain are as follows:

- maximum drop diameters greater than $500 \mu m$;
- pressure altitude range: 0 to 22,000 feet MSL;
- maximum vertical extent: 7,000 feet;
- horizontal extent: Standard distance of 17.4 nautical miles;
- total liquid water content;
- drop diameter distribution according to Figure 8.9, in Appendix 8.1;
- and an altitude and temperature envelope according to Figure 8.10, in Appendix 8.1.

From Figure 8.9 in Appendix 8.1, it can be seen that for $MVD < 40\mu m$, roughly 25% of the drops have a diameter greater than $500\mu m$ and contribute to freezing rain. For $MVD > 40\mu m$, about 70% of the drops have a diameter greater than $500\mu m$ and a maximum drop diameter of around $2500\mu m$. Hence, they also contribute to freezing rain.

Figure 8.10 in Appendix 8.1, gives an overview of the ambient conditions in which freezing drizzle occurs. At 12 kft the ambient temperature is 0 degrees. Freezing rain only occurs up to -13 degrees, below 12 kft.

Liquid Water Content

The liquid water content for freezing drizzle and freezing rain conditions for horizontal extents other than the standard 17.4 nautical miles can be determined by the value of the liquid water content determined from Figure 8.11 for freezing drizzle and Figure 8.12 for freezing rain, in Appendix 8.1, multiplied by the factor provided in Figure 8.13, which is defined by the following equation:

$$S = 1.266 \cdot 0.213 \log_{10}(H)$$

where:

S = Liquid Water Content Scale Factor (dimensionless);

H = horizontal extent in nautical miles.

2.3.3 Compliance of Boeing 737 MAX To The Icing Conditions

In order for the Boeing 737 MAX to be certified, it must demonstrate that it can fly safely at any icing condition, meaning to show compliance with subpart F - Equipment- Ice protection and Super cooled large icing conditions.

Through research into several websites, the operating conditions of a typical flight path for a Boeing 737 MAX were found and outlined below:

- Cruising altitude between 31,000 - 38,000 ft [24];
- 10 minutes after takeoff to reach cruising altitude [24];
- Cruising speed of 453 knots [25].

From the values, found it can be seen that the cruising altitude of a Boeing 737 MAX is above the altitude in which icing occurs (22 kft). Hence, icing is only likely to occur while parked, ascending and descending. The time for ascent and descent is around 10 minutes and ice accretion will occur here due to CM, IM, freezing drizzle and/or freezing rain. During ascent and descent there will be times when the speed is lower than 430 knots [26]. It is at these times that ice accretion is likely to occur.

The normative atmospheric operational conditions for the aircraft must hence be below the maximum atmospheric conditions described in this section to prevent critical ice accretion.

2.4 Problem Identification

In this part of the literature study, the detailed problem of icing protection on an aircraft exposed to an airflow. The icing changes the aerodynamics of a wing and thus its required increase in thrust power to maintain a constant velocity. In Effect of Ice Accretion on Aircraft Flight Dynamics by M.B. Bragg[27], a linear increase in the required thrust can be seen as a function of the duration of the flight. Due to the ice accumulation on the wings and tail, the lift coefficient deteriorates. To maintain altitude this means the flight speed and thus thrust has to be increased. This increase in required thrust lowers the fuel efficiency of the aircraft as the air resistance increases non-linearly. Because of this, more fuel is required to maintain the required energy required for the flight duration.

2.4.1 Bleed air Ice Protection System

A common type of systems to prevent ice from forming on the wing is to use the bleed air from the engine. However, the exhaust air of modern jet engines is not sufficiently hot to provide adequate heat transfer to combat ice forming on the wings of the plane. To fully heat the plane, the hot air would have to be extracted before entering the turbine. This however comes with a drawback of lowering the thermal efficiency of the engines. This decrease also leads to a decrease in the amount of power dedicated to propulsion[23]. When using a traditional bleed air system, the decrease is found to be around 6.6%, however, using Loop Heat Pipes to use the waste heat from the engine can decrease this to about 0.38%[28]. A more efficient way to provide this heat could be to use an electrical heating element as such an installation is more thermally efficient than using bleed air in combination with heat exchangers. Such a system can be very lightweight and operate very quickly when a threshold of ice is accumulated on the plane wings[23].

2.4.2 Fluid based Ice Protection System

Using fluids for ice removal does not come with a lot of mechanical or thermal drawbacks as the anti-icing fluid does not have to be heated and this method does not cost much power. The only increase in power comes from the added weight to the plane, however, almost all IPS's suffer from this drawback. The method also clearly lacks the ability for longer flights, making it more suited for smaller aircraft. One of the problems associated with this type of system originates from a different corner of science. Namely toxicology as anti-icing systems used in aircraft are toxic to humans and the environment[29]. When implementing such a system into an aircraft, laws regarding the maximum amount of these substances into the environment should be taken into account.

2.4.3 Pneumatic boots

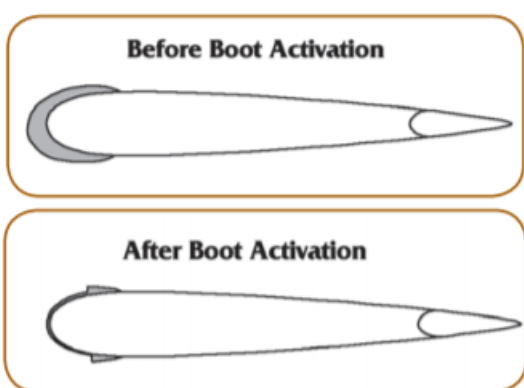


Figure 2.19: Negative aerodynamic effects of pneumatic boots [30]

The most common anti-icing system on small planes with a propeller or small turbojets is the use of pneumatic boots. Although this system is able to delete the ice from the wings, there are some serious disadvantages with respect to aerodynamics. Because this system works only periodically between inflated and not inflated (see figure 2.8), ice will still be formed between the cycles. This has still a negative result on the aerodynamics of the plane. Another negative effect is that in between or at the sides of the system also ice is formed that cannot be removed. This residual icing ridge can be very dangerous because it blocks the air flows and thus has a negative effect on the aerodynamics. Both aerodynamic effects are shown in figure 2.19.

Both negative effects result in a different angle of attach with respect to a clean wing. This results in a lower lift coefficient, requiring more power to stay at the same altitude at a constant velocity. The system does not require heat, so there will be no thermal issues.

2.4.4 EESS (Electro-Expulsive Separation System)

This system works almost the same as the pneumatic boots system. The major difference is the activation of the boots. Where pneumatic boots use air, the EESS system uses electromagnets to activate. This makes a major difference because while the pneumatic boots work slow, the EESS can remove the ice layers way faster[23]. The time between each cycle will be lower so the situations in figure 2.19 will have less ice. This results in less negative effects of aerodynamics, but they still exist. So there will be a need for less power than pneumatic boots do but more than without aerodynamic issues. The system does not require heat, so there will be no thermal issues.

2.4.5 EIDI (Electro-Impulse Deicing)

The EIDI system uses electro impulse actuators that are embedded in the wing. because of this, the shape of the wing does not have to change, so the lift coefficient will be the same, resulting in the same power usage. Another advantage is that no heat is needed so there are no thermal issues. However, there are some disadvantages with this type of system. Because the system uses electro-impulses, these may interfere with sensors, which can result in failure of the sensors or wrong results. Because the impulses cause stresses in both directions, the system is prone to fatigue, what can cause failure of the structure of the wing. At last the vibrations of the impulses can cause noise that the passengers can hear. The response that the passengers can have to this noise is a big disadvantage.

Chapter 3

External Flows and Heat Exchange

3.1 Trajectories of Droplets

The goal of this section is to determine the trajectories of the droplets when they hit the airplane wing. First a velocity potential around the wing was determined. Next, droplets of different sizes were input into the velocity potential field to see how they behave and which parts of the wing they hit.

3.1.1 Derivation of Potential Flow

The first step in determining the trajectories, is to derive the velocity potential function. The most critical location of the airfoil to be analyzed is the leading edge as that is the location where most ice accretion is going to take place. For simplification in calculation, the leading edge can be modeled as a cylinder. This assumption is well founded as the geometrical shape of the leading edge facing the wind is similar to the curve of a cylinder.

The situation will be analyzed in 2D in the x and y-direction along the leading edge. The span-wise direction (z-direction in this case) can be left out as the situation in the x and y-direction can be assumed to simply be occurring along the whole z-direction. From fluid mechanics, a potential flow is described using the velocity potential (ϕ) which is a function of time and space. The gradient (∇) of the velocity potential gives the velocity field (\vec{U}). The relation is shown below in equation (3.1).

$$\vec{U} = \nabla\phi \quad (3.1)$$

An incompressible flow can be assumed as the aircraft will be flying at low Mach number speeds. As a result the \vec{U} has zero divergence. Using vector calculus this means:

$$\nabla \cdot \vec{U} = 0 \quad (3.2)$$

Hence,

$$\nabla^2\phi = 0 \quad (3.3)$$

If ϕ is defined as $\phi(x, y)$. Then:

$$u = \frac{\partial\phi}{\partial x} \quad (3.4)$$

$$v = \frac{\partial \phi}{\partial y} \quad (3.5)$$

Substituting equation (3.4) and (3.5) into equation (3.3) gives the relation below:

$$\frac{\partial^2 \phi}{\partial x^2} + \frac{\partial^2 \phi}{\partial y^2} = 0 \quad (3.6)$$

From here trial and error will be used to obtain an equation for $\phi(x, y)$ that satisfies the relation in equation (3.6) for the cylinder. The correct solution is shown below:

$$\phi(x, y) = U_o x + \frac{U_o a^2 x}{x^2 + y^2} \quad (3.7)$$

Where,

- U_o is the constant velocity of air
- a is the radius of the cylinder

For this situation it is more convenient to use 2D cylindrical coordinates using the transformation below:

$$r = \sqrt{x^2 + y^2} \quad (3.8)$$

$$\theta = \arctan\left(\frac{y}{x}\right) \quad (3.9)$$

Equation (3.7) can hence be written as:

$$\phi(r, \theta) = U_o \left(1 + \frac{a^2}{r^2}\right) r \cos \theta \quad (3.10)$$

3.1.2 Plotting The Velocity Field

In this section the equation of ϕ for the cylinder found above in equation (3.10) will be used to determine the velocity field around the cylinder and plot them in a graph. First the partial derivatives of ϕ , U_r and U_θ were calculated:

$$U_r = \frac{\partial \phi}{\partial r} = U_o \left(1 - \frac{a^2}{r^2}\right) \cos \theta \quad (3.11)$$

$$U_\theta = \frac{1}{r} \frac{\partial \phi}{\partial \theta} = -U_o \left(1 + \frac{a^2}{r^2}\right) \sin \theta \quad (3.12)$$

The components of U_r and U_θ in the x and y direction were taken and summed up to obtain equations for the horizontal velocity (U) and vertical velocity (V):

$$U = U_r \cos \theta - U_\theta \sin \theta \quad (3.13)$$

$$V = U_r \sin \theta + U_\theta \cos \theta \quad (3.14)$$

Plotting U and V for a grid of x and y values gives the velocity field as shown in Figure 3.1 below.

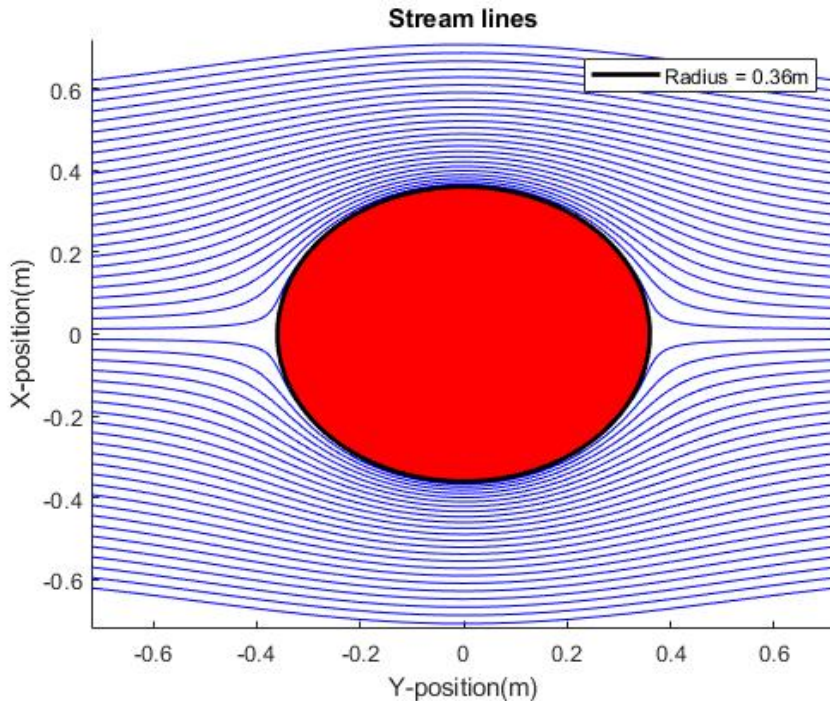


Figure 3.1: Velocity field around a cylinder represented using streamlines

3.1.3 Plotting Trajectories of Droplets

Before proceeding further, a few assumptions had to be made about the droplets. These assumptions were made to simplify the problem and to enable easier calculations. In this section, parameters relating to the droplet will be indicated with " d " while those relating to air will be indicated with " a ".

General Assumptions On The Droplets:

- The droplets are considered to be perfect spheres;
- The droplets do not change shape throughout their trajectory, hence volume and density are constant;
- For simplification, the airfoil of the wing will be modeled as a cylinder;
- The droplets are considered to be sufficiently small that they do not influence the velocity potential field;
- And the starting velocity of the droplet is equal to the velocity of potential field.

Forces On A Droplet:

- Drag force (F_D);
- Buoyancy force (F_B);

- And gravity (F_G).

Although other forces do occur on a droplet, the 3 forces above are the most dominant ones. Forces such as Basset force and virtual mass force are very small here and can be considered as negligible.

Using Newton's 2nd Law, the forces acting on the droplet were equated to it's mass (m_d) times it's acceleration (\vec{a}_d):

$$\vec{F}_D + \vec{F}_B + \vec{F}_G = m_d \vec{a}_d \quad (3.15)$$

The forces mentioned above are defined as:

$$\vec{F}_D = \frac{1}{2} \rho_a |\vec{u}_a - \vec{u}_d| (\vec{u}_a - \vec{u}_d) A_d C_d \quad (3.16)$$

$$\vec{F}_B = (\rho_a - \rho_d) V \vec{g} \quad (3.17)$$

$$\vec{F}_G = m_d \vec{g} \quad (3.18)$$

Hence, the overall equation is formed by substituting equations (3.16), (3.17), (3.18) into (3.15):

$$\frac{1}{2} \rho_a |\vec{u}_a - \vec{u}_d| (\vec{u}_a - \vec{u}_d) A_d C_d + (\rho_a - \rho_d) V \vec{g} + m_d \vec{g} = m_d \vec{a}_d \quad (3.19)$$

From equation (3.19) it can be seen that \vec{u}_d and \vec{a}_d are present as variables while A_d is the area which makes will make contact with the wing, C_d is the drag coefficient settled to be 0.47 [31], m_d is the mass of the droplet and g is the gravitational acceleration. Hence, equation (3.19) is a vector equation with a pair of 2nd order differential equations (one in x direction and one in y direction). These differential equations were solved using Matlab and an equation for the displacement of the droplet in the x direction ($x_{d,x}$) and y direction ($x_{d,y}$) was obtained.

The steps to solve with the equation 3.19 with Matlab are listed below

1. Divide equation 3.19 in x-axis and y-axis with the acceleration terms in one side of the equations:

$$a_x = \frac{1}{2m_d} \rho_a |\vec{u}_a - \vec{u}_d| (\vec{u}_a - \vec{u}_d x) A_d C_d + \frac{(\rho_a - \rho_d) V \vec{g}}{m_d} + \vec{g} \quad (3.20)$$

$$a_y = \frac{1}{2m_d} \rho_a |\vec{u}_{ay} - \vec{u}_{dy}| (\vec{u}_{ay} - \vec{u}_{dy} y) A_d C_d + \frac{(\rho_a - \rho_d) V \vec{g}}{m_d} + \vec{g} \quad (3.21)$$

2. Then the two second order differential equation are converted into first order differential equations.

3. The function `ode45` in Matlab is called with initial inputs: initial position of the droplet and the velocity of air at that initial position. The output is the position of after a step time of 1^{-6} seconds.
4. Then the new inputs are the positions found in the previous step and the velocity of air at that position.
5. This is repeated until the droplets either hit the wing or passes over it.

Using the x and y displacements following the steps above, the trajectory of the droplet in the velocity field was plotted. Different droplet sizes were tested for by varying the diameter of the droplets. Figures 3.2, 3.3, 3.4 below show the trajectory of small, medium and large sized droplets. The small and medium droplet sizes are likely to occur during the continuous maximum icing and intermittent icing. The large droplet sizes are likely to occur during supercooled icing conditions such as freezing rain and freezing drizzle. The droplet diameters were chosen in reference to section 2.3.2.

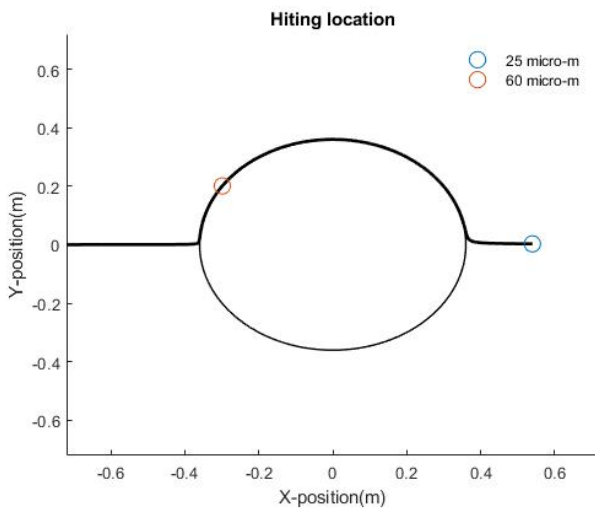


Figure 3.2: Small droplets

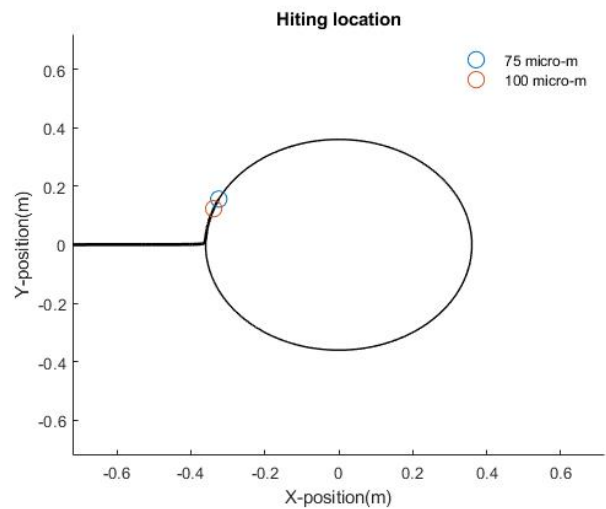


Figure 3.3: Medium droplets

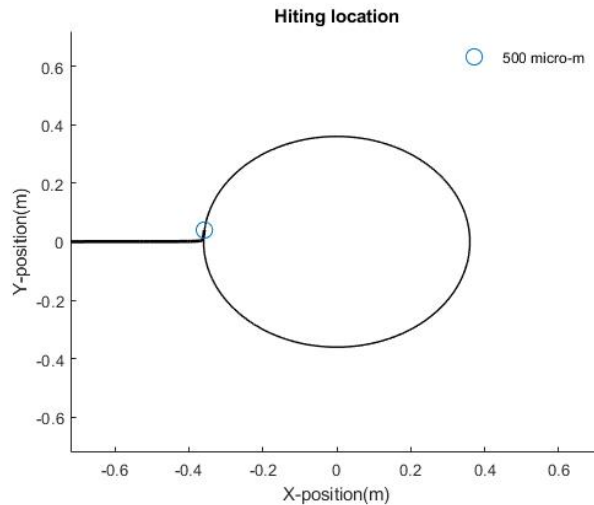


Figure 3.4: Large droplets

The initial position of the droplets were chosen to be [0.72, 0.0005] for all droplets sizes, the position in the y-axis 0.005 was chosen to make sure the droplet hit the wing. If higher values for the y-axis were chosen, all the droplets would never hit the wing. Due to this the droplets initially follow a very similar path until they hit the cylinder. The deviation in their trajectories initially therefore is too small to be seen in the above figures. From the plotting of trajectories, it can be seen that really small droplets of diameter $10\mu\text{m}$ simply follow the velocity field around the cylinder without impacting it. However as the droplet diameter increases, all the droplets tend to hit the front of the cylinder which in this case would be the leading edge of the wing. The large sized droplets are found a close to the stagnation point while the medium sized ones are a bit further away.

3.2 Mass and energy balance

The calculation of the energy and mass are necessary to evaluate the ice accumulation to do that the Messinger-balanced [32] is applied. The analysis is done between the incoming and outgoing mass rates and energies, a cylindrical control volume and two plates are used to analyse the present case, one plate for the top of the wing and the other for the bottom. The control volume has the following boundaries. The mass and energy balance are shown in the figure 3.5.

- The control volume is considered 2D.
- The bottom boundary is the layer of ice formed on the wing.
- The left and the right boundaries were chosen arbitrarily along the wing , the size is sufficiently small to allow the calculations on the surface.
- The depth of the volume has the unit length.

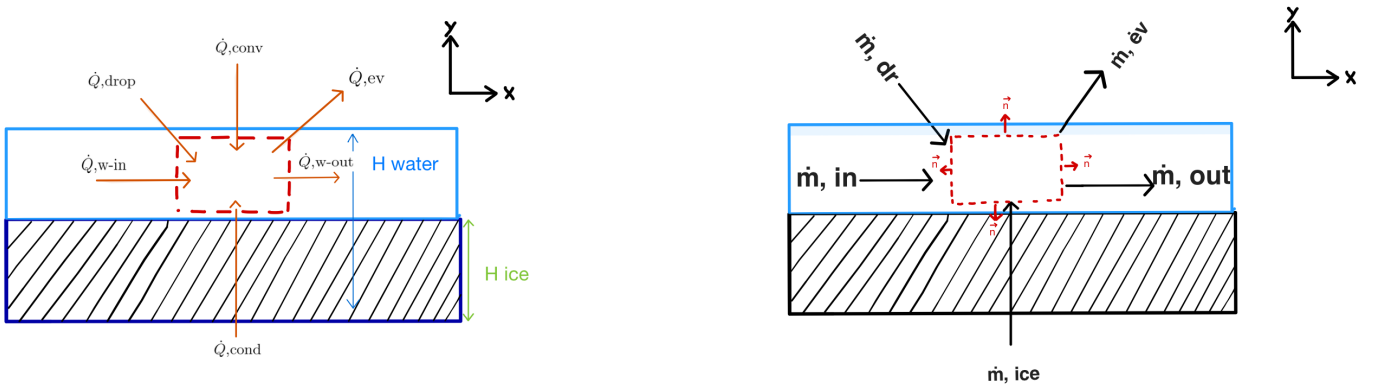


Figure 3.5: Messinger balance. Left: energy balance. Right: mass balance

3.2.1 Assumptions

In order to calculate accurate values for the mass and energy balance some assumptions need to be done.

- The flow will be considered as steady state. It means that process is independent of time.
- The flow is incompressible. The density is constant, because the size of the control volume is sufficiently small.
- The gravity will be neglected due to the small size of the droplet and the influence of gravity is null.

3.2.2 Mass balance

The basic equation of the mass balance is :

$$\int_{V(t)} \frac{\partial \rho}{\partial t} dV + \int_{A(t)} \rho(u_j n_j) dA = 0 \quad (3.22)$$

Where:

- The integral $\int_{V(t)} \frac{\partial \rho}{\partial t} dV$ expresses the mass rate of change due to the density rate of change [33].
- The integral $\int_{A(t)} \rho(u_j n_j) dA$ expresses the mass rate of change due the growth rate of the blob.[33]

Due to the assumptions made (section 3.2.1) , the new expression can write as:

$$\rho \int_{A(t)} (u_j n_j) dA = 0 \quad (3.23)$$

The expression was taken based on figure 3.5 (right):

- \dot{m}_{in} is mass rate that enters in the control volume.
- \dot{m}_{out} describes the part of the incoming water that does not freeze to the surface. This flow then leaves the control volume.
- \dot{m}_{ice} represent the mass rate that become ice over the wing surface
- \dot{m}_{ev} is the mass rate that evaporates and leaves the control volume at the height. The water will evaporate due to the contact with the de-icing system.
- \dot{m}_{dr} represents the droplets that enter the control volume.

The mass rate that enter in the control volume is expressed by the equation. The boundaries taken for the integral are from 0 to the width in the x-axis and for y-axis are from h_{ice} to h_{water} .

$$\dot{m}_{w,in} = \int_{h_{ice}}^{h_{water}} \int_0^w \rho(u_{in} \cdot (-1)) dx dy = \int_{h_{ice}}^{h_{water}} \rho(-u_{in}) dy \quad (3.24)$$

The outcoming mass rate is the remaining that does not freeze in the surface or evaporate on the wing , the equation that describe it is the below one.

$$\dot{m}_{w,out} = \int_{h_{ice}}^{h_{water}} \int_0^w \rho(u_{out} \cdot 1) dx dy = \int_{h_{ice}}^{h_{water}} \rho(u_{out}) dy \quad (3.25)$$

The resulting mass balance is:

$$\dot{m}_{ev} - \dot{m}_{out} - \dot{m}_{ice} - \dot{m}_{ev} + \dot{m}_{dr} = 0 \quad (3.26)$$

The mass rate of the droplets that enter in the control volume is described by:

$$\dot{m}_{dr} = \beta \cdot LWC \cdot U \cdot w \cdot s \quad (3.27)$$

In the equation 3.27 the term U describe the velocity field, s is the depth, w the width along the x-axis, LWC is the liquid water content of the droplet and β its equivalent collection efficiency.

The evaporation rate is represented with the following formula by:

$$\dot{m}_{ev} = \frac{h_v(T - T_i)A}{\lambda_i} \quad (3.28)$$

3.2.3 Energy Balance

Based on the mass balance and by using the same principle the following energy balance is obtained.

Figure 3.5 left, shows the incoming and outgoing energy in the system, as result of the graph the-follow equation is found [32]:

$$\dot{Q}_{w-in} + \dot{Q}_{drop} + \dot{Q}_{conv} + \dot{Q}_{cond} + \dot{Q}_{KE} + \dot{Q}_U - \dot{Q}_{ev} - \dot{Q}_{w-in} = 0 \quad (3.1)$$

Where:

\dot{Q}_{w-in} = The rate of heat transfer of the water that did not freeze or evaporate.

\dot{Q}_{w-out} = The rate of heat transfer of the runback water.

\dot{Q}_{drop} = The rate of heat transfer of the incoming drops.

\dot{Q}_{cond} =The rate of heat transfer due to the anti icing system between the skin and the ice.

\dot{Q}_{conv} =The rate of heat transfer of the motion of the fluid such as air.

\dot{Q}_{ev} = The rate of heat transfer required to evaporate the liquid water.

\dot{Q}_{KE} = The rate of heat transfer provided by the kinetic energy of the incoming water droplets.

\dot{Q}_U =The rate of heat transfer of the internal energy that is converted to heat.

The first law of thermodynamics states that the energy change of a blob of material equals the heat added to the blob plus the work done.The relation that describes it is:

$$Energy(t) = \int_{V(t)} \rho(x, t) E(x, t) dV. \quad (3.2)$$

The amount of heat added to the blob per unit time can be written as:

$$\int_{S(t)} q \cdot (-n) dS = - \int_{S(t)} q \cdot n dS = - \int_{S(t)} q_j n_j dS \quad (3.3)$$

where $(-\mathbf{n})$ was taken instead of \mathbf{n} since it is about the heat flux towards $V(t)$. The amount of work done on the blob per unit time can be written as:

$$\int_{S(t)} t_i u_i dS + \int_{V(t)} \rho g_j u_j dV \quad (3.4)$$

Where:

- The integral $\int_{S(t)} t_i u_i dS$ denotes the work rate done by the surrounding fluid (stress);
- The integral $\int_{V(t)} \rho g_j u_j dV$ denotes the work rate done by the surrounding fluid (stress).

The first law of thermodynamics for the blob now becomes.

$$\frac{d}{dt} \int_{V(t)} \rho E dV = - \int_{S(t)} q_j n_j dS + \int_{S(t)} \sigma_{ij} n_j u_i dS + \int_{V(t)} \rho g_j u_j dV \quad (3.5)$$

With the Reynolds transport theorem, the expressions can be written as:

$$\int_{V(t)} \frac{\partial}{\partial t} (\rho E) dV + \int_{S(t)} (\rho E u_j - \sigma_{ij} u_i - k \frac{\partial T}{\partial x_j}) n_j dS = \int_{V(t)} \rho g_j u_j dV. \quad (3.6)$$

Each parameter of the equation describe a particular case whose are mentioned above:

- $\int_{V(t)} \frac{\partial}{\partial t} (\rho E) dV$ expresses the energy rate of change due to the total energy rate of change.
- $\int_{S(t)} \rho E u_j n_j dS$ expresses the energy rate of change due convection.
- $\int_{S(t)} -\sigma_{ij} u_i n_j dS$ expresses the energy rate of change due work done by stress.
- $\int_{S(t)} -k \frac{\partial T}{\partial x_j} n_j dS$ expresses the energy rate of change due conduction.
- $\int_{V(t)} \rho g_j u_j dV$ expresses the energy rate of change due work done by gravity.

The assumption mentioned in the section 3.2.1 will work for the energy balance, and the new equation will look like:

$$\int_{S(t)} \rho E u_j dS - \int_{S(t)} \sigma_{ij} u_i n_j dS = \int_{S(t)} k \frac{\partial T}{\partial x_j} n_j dS \quad (3.7)$$

Due to the assumptions of an inviscid flow the second term changes:

$$\sigma_{ij} = -p\delta_{ij} + \mu \left(\frac{\partial u_i}{\partial x_j} + \frac{\partial u_j}{\partial x_i} \right) - \frac{2}{3} \mu \delta_{ij} \frac{u_k}{x_k} = -p\delta_{ij}, \quad \delta_{ij} = \begin{cases} 0, i \neq j \\ 1, i=j \end{cases} \quad (3.8)$$

As a result of the change due to the inviscid fluid. It will look like:

$$\int_{S(t)} \rho E u_j n_j dS - \int_{S(t)} -p u_j n_j dS = \int_{S(t)} (\rho E + p) u_j n_j dS \quad (3.9)$$

In equation 3.9 is possible to substitute it with the definition of the enthalpy.

$$h \equiv E + \frac{p}{\rho} \Rightarrow h\rho = E\rho + p \Rightarrow \int_{S(t)} (h\rho) u_j n_j dS \quad (3.10)$$

Which result in:

$$\int_{S(t)} (H\rho) u_j n_j dS = \int_{S(t)} k \frac{\partial T}{\partial x_j} n_j dS = - \int_{S(t)} q_i n_j dS \quad (3.11)$$

The enthalpy will help to express the incoming and outgoing energy in the control volume, the kinetic energy will be neglected. The new equations could be expressed in term of enthalpy flow in and out of the control volume.

$$\int_{h_{ice}}^{h_{water}} (h_{w,in}\rho) u_j n_j dS = \dot{Q}_{w,in} = \dot{m}_{in} H_{w,in} = \dot{m}_{in} (C_p(T_{in} - T_{surr})) \quad (3.12)$$

$$\int_{h_{ice}}^{h_{water}} (h_{w,out}\rho) u_j n_j dS = \dot{Q}_{w,out} = \dot{m}_{out} H_{w,out} = \dot{m}_{out} (C_p(T_{out} - T_{surr})) \quad (3.13)$$

Now it is possible to write the complete energy balance for the case in the control volume:

$$\dot{Q}_{w-in} = \dot{m}_{in} (C_{p_{water}}(T_{in} - T_{surr})) \quad (3.14)$$

$$\dot{Q}_{w-out} = \dot{m}_{out} (C_p(T_{out} - T_{surr})) \quad (3.15)$$

$$\dot{Q}_{KE} = h_c(T_e + \frac{r \cdot U_e^2}{2c_{pa}} - T_\infty) \Delta s \quad (3.16)$$

$$\dot{Q}_{conv} = h_c(T_{surr} - T_\infty) \Delta s \quad (3.17)$$

$$\dot{Q}_{cond} = kA \frac{T_{sur} - T_{ice}}{L} \quad (3.18)$$

$$\dot{Q}_{drop} = \dot{m}_d C_{pw}(T_\infty - T_{surr}) \quad (3.19)$$

$$\dot{Q}_{evap} = \dot{m} \cdot c_p \cdot \Delta T \quad (3.20)$$

The analysis that was carried out before regarding the balance of masses and energies serves to be able to fulfill the principle of the conservation of mass and energy, since nothing is created or destroyed, it can be transformed into another mass or energy.

3.2.4 Local Heat Transfer

The heat transfer coefficient (h), is a quantitative characteristic of convective heat transfer from the wing to the surrounding air. What this quantity indicates is the heat loss per unit area and per Kelvin. Therefore with this value it is possible to predict the rate of the wing to cool down. The following formula is normally used:

$$\dot{Q} = h \cdot A(T_2 - T_1) \quad (3.21)$$

Where T_2 is the temperature of the surrounding, in this case would be the temperature of the air during the flight. T_1 is the temperature of the wing, the wing can increase in temperature because of the de-icing system.

Previous to calculate the heat transfer coefficient, two main parameters should be found: the Velocity Boundary Layer and the coefficient of friction. The heat transfer coefficient will be calculated by modeling the leading edge as a cylinder while the top and bottom part of the wing will be flat surfaces.

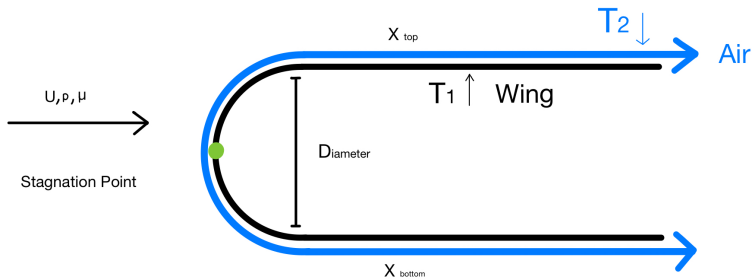


Figure 3.6: Wing Profile

Velocity Boundary layer

The velocity boundary layer δ is described as the layer where the flow velocity of the fluid is influenced by the dynamic viscosity μ , also the velocity is equal to zero in the wall due to the shear stress producing a laminar flow. The equation for the boundary layer can be obtained from the continuity equation and the momentum conservation.

$$\frac{\partial u}{\partial x} + \frac{\partial v}{\partial y} = 0 \quad (3.22)$$

$$u \frac{\partial u}{\partial x} + v \frac{\partial u}{\partial y} = \nu \frac{\partial^2 u}{\partial y^2} \quad (3.23)$$

Using the Blasius solution for flat plate, a new relation for the velocity boundary layer is found, the new equation is dependent on the dimensionless Reynolds number. The complete derivation can be found in the appendix:

$$\delta(x) = \frac{4.91x}{\sqrt{Re(x)}} \quad (3.24)$$

$$Re(x) = \frac{Ux}{\nu} = \frac{Ux\rho}{\mu} \quad (3.25)$$

The velocity boundary along the length of the wing is shown in the figure 3.7, in order to plot the velocity layer the assumption of laminar is taken to make a simple analysis and the data used for plot the velocity layer are mentioned in the table 3.1.

Symbol	Description	Value
U	Velocity of air	86 m/s
T _s	Temperature of the surface	50 °C
T _∞	Temperature of the air	-10 °C
T _f	Film Temperature	20 °C
ν	Dynamic Viscosity	1.825·10 ⁻⁵
C _p	Specific heat	1007 J·kg ⁻¹ ·K ⁻¹
k	Thermal conductivity	0.02514 W·m ⁻¹ K ⁻¹
P _r	Prandtl Number	0.7309
W	Wingspan	2 m

Table 3.1: Data for plot velocity boundary layer

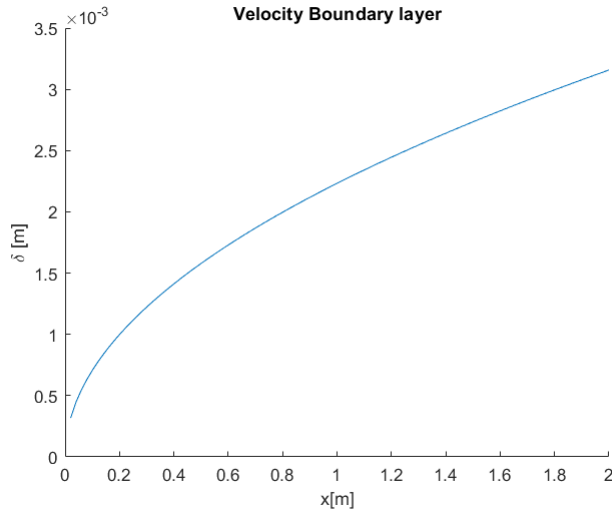


Figure 3.7: Velocity boundary layer

Friction coefficient

The friction coefficient C_f is a dimensionless number generated by the viscosity of the fluid and the development of it. The expression for the friction coefficient can be derived from the shear stress:

$$\tau_{wall} = \mu \frac{\partial u}{\partial y} \Big|_{y=0} \quad (3.26)$$

Using the stream function and relation found during the derivation(8.2.1) of the equation, the new expression can be rewritten as:

$$C_f = \frac{0.664}{\sqrt{Re(x)}} \quad (3.27)$$

Local heat transfer coefficient along a flat plate

To get the local heat transfer Coefficient it is necessary to use the energy equation and the thermal boundary layer. With this information, a relation for the heat transfer coefficient can be found in Equation 3.29. The derivation can be found in Appendix 8.2.2

$$u \frac{\partial \theta}{\partial x} + \nu \frac{\partial \theta}{\partial y} = \alpha \frac{\partial^2 \theta}{\partial y^2} \quad (3.28)$$

$$h(x) = 0.332 Pr^{\frac{1}{3}} k \sqrt{\frac{V}{\nu x}} \quad (3.29)$$

Thermal Boundary Layer

The thermal boundary layer can be seen in the following equation:

$$\left. \frac{\partial T}{\partial y} \right|_{y=0} = (T_\infty - T_s) \left. \frac{\partial \theta}{\partial y} \right|_{y=0} = (T_\infty - T_s) \left. \frac{\partial \theta}{\partial \eta} \right|_{\eta=0} \left. \frac{\partial \eta}{\partial y} \right|_{y=0} \quad (3.30)$$

$$\left. \frac{\partial T}{\partial y} \right|_{y=0} = 0.332 Pr^{\frac{1}{3}} (T_\infty - T_s) \sqrt{\frac{V}{\nu x}} \quad (3.31)$$

Local heat coefficient across the cylinder

The correlation (empirical/experimental) was used to get the local heat transfer coefficient along the smooth cylinder. The distance on the circumference from the front stagnation point, and the x represents the arc distance.

$$Nu_{cyl} = \frac{hD}{k} = 0.3 + \frac{0.62 \cdot Re^{1/2} Pr^{1/3}}{[1 + (\frac{0.4}{Pr})^{2/3}]^{1/4}} \left[1 + \left(\frac{Re}{282000} \right)^{5/8} \right]^{4/5} \quad (3.32)$$

The Nusselt number was used to found the local heat transfer coefficient across the cylinder.

$$h_{cyl} = \left[0.3 + \frac{0.62 \cdot Re^{1/2} Pr^{1/3}}{[1 + (\frac{0.4}{Pr})^{2/3}]^{1/4}} \left[1 + \left(\frac{Re}{282000} \right)^{5/8} \right]^{4/5} \right] \frac{k}{D} \quad (3.33)$$

Local heat transfer coefficient along the wing

The wing's leading edge is represented as a cylinder and a top flat surface and bottom flat surfaces. Therefore, the local heat transfer coefficient can be obtained by combining the equation for the cylinder and the flat surfaces. This can be done for the top and the bottom surface. The transition point between cylinder and flat will be considered at the distance of the radius of the cylinder in the present case is 0.16 m.

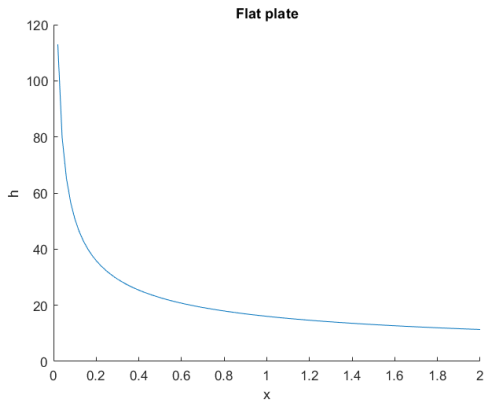


Figure 3.8: Heat transfer coefficient flat plate

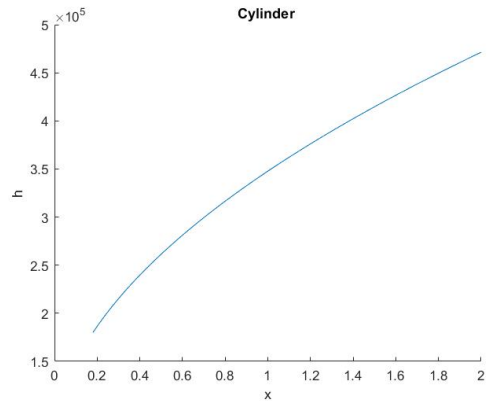


Figure 3.9: Heat transfer coefficient cylinder

The derivation for the heat transfer coefficient is a fundamental part, because with it the rate of heat loss can be calculated. It gives information about the energy that is need to be supply on the surface of the wing to avoid the formation and accumulation of ice. It is calculated along the wing, the critical parts for the heat transfer can be known and a suitable location for an anti-icing can be found.

3.3 Simulations using 2DFOIL-ICE

Using the 2DFOIL-ICE program the streamlines and the heat coefficient were compared and checked. Also the amount of heat needed to keep the wing ice free was calculated using the program.

3.3.1 Tests

Before comparing and calculating, the right assumptions have to be made. Because there are a lot of conditions where planes fly in, some tests have to be done. In Table 3.2 below are different variables, such as altitude, temperature and liquid water content. These values are found in section 2.1.2. A few combinations of these variables are chosen for 9 tests, since not all combinations are realistic. The first tests give an indication of the amount of ice accretion; the tests done with greater droplet sizes are used for the comparison with the results of the numerical solver.

Variable	Values to test				
Altitudes [m]	1000	1500	5000	-	-
Temperature [K]	263.15	267.15	271.15	-	-
Droplet diameter [μm]	15	35	50	100	500
LWC [g/m ³]	0.25	1.6	3.0	-	-
Time step (s)	1200				

Table 3.2: The variables and values to test

The last variable is the pressure at different altitudes and temperatures; that can be found by using equation 3.34

$$P(h, T) = P_0 * \exp \frac{Mgh}{RT} \quad (3.34)$$

$$M = 0.029 \frac{\text{kg}}{\text{mol}}$$

$$g = 9.8 \frac{\text{m}}{\text{s}^2}$$

$$R = 8.13 \frac{\text{J}}{\text{mol*K}}$$

$$P_0 = 100000 \text{Pa}$$

Here, h is the altitude in [m] and T the temperature in [K]. All tests can be found in the appendix 8.3

3.3.2 Comparing the 2DFOIL-ICE simulations to the cylinder simulations

To check if the flow around a cylinder resembles the real flow around an airfoil, the results from the potential flow and numerical solver are compared to the results from the 2DFOIL-ICE-software. The inputs in the numerical solver and the software are as similar as possible (airspeed and droplet size). The results taken from the software are the worst-case scenarios for the airfoil. The inputs used for the software are shown in Table 3.3. The droplet-trajectories of the cylinder-tests tend to lie around the cylinder if the droplets are small. The size is then around 10 μm . This was already seen in the results of the numerical solver. If the droplet size increases, the droplets impact more to the leading edge of the wing. The 2DFOIL-ICE software provides more insight in what the airfoil experiences with increasing droplet size. These results can be compared to the results of the other calculations. The bigger droplets are less influenced by the airflow that moves around the airfoil, thus they impact

Droplet diameter [μm]	50	100	500
Airspeed [m/s]	86	86	86
Temperature [K]	263.15	263.15	263.15
LWC [$\frac{\text{g}}{\text{m}^3}$]	3	3	3
Pressure [Pa]	81 917	90 908	90 908

Table 3.3: The variables and values used test the streamlines

the wing in the direction they were in already. This trend is seen in the software results as well. The tests with the small droplets, 50 μm , do impact the wing, but the trajectories and streamlines are close to the shape of the airfoil; this is seen in figures 3.10 and 3.11. This closeness decreases when the droplet size increases. The trajectories of the bigger droplets are not deviating much from their original flow and impact a large area on the leading-edge. The increase with the medium-sized droplets is seen in the figures 3.12 and 3.13. The effects of the large droplets are seen in figures 3.14 and 3.15. A big difference between the two solvers is that the numerical solution shows just one trajectory, thus one impact location. This does not show that the droplets will impact on a larger area if their size increases. The results from the software, however, do show the different trajectories from multiple droplets. This gives a more clear image of the impacting locations of droplets coming from a cloud onto the wing.

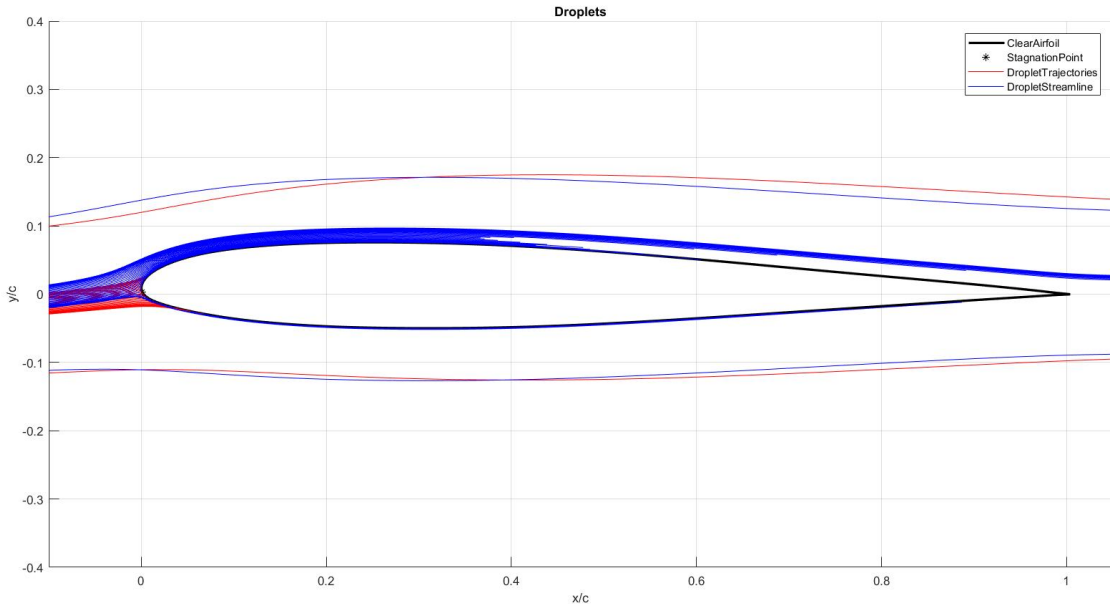


Figure 3.10: Droplet trajectories, diameter 50 micrometers

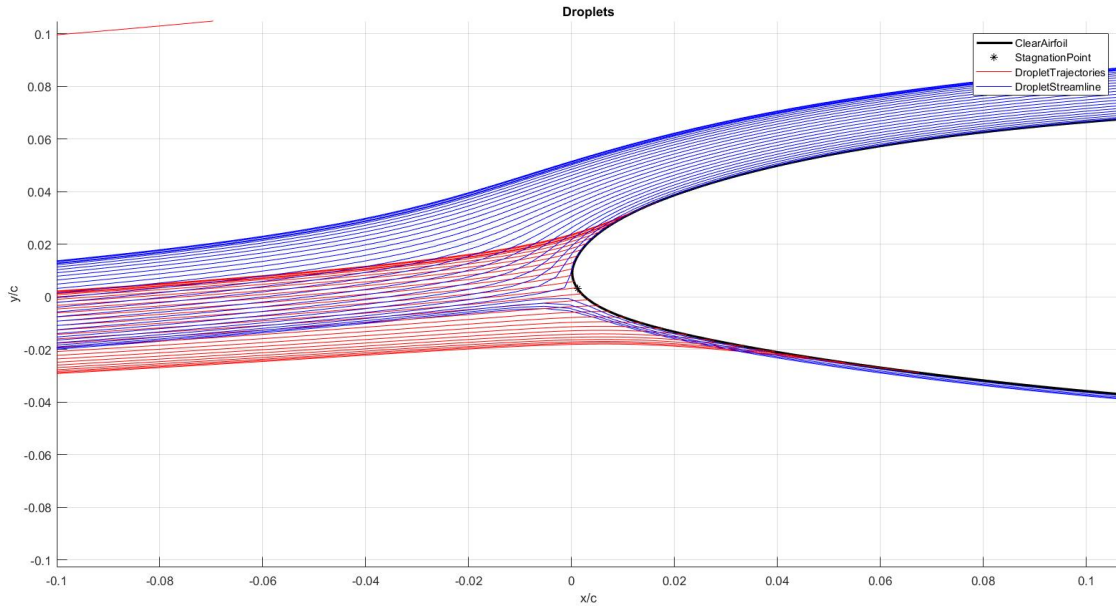


Figure 3.11: Close-up of the droplet trajectories, diameter 50 micrometers

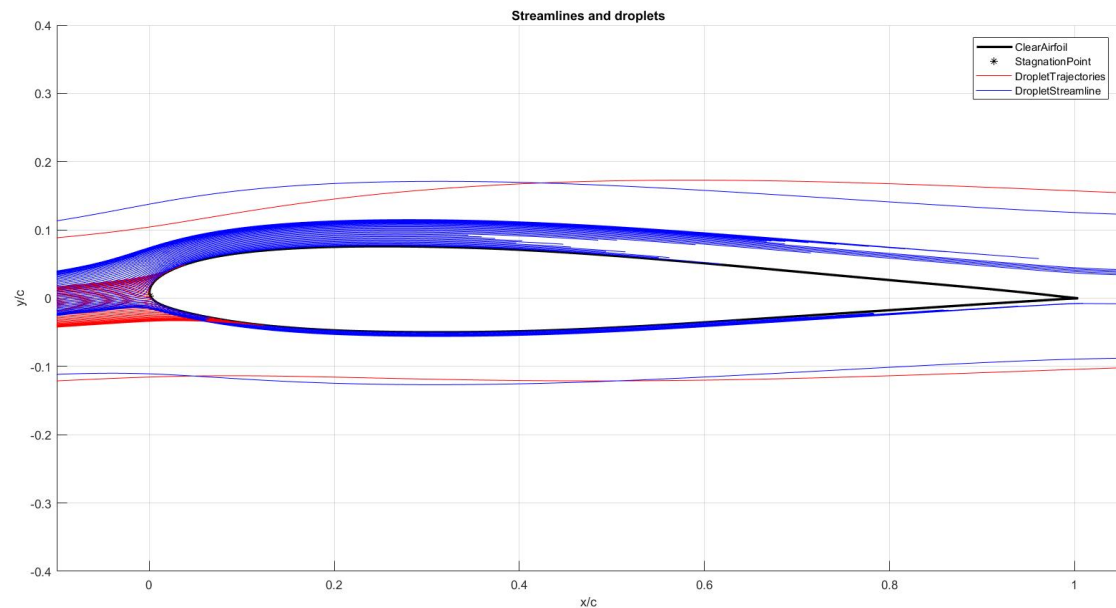


Figure 3.12: Droplet trajectories, diameter 100 micrometers

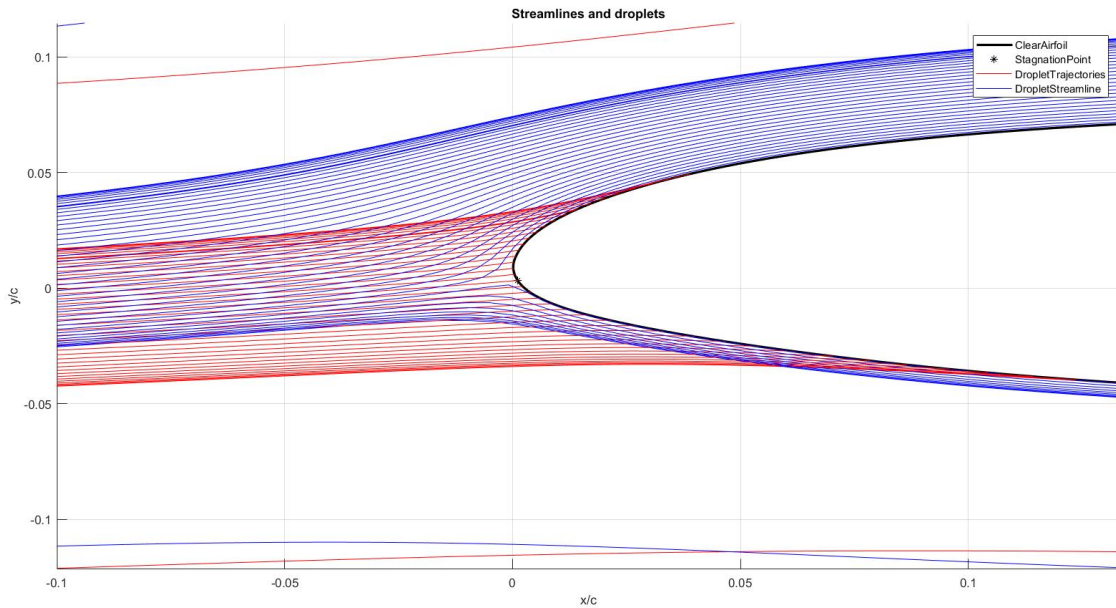


Figure 3.13: Close-up of the droplet trajectories, diameter 100 micrometers

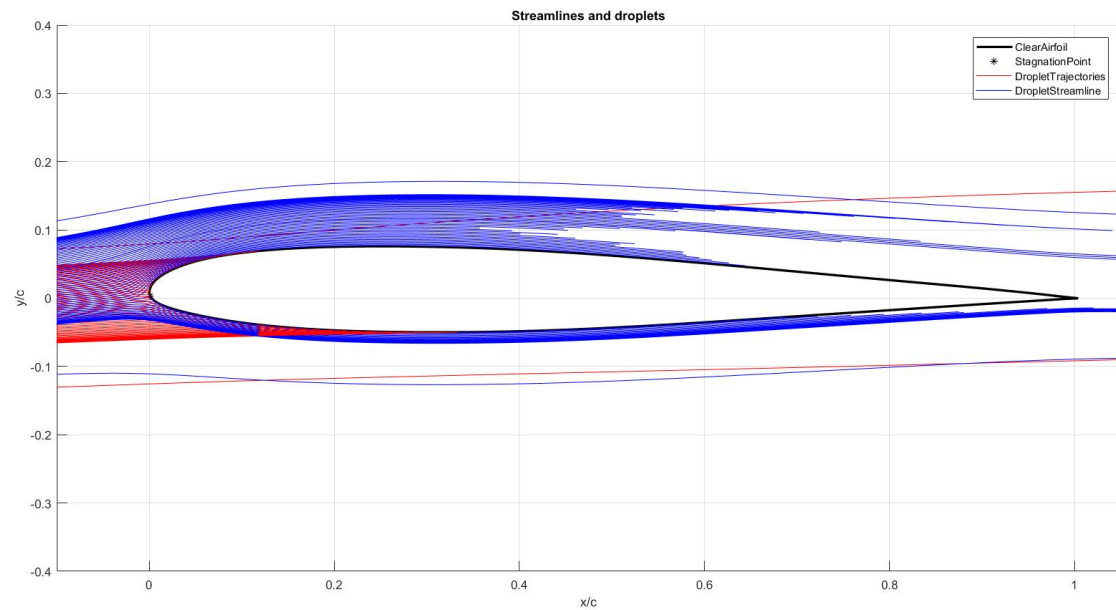


Figure 3.14: Droplet trajectories, diameter 500 micrometers

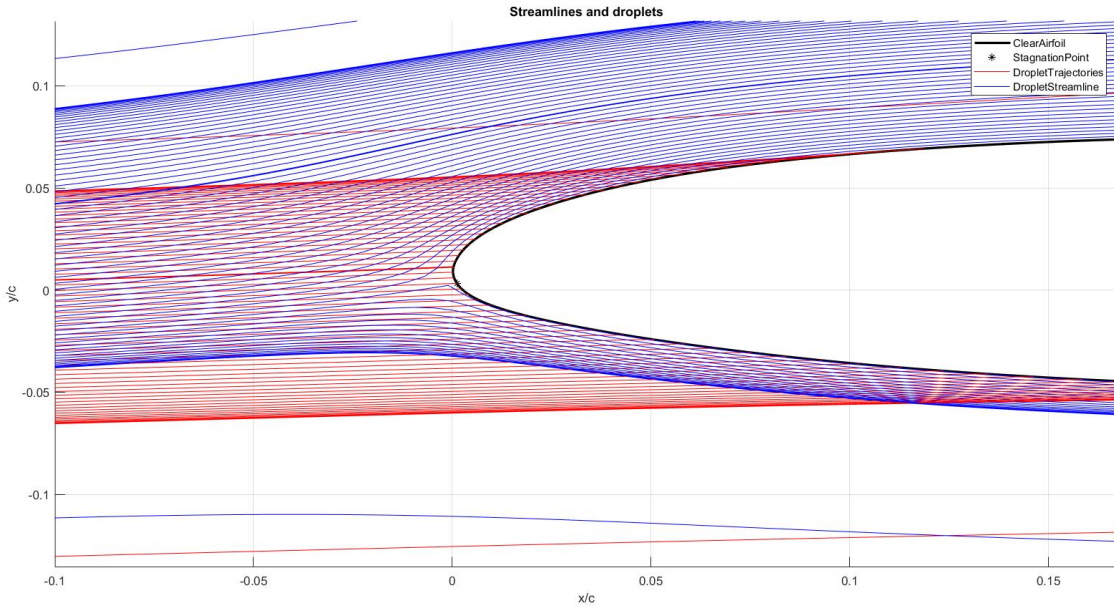


Figure 3.15: Close-up of the droplet trajectories, diameter 500 micrometers

3.3.3 Keeping the wing ice free using 2DFOIL-ICE

For calculating how to keep the wing ice free, the software 2DFOIL-ICE is used. The program has the option to add heating to the wing. Two options are possible: a constant heat flux or constant temperature. In the tests a constant temperature is chosen. The conditions of test 8 are chosen because those are the conditions with the thickest ice accretion so the worst case scenario. If the heat flux is enough to melt all the ice in this scenario the heat flux is enough to melt the ice in all scenarios.

2DFOIL-ICE has multiple anti ice systems to simulate, a constant heat flux, a constant temperature and clear the wing of ice. All were tested but the simulation to clear the ice from the wing is the most efficient simulation because it didn't keep the temperature or heat flux constant. A constant heat flux gives multiple temperatures but will cost too much energy because every part will be heated evenly. A constant temperature will give the whole area the same temperature to keep the ice off but this way will cost the most energy. Because the simulation that keeps all ice from the wing uses different temperatures and heat fluxes on different areas of the airfoil, the simulation will be more energy efficient and realistic. It will be more realistic because not all parts of the wing will need the same amount of energy.

The heating area of the simulation ($s - s_{stag}$) is the stagnation point to 0.2/c, on the top and 0.4 of the bottom because 0.2 on the top and 0.4 on the bottom of the airfoil is the most important part of the airfoil. 0.4 of the bottom is because the airfoil is under an angle of 2 degrees, the cruising angle of attack. From section 2.1.3 it can be seen that ice accretion mostly forms in the first 20% of the top and 40% of the bottom of the airfoil and if it's less the ice will cause the wing to stall and the plane to fall.

Test 8 was done again with the same parameters:

Altitude: 1000 [m]

Temperature: 263.15 [K]

Droplet diameter: 500 [μm](only at low altitudes, for freezing rain. Worst case scenario assumption)

LWC: 3 [$\frac{\text{g}}{\text{m}^3}$]

Pressure: 90 908 [Pa]

As a result the heat flux is shown in Figure 3.16

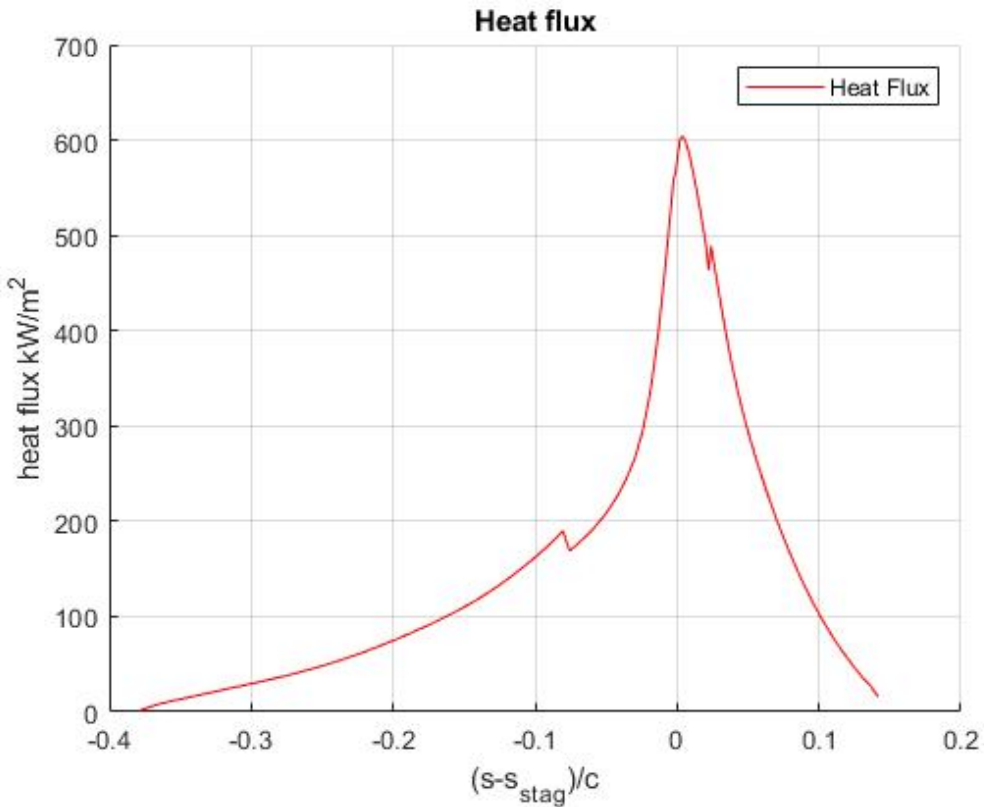


Figure 3.16: The heatflux against the distance from the stagnation point divided by the chord length

Amount of energy

To calculate the amount of energy first the area has to be integrated over the heating area ($s - s_{stag}$). So all the area under the curve: $q = 78 \frac{\text{kW}}{\text{m}^2}$. This is calculated with Matlab using the trapz function.

$$q = \frac{Q}{A} \quad (3.35)$$

$$A = s * c \quad (3.36)$$

q = area under the curve $[\frac{\text{kW}}{\text{m}^2}]$

Q = energy $[\text{kW}]$

A = area of the wing $[\text{m}^2]$

c = chord length $[\text{m}]$

s = length of the wing $[\text{m}]$

Using equation 3.35 and 3.36 the total energy can be calculated. The chord length is 3.6 m and the length of the wing is 13 m so the area of the wing is 46.8 m^2 . Using equation 3.35: $q * A = Q$ so $78 * 46.8 = 3650.4$

So the total energy usage is: 3650.4 kW

The temperature

Because the temperature is not constant and the temperature is needed in further calculations. The mean temperature is 349 K using the mean function in Matlab.

Chapter 4

Internal Flows and Heat exchange

4.1 Introduction

In this chapter various ways of supplying heat energy to prevent icing will be analysed. 4 different methods will be outlined and compared to see which method proves to be the most efficient. In section 3.3.3 the worst possible conditions for the entire wing was taken. However in this section, the atmospheric conditions and the heat needed to only break apart the ice (not completely melt it) are taken. Hence the data set from 2DFOIL-ICE of " $\dot{q}_{cond,droplet}$ " alone is taken instead of the total heat flux. This is done to obtain a more efficient anti-icing system by reducing the amount of "waste heat". Also only a section of the wing will be analysed here and not the entire wing (as was done in section 3.3.3) as the heating elements will only be placed near the leading edge of the airfoil.

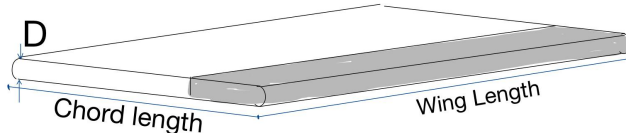


Figure 4.1: Representation of wing for a BOEING 737

To make the calculation possible some assumptions and remarks are presented:

- The wing is taken as a cylinder with flat top and bottom as in section 3.2.4, see Figure 4.1.
- The length of the wing (L_{wing}) is 13 m [34].
- The radius (0.36m) of the cylinder is 10% of the chord length, L_{chord} (3.6m).
- The atmospheric conditions are:

Droplet size [μm]	50
Pressure [kpa]	81 917
Airspeed [m/s]	86

Table 4.1: Atmospheric conditions during cruising

- The surface temperature on the wing is 50°C . This is the temperature found using the atmospheric conditions in Table 4.1 above using 2DFOIL-ICE-ICE
- The maximum amount of heat flux that needs to be transferred to the frozen droplets is $\dot{q} = 6.8 \text{ kW/m}^2$ as seen in Figure 4.2, which is calculated with the software 2DFOIL-ICE as the heat flux conducted to the droplets to break them apart. The total area in which this heat flux acts is 26.07 m^2 , calculated using the Figure 4.1 as reference. Then the total amount of heat to keep the wing free of ice is $\dot{Q}_{total} = 177.2 \text{ kW}$.

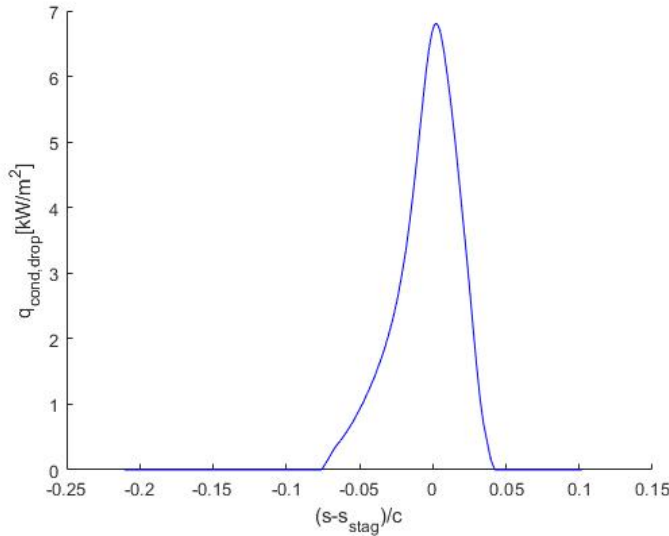


Figure 4.2: Heat flux to frozen droplets.

- In Figure 4.1, the grey part represents where the anti-icing system works on, this is from the leading edge to 20% of the chord (0.72 m), which is where accretion happens the most as can be seen in Figure 3.14.

4.2 Electric Heating Mats

In this method, electric heating mats will be placed along the leading edge of the wing. The heating mats will be located on the inner side of the airfoil. These heating mats are most commonly made of composite materials. The contribution of the heating mats will be assessed over the wing wall thickness and along the wing (in chord wise direction).

4.2.1 Over Wing Wall Thickness

Since we are only interested in the temperature difference over the wing wall thickness, only the y -direction is to be considered. It can be assumed that the 3 layers shown in Figure 4.3 can be considered as plane wall layers. The wing wall is assumed to be made of aluminium ($k_{al} = 205 \text{ W/mK}$). \dot{Q}_1 is the heat transferred by conduction from the surface of the heating mat to the outer surface of the wing wall. \dot{Q}_2 is the heat transferred from the wing wall to the ice layer. \dot{Q}_2 was taken from Figure 4.2 and has a value of 177.2 kW. Due to energy conservation, all the heat produced by the heating

mats is transferred to the ice. Hence, $\dot{Q}_1 = \dot{Q}_2$. The temperature T_{wing} is the temperature at the outer surface of the wing wall and was also found from 2DFOIL-ICE.

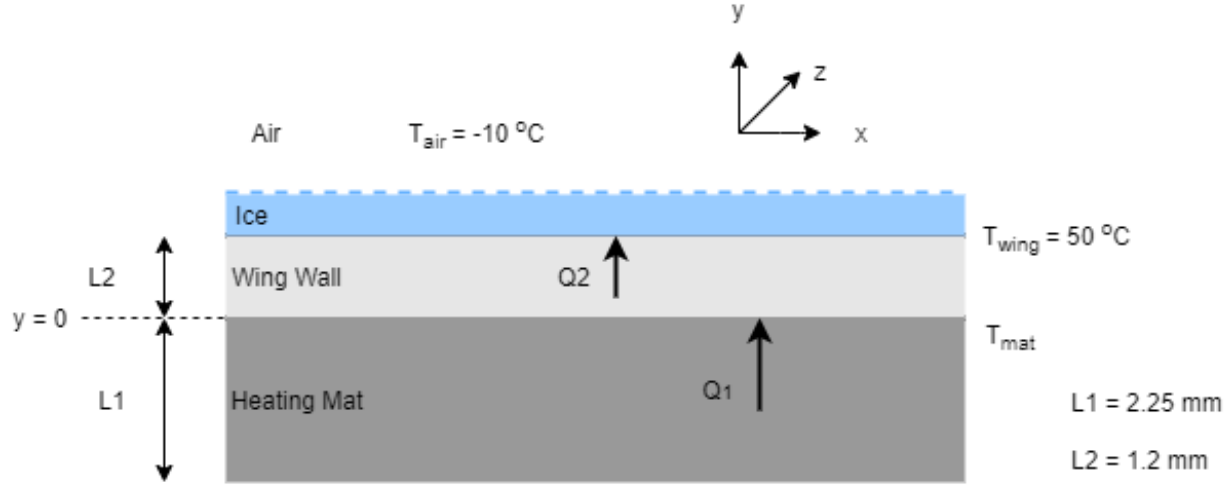


Figure 4.3: Overview of plane wall layers showing the location of the electric heating mats

We are interested in T_{mat} and therefore need to look at the heat transfer of \dot{Q}_1 . Since only conduction takes place here, the general heat diffusion equation for a rectangular coordinate system can be used and is stated in equation (4.1) below:

$$\frac{\partial}{\partial x} \left(k \frac{\partial T}{\partial x} \right) + \frac{\partial}{\partial y} \left(k \frac{\partial T}{\partial y} \right) + \frac{\partial}{\partial z} \left(k \frac{\partial T}{\partial z} \right) + \dot{e}_{gen} = \rho c \frac{\partial T}{\partial t} \quad (4.1)$$

A few assumptions are formed to simplify this equation:

- Steady state, meaning the temperature doesn't change over time: $\frac{\partial T}{\partial t} = 0$
- 1D, as only the y-direction is considered: $\frac{\partial T}{\partial x} = 0$ and $\frac{\partial T}{\partial z} = 0$
- No heat generation: $\dot{e}_{gen} = 0$

The simplified equation is shown below and can be solved for $T(y)$ (temperature distribution in y-direction) using the boundary conditions stated:

$$\frac{\partial}{\partial y} \left(k \frac{\partial T}{\partial y} \right) = 0 \quad (4.2)$$

$$BC_1: T(y = L_2) = T_{wing} = 50 \text{ } ^\circ\text{C}$$

$$BC_2: -k_{al}A \frac{\partial T(0)}{\partial y} = \dot{Q}_1 = 177.2 \text{ kW}$$

Solving this differential equation yields:

$$T(y) = -\frac{\dot{Q}_1}{k_{al}A}y + \frac{\dot{Q}_1}{k_{al}A}L_2 + T_{wing} \quad (4.3)$$

A is the area across which this heat transfer occurs and can be calculated using the equation below:

$$A = L_{wing} \cdot L_{chord} = 46.8 \text{ m}^2 \quad (4.4)$$

Substituting the values of \dot{Q} , k_{al} , A, L_2 and T_{wing} into equation (4.3) gives the expression below for the temperature distribution along the wing wall in the y-direction

$$T(y) = -109y + 50.13 \quad (4.5)$$

T_{mat} occurs at $y = 0$ m. Substituting this into equation (4.5) gives us the value for T_{mat}

$$T_{mat} = T(y = 0) = 50.13^\circ\text{C} \quad (4.6)$$

Hence the temperature difference between the inner and outer surface of the wing wall is as follows:

$$\Delta T = 50.13 - 50 = 0.13^\circ\text{C} \quad (4.7)$$

Since the ΔT is very small, it can be concluded that the wing wall has a negligible effect on the temperature required by the heating mats. In other words, the presence of the wing wall can be completely omitted in this situation without any significant consequence.

4.2.2 Along The Wing

The electric heating mats are only present near the leading edge of the airfoil. However, heat transfer still occurs along the wing to the tail region of the airfoil. Hence, in this case the x-direction alone will be studied. Since the airfoil is hollow, convective heat transfer occurs along with conduction. As a result, the heat transfer along the wing can be assumed to be like the heat transfer along a fin. The base of the fin would in this case be the heating mats. Figure 4.4 shows how the airfoil is represented as a rectangular fin.

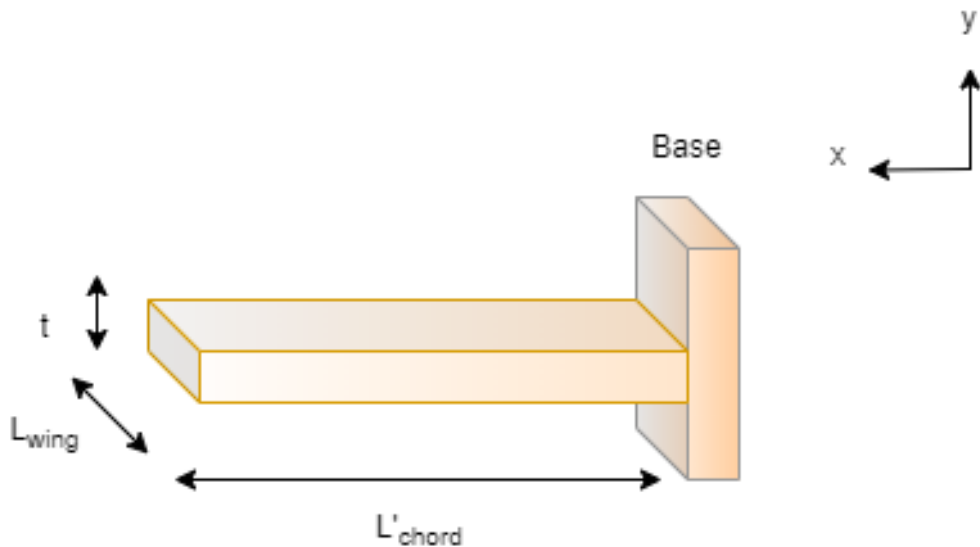


Figure 4.4: Simplification of airfoil along the wing as a rectangular fin

The values of L_{chord}' and t are determined from the geometry of the simplified wing referring to Figure 4.1. The value of h was obtained from section 2.2.3. T_b equals to T_{mat} from section 4.2.1. The values are listed below in Table 4.2.

Variable	Value
L_{chord}'	2.88 m
t	0.72 m
h	205 W/m K
T_b	50.13 °C
T_∞	-10 °C

Table 4.2: Values for fin

First the value of m is calculated using the equation below for a rectangular fin:

$$m = \sqrt{\frac{2h}{k_{alt}}} = 1.52 \quad (4.8)$$

It is assumed that convection does occur at the tip or in other words the tip is not adiabatic. Hence, there is no need to use corrected length (L_c) here. The temperature distribution along the fin for such a case is described by the equation below:

$$\frac{T(x) - T_\infty}{T_b - T_\infty} = \frac{\cosh m(L - x) + (h/mk)\sinh m(L - x)}{\cosh mL + (h/mk)\sinh mL} \quad (4.9)$$

The equation (4.9) can be rearranged to make $T(x)$ the subject. To determine the temperature at the end of the fin (the tail edge of the airfoil), the value of $x = L_{chord}'$ is taken:

$$T(L) = \frac{\cosh m(L'_{chord} - L'_{chord}) + (h/mk)\sinh m(L'_{chord} - L'_{chord})}{\cosh mL'_{chord} + (h/mk)\sinh mL'_{chord}} \cdot (T_b - T_\infty) + T_\infty = -9.02^\circ C \quad (4.10)$$

Hence the temperature difference along the wing is as follows:

$$\Delta T = 50.13 - (-9.02) = 59.15^\circ C \quad (4.11)$$

The ΔT is a reasonable value and the temperature at the end tail edge also lines up with the surrounding air temperature (-10 °C).

4.2.3 Conclusion

In conclusion, the values of ΔT for over the wing wall and along the wing are both reasonable and realistic values. However the power needed to run these heating mats is quite large. An aircraft the size of the Boeing 737 MAX would have about 8 heating mats present [35]. Each heating mat requires about 200kW of power [35]. Hence, a total of 1600kW is needed to power these heating mats.

4.3 Heating through radiation and free convection

4.3.1 Radiation

In this section an analysis is carried out to verify if it is possible or how efficient it is to heat the outer surface of the wing by means of radiation only. The wing is seen as a cylinder of length ($L_{wing} = 13m$) made of carbon and diameter $D_2 = 0.36m$ which is 10% of the chord length of the airfoil for the Boeing

737 (3.6m). In the other hand, the heated object is seen as another cylinder of similar length which should be inside the wing, it is assumed to be made of aluminum alloy with diameter D_1 , see Figure 4.5.

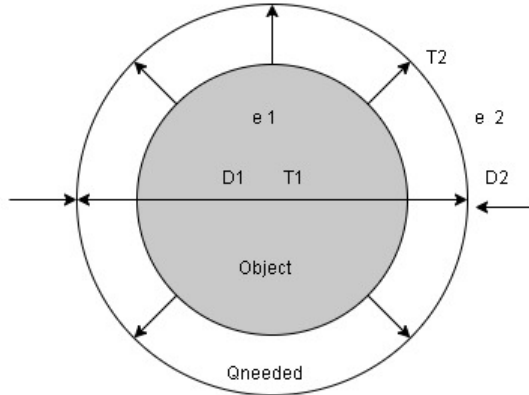


Figure 4.5: Radiation between cylinders

In the introduction of this chapter the amount of energy needed to keep the temperature of the wing at 50 was calculated to be 177.27W. Therefore, the goal is to verify if it is possible to find the right diameter D_1 for the heating object to be placed inside of the carbon wing.

The known variables are:

- Temperature of heated object is the maximum working temperature of the aluminum alloy: 608 K [?].
- Maximum emissivity of Aluminum alloy (ϵ_1): 0.80 [36]
- Emissivity of carbon(ϵ_2): 0.81 [37].
- It is assumed the temperature through the wing is the same.

The equation of heat transfer by radiation between two cylinders is shown in equation (4.12) [38]:

$$\dot{Q} = \frac{\sigma(T_1^4 - T_2^4)}{\frac{1}{\epsilon_1} + \frac{A_1}{A_2}(\frac{1}{\epsilon_2} - 1)} \quad (4.12)$$

Where σ is the Stephan-Boltzmann constant $5.67 \cdot 10^8$, A_1 is the area of the heated object and A_2 the area of the wing, in the same way with temperature $T(1$ and $2)$, and the emissivity ϵ (1 and 2). This can be seen in Figure 4.5.

The equation (4.12) is rewritten to find A_1 :

$$A_1 = \frac{\epsilon_2 A_2 \dot{Q}}{-(\epsilon_2 - 1)\dot{Q} + \sigma \epsilon_1 \epsilon_2 A_2 (T_1^4 - T_2^4)} \quad (4.13)$$

Where $A_1 = \pi D_1 \cdot L_{wing}$ and $A_2 = \pi D_2 L_{wing}$, giving the equation for the diameter of the heated object to be determined with the equation (4.14):

$$D1 = \frac{\frac{\epsilon_2 A_2 \dot{Q}}{\pi L_{wing}}}{-(\epsilon_2 - 1)\dot{Q} + \sigma \epsilon_1 \epsilon_2 A_2 (T_1^4 - T_2^4)} \quad (4.14)$$

The values for each of the known variables in equation (4.14) are listed in the table below:

Variable	Symbol	Value
Power input	\dot{Q}	177.27kW
Emissivity alum	ϵ_1	0.8
Emissivity carbon	ϵ_2	0.81
Chord BOEING737	D_2	3.6 m
Boltzmann Con.	σ	$5.67 \cdot 10^8$
Wing Length	L_{wing}	13m[34]
T°object	T_1	608 °K
T°wing	T_2	323°K

Table 4.3: Variables for equation 4.14

After replacing the variables into equation (4.14), D_1 can be found to be $0.511m$, which is bigger than the diameter of the wing itself by $15cm$, for that reason it is concluded that: heating the wing surface through radiation only is not possible. However, for the sake of completion one way to improve heat transfer between the hot object and the wing by radiation is: to find material with as high emissivity factor as possible ($= 1$) and to choose a material with a higher working temperature(around $650K$), given these conditions the diameter changes to $D_1 = 0.35m$, which can be fitted inside the wing. However bodies with high emissivity are usually made of material that can not work at high temperatures or are too heavy to be used in this operations [37].

4.3.2 Free convection

In this section an analysis is carried to verify if it is possible to heat the outer surface of the wing by means of free convection only. The situation is similar in to the previous section 4.3.1, where two horizontal cylinders of diameter D_1 and D_2 are taken to represent the wing and the hot object respectively, see Figure 4.5. Subsequently, the hot object and wing surface are not directly in contact but rather there is a layer of air in between, the thickness of this layer is assumed to 5 cm meaning that the hot object has a diameter D_1 of $0.31m$.

Furthermore, it is assumed that: heat transfer is stable,, radiation heat transfer is neglected, the air in between the cylinder is an ideal gas. With this condition, natural convection per unit length between two cylinders is described by the equation (4.15) [38]:

$$\dot{Q}_{convection} = \frac{2 \cdot \pi \cdot k_{eff}}{\ln \frac{D_2}{D_1}} \cdot (T_1 - T_2) \quad (4.15)$$

where k_{eff} is the effective thermal conductivity determined by[38] :

$$k_{eff} = k_{air} \cdot 0.386 \left(\frac{Pr}{0.861 + Pr} \right)^{0.25} \cdot (F_{cyl} \cdot Ra_l)^{0.25} \quad (4.16)$$

F_{cyl} is the geometry factor for cylinders times the Rayleigh number (Ra_L) :

$$F_{cyl} \cdot Ra_L = \frac{\ln\left(\frac{D_2}{D_1}\right)^4}{L_c^3 \cdot (D_1^{-\frac{3}{5}} + D_2^{-\frac{3}{5}})^5} \cdot \frac{g \cdot \beta \cdot (T_1 - T_2) \cdot L_c}{\nu^2} \cdot Pr \quad (4.17)$$

k_{eff} is applicable for $0.70 \leq Pr \leq 6000$ and $10^2 \leq F_{cyl} \cdot Ra_L < 10^7$.

Variable	Symbol	Value
T° object	T_1	543 K
T° wing	T_2	323 K
Laminar Temp.	T_{lam}	436.5K
Thermal cond. air	k_{air}	0.04104 W/m
Prandtl Num.	Pr	0.7014
Thermal coduc.	k	0.03511 W/mK
Kinematic Viscos.	ν	$2.975 \times 10^{-5} \text{ m}^2/\text{s}$
Characteristic length	L_c	50mm
Gravity	g	9.8 m/s^2
$\beta = T_{lam}^{-1}$		539^{-1} K^{-1}

Table 4.4: Variables for equation 4.17

The values for equations 4.15, 4.16 and 4.17 are listed in Tables 4.3 and 4.4. Where the laminar temperature is the average between the wing and the hot object, the characteristic length is half of the distance between cylinders. Finally, after replacing the variables in equations 4.15, 4.16 and 4.17 accordingly, the values found are listed below in Table 4.5.

Variable	Value
$F_{cyl} \cdot Ra_l$	12
$k_{eff} [\text{W/m}]$	0.07594
$\dot{Q} [W]$	9258.7
$\dot{Q}_{needed} [kW]$	177.27
efficiency	0.052

Table 4.5: Free convection results

As can be seen in Table 4.5 the efficiency is very low. In order to improve the heat transfer it could be possible to increase the increase the temperature and reduce the space in between the cylinders, however after taking unrealistic temperature of 3500 K and a space of 1cm, the efficiency is calculated to be 1.05 . This gives the conclusion that heating the wing of an aircraft using free convection is not beneficial.

4.4 Forced convection

In this section forced convection is studied through a pipe at the leading edge of the wing, with a diameter of $D=0.36\text{m}$ and length $L=13\text{m}$, see figure 4.6.

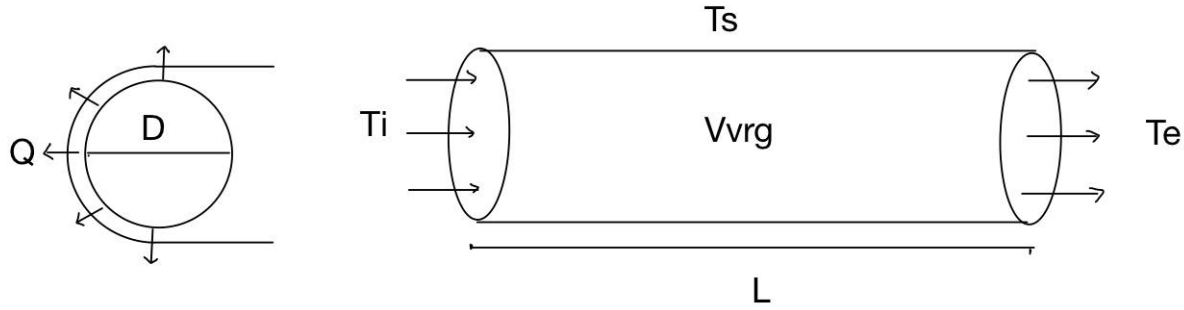


Figure 4.6: Pipe along at the leading edge

Bleed air from the exhaust engine at temperature of 200 °C and initial pressure of 275 kPa are used to keep the surface at a temperature of 50°C. Also, the heat required to keep that surface temperature is 177.27 kW which was calculated from 2DFOIL-ICE and explained in the introduction of this chapter 4.1.

In order to calculate the average speed of the fluid T_{vrg} , it is assumed that the bleed high pressure air enters the pipe which is at atmospheric pressure meaning at 85kPa (1500m above sea level) undergoes a pressure drop $\Delta P = 275kPa - 101kPa = 174kPa$, from here Bernoulli's equation is used in equation (4.18):

$$\frac{\rho \cdot v^2}{2} + \rho \cdot g \cdot h + P = \text{constant} \quad (4.18)$$

can be rearranged to find V_{vrg} :

$$V_{vrg} = \sqrt{\Delta P \cdot \frac{2}{\rho}} = 713 \text{ m/s.} \quad (4.19)$$

With the density $\rho = 0.7459 \text{ kg/m}^3$ taken at the altitude of 1500 m.

The next step is to determine the Reynolds number(Re), for which the properties of the fluid (air) is taken at the bulk temperature $T_b = \frac{528+50}{2} = 289^\circ\text{C}$ and 1 atm: Specific heat $C_p = 1044 \text{ J/kg}$, density $\rho = 0.6158$, thermal conductivity $k=0.04418 \text{ W/m}\cdot\text{K}$, Kinematic viscosity $\nu = 4.765e-5 \text{ m}^2/\text{s}$, Prandtl number $\text{Pr}=0.6935$

Then:

$$Re = \frac{V_{vrg} \cdot D}{\nu} = 5,4 \cdot 10^6 \quad (4.20)$$

As $Re > 1000$ the flow is considered turbulent [38].The hydrodynamic (Lh) and thermal (Lt) entry lengths can be calculated:

$$Lh = Lt = 10D = 10 \cdot 0.36 \text{ m} = 3.6 \quad (4.21)$$

The flow then is assumed to be fully developed, since the entry length is relatively small to the length of the pipe. Therefor Petukhov equation [38] 4.23 is used to calculate the Nussel number:

$$f = 0.184 Re^{-0.2} \quad (4.22)$$

f is the friction factor for smooth surfaces.

$$Nu = \frac{(f/8)(Re - 1000)Pr}{1 + 12.7(f/8)^{0.5}(Pr^{2/3} - 1)} = 3.98 \cdot 10^3 \quad (4.23)$$

From here the heat transfer coefficient of the fluid through the pipe is calculated from:

$$h = \frac{k \cdot Nu}{D} = 488.75 W/m^2 \quad (4.24)$$

The mass flow rate \dot{m} can be calculated given the cross sectional $Ac = \pi(D/2)^2$:

$$\dot{m} = Ac \cdot V_{vrg} \cdot \rho = 54,2 kg/s \quad (4.25)$$

Then the exit temperature can be calculated with [38] :

$$Te = Ts - (Ts - Ti) \exp \frac{-hAs}{\dot{m}C_p} = 496^\circ C. \quad (4.26)$$

In the same way the log mean temperature difference ΔT_{lm} can be calculated:

$$\Delta T_m = \frac{Ti - Te}{\ln(\frac{Ts - Te}{Ts - Ti})} = -461^\circ C \quad (4.27)$$

Assuming that heat is transferred to just one half of the cylinder "the half that is in contact with the leading edge", as seen in figure 4.6, then the surface area for heat convection is:

$$As = 0.5\pi DL = 7.3 m^2 \quad (4.28)$$

With the area of transfer heat through convection (equation 4.28), the change in temperature(equation 4.27) and the heat transfer coefficient(equation 4.24); the total heat that the pipe can give is then:

$$\dot{Q} = hAs|\Delta T_m| = 1657 kW \quad (4.29)$$

then the efficiency is calculated to be; the heat needed which was calculated with the software 2DFOIL-ICE Q_{needed} (presented in the introduction 4.1 of this chapter) over the heat calculated from the pipe:

$$n = \frac{\dot{Q}_{needed}}{\dot{Q}_{pipe}} = 9.34 \quad (4.30)$$

The efficiency for forced convection with the current situation is 800% more than is needed, meaning that the heating loss is highly not beneficial. Also, the mass flow needed is considerably greater to the impinging jets in section 4.5. The solution to heat and so the efficiency to a most beneficial values is: to decrease the diameter as much as possible. After some iteration the diameter is found to be $0.037m$ to be and efficiency of 1.012. However the diameter is so small that the heat would be concentrated in a small section of the wing, this could be improved by adding more pipes but it would mean to increase the efficiency again above 1.

4.5 Impinging Jets

In this section, the use impinging jets to provide the heat flux required for the anti-icing process will be investigated. Impinging jets work on the principle of convective heat transfer. A fluid is passed through a tube, exits via a nozzle and hits a desired surface. Depending on the temperature of the fluid used in the situation, impinging jets can be used to either cool down or heat up the surface they hit. In other words, if fluid is used that is hotter than the surface temperature, they will heat up the surface. The basic working principle of an impinging jet is shown below in Figure 4.7.

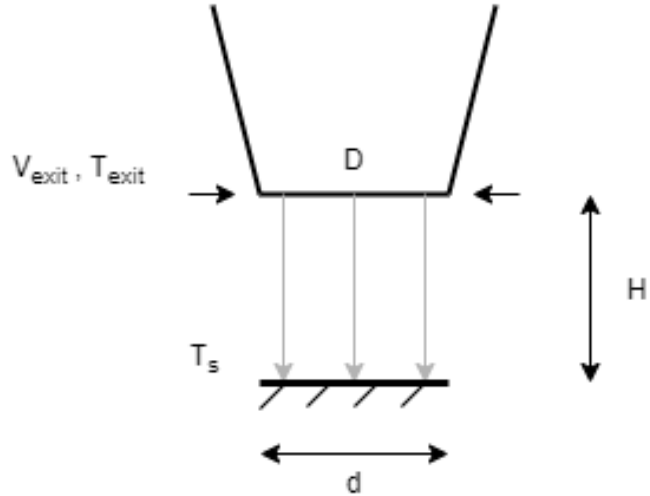


Figure 4.7: Simple representation of impinging jet for a circular nozzle

In Figure 4.7 above:

- H is the difference in height between nozzle tip and surface [m]
- D is the diameter of nozzle [m]
- d is the diameter of impinged area [m]
- V_{exit} is the exit velocity of fluid [m/s]
- T_{exit} is the exit temperature of fluid [$^{\circ}\text{C}$]
- T_s is the temperature of impinged surface [$^{\circ}\text{C}$]

To apply these impinging jets inside an airplane wing, a little more complex setup is required. This setup can be seen in Figure 4.8 [39]. In the case of an aircraft, the fluid for the impinging jets will be the bleed air from the compressor. This bleed air (normally at a temperature of 400 - 800 K) is transported to the inside of the wing, where it exits out of the nozzles of a piccolo tube. A piccolo tube (refer to Figure 5.2 [40]) is a tube with multiple circular nozzles that is used to direct the bleed air onto the leading edge of the airfoil. The piccolo tube is indicated by (1). The hot air is released into the front-bay (2) and heats up the leading edge from the inside. The hot air then rises up and passes through the slot (3) into the rear bay (4). From there it exits the airfoil through the exhaust holes (5).

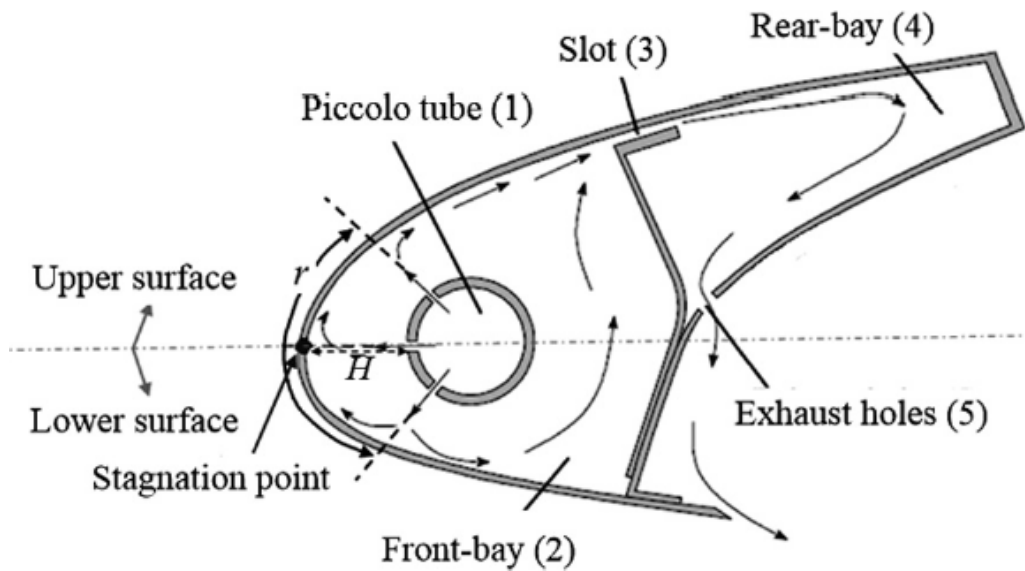


Figure 4.8: Side view of the inside of an airfoil with the impinging jet mechanism

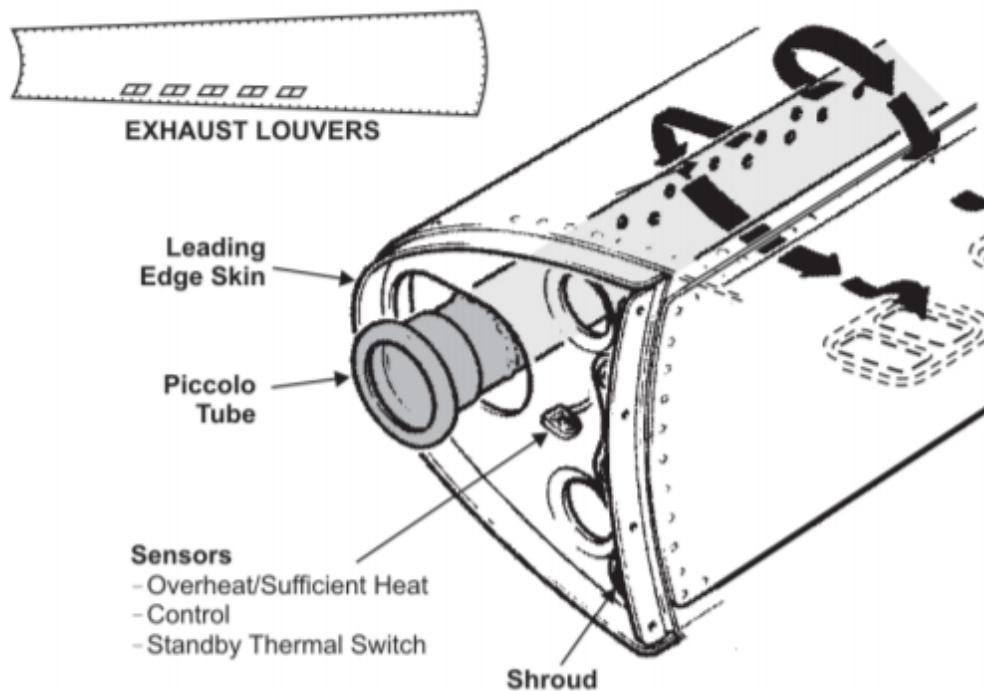


Figure 4.9: Closeup to show piccolo tube

Some of the variables such as H, D, d and V_{exit} have to be set. They were taken from a report [39] which had experiments very similar to what is being analyzed in this section. T_{exit} was taken from the project description and T_s was found in 2DFOIL-ICE. The values are shown in Table 4.7 below. The value of d was found by setting the jet impingement angle (α) to 40 °.

Variable	Value
H	24 mm
D	3.5 mm
d	20 mm
V_{exit}	550 m/s
T_{exit}	526 °C
T_s	50 °C

Table 4.6: Values of variables to be set

For now the mass flow in a single nozzle of the piccolo tube will be considered. First, the Nutseel number needs to be calculated. The formula below is specific for the geometry of a single circular nozzle [41]:

$$\bar{Nu} = Pr^{0.42} G \left[2Re^{1/2} (1 + 0.005Re^{0.55})^{1/2} \right] \quad (4.31)$$

where,

$$G = 2A_r^{1/2} \frac{1 - 2.2A_r^{1/2}}{1 + 0.2(H/D - 6) A_r^{1/2}} \quad (4.32)$$

$$A_r = \frac{D^2}{4(d/2)^2} \quad (4.33)$$

A_r is to be determined using equation (4.33). The value of A_r can then be substituted into equation (4.32) to find a value for G.

Next, the Re has to be calculated. Before this can be done, the film temperature (T_f) has to be determined. The T_f will be used to check the tables for the fluid properties.

$$T_f = \frac{T_{exit} + T_s}{2} = \frac{526 + 50}{2} = 288^\circ C \quad (4.34)$$

Using the T_f , values for ν , Pr and k were found. The values are shown in the table below

Variable	Value
ν	$4.765 \times 10^{-5} m^2/s$
Pr	0.6935
k	0.04418 W/m K
c_P	1044 J/kg K

Table 4.7: Values for properties of air at 1 atm

Now the Re can be determined using the equation below:

$$Re = \frac{V_{exit}D}{\nu} = 40,400 \quad (4.35)$$

Filling in Pr, G and Re into equation (4.31) gives \bar{Nu} :

$$\bar{Nu} = 117.9 \quad (4.36)$$

With this, the heat transfer coefficient (\bar{h}) can be calculated using equation below:

$$\bar{h} = \frac{k\bar{Nu}}{D} = 1490W/mK \quad (4.37)$$

From here, \bar{h} can be used to calculate the heat flux (\dot{Q}) using the equation below:

$$\dot{Q} = \bar{h}A_{impinged}(T_{exit} - T_s) = 0.2225kW \quad (4.38)$$

Finally the mass flow (\dot{m}) through a single nozzle can be determined using the equation below:

$$\dot{m} = \frac{\dot{Q}}{c_P(T_{exit} - T_s)} = 4.477 \cdot 10^{-4}kg/s \quad (4.39)$$

The number of nozzles (n) was set to 800. Hence the total mass flow and \dot{Q}_{total} can be determined and are shown below:

$$\dot{m}_{total} = n \cdot \dot{m} = 0.3582kg/s \quad (4.40)$$

$$\dot{Q}_{total} = n \cdot \dot{Q} = 178kW \quad (4.41)$$

Looking through and comparing the values, it can be seen that \dot{m}_{total} is a very feasible value and \dot{Q}_{total} also matches the \dot{Q} required for anti-icing. Hence, the impinging jet method is a feasible method to be considered for the final design of the anti-icing system.

4.6 Conclusion

After analyzing the multiple methods to achieve the heat required for anti-icing, one of the system needs to be chosen for the final design. Radiation was deemed as not feasible as the diameter of the cylinder required exceeded the dimensions of the airfoil. Free convection was not opted for as it was not able to produce the required amount of heat. Forced convection was also not suitable as finding the balance to obtain just the right amount of heat was problematic. The electric heating mats proved to be a good solution but required a lot of external power to be supplied. Hence the impinging jets method was chosen as it was able to produce the heat required within a very reasonable mass flow. It also makes use of bleed air from the compressor which further improves the efficiency of the compressor.

Chapter 5

Design of An Anti-icing System

5.1 Temperature difference along the wing

The temperature difference is visible by using the the Partial Differential Equation(PDE).This is a MatLab tool box which can solve differential equations using finite elements method by dividing the wall of the wing into small triangles and by calculating the temperature of each segment. Only the front of the wing is considered because heat is only added at the front of the wing.

The wing has a wall thickness of 2 mm, considering a outer temperature of 0°C. The figure ?? shows that the maximum temperature difference is in the stagnation point and decreases when moving away from this point.

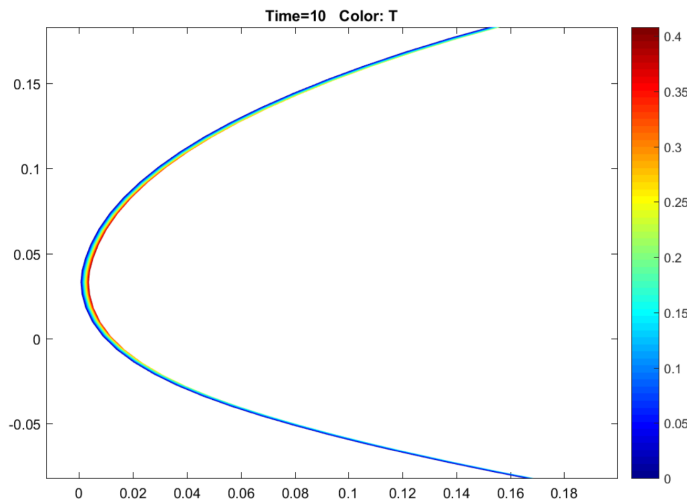


Figure 5.1: Temperature distribution

5.2 Choice of Anti-icing - Impinging Jets

In section 4, multiple anti-icing method were looked into. After evaluating each of the methods, the impinging jets solution came out on top. In this section, the system of the impinging jets will be optimized to achieve the most efficient results possible.

The optimization will be done by analyzing the optimal layout of the nozzles on the piccolo tube. This is done by finding the optimal (H/D) value in the x and y-direction related to Figure 4.7. Figure 5.2 shows the coordinate system that will be used for this section. With respect to the airfoil, the x-direction is along the chord length and the y-direction is along the leading edge. This is shown in Figure 5.3.

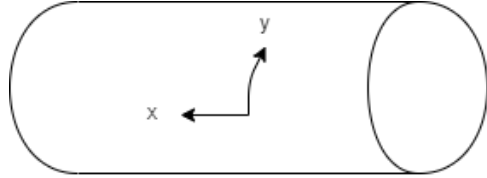


Figure 5.2: Coordinate system on the piccolo tube

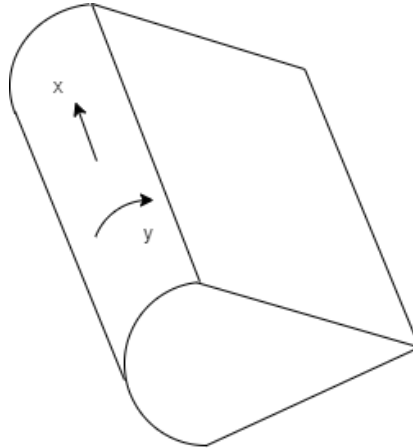


Figure 5.3: Coordinate system on the airfoil

5.2.1 Nusselt Number For Impinging Jets

The Nusselt number of the jets (Nu_{jet}) is the Nu values that an impinging jet can provide. The Nu_{jet} can be plotted as a function of the distance from the stagnation point (R) over the diameter of the nozzle (D). The R can either be in the x or y-direction. This Nusselt number can only be found from experiments. Figure 5.4 shows the experimental data determined in [39]. Out of the 3 values for (H/D) plotted in Figure 5.4, the (H/D) value of 6.63 was chosen as it was the most feasible to be used within the dimensions of the airfoil. The y-axis is ξ_x and it is the percentage of the $Nu_{jet}/Nu_{jet,max}$. The $Nu_{jet,max}$ in this case is the Nu_{jet} at the stagnation point, which was calculated above in section 4.5 to be 117.9. Hence by multiplying all the data points by $Nu_{jet,max}/100$, the data set for Nu_{jet} is obtained. Equation (5.1) below shows this conversion.

$$Nu_{jet} = \frac{Nu_{jet,max}}{100} \cdot \xi_x \quad (5.1)$$

Figure 5.5 shows the graph obtained from Figure 5.4. The data set for (H/d) = 6.63 was exactly copied and re-plotted using the 'polyfit' function on Matlab.

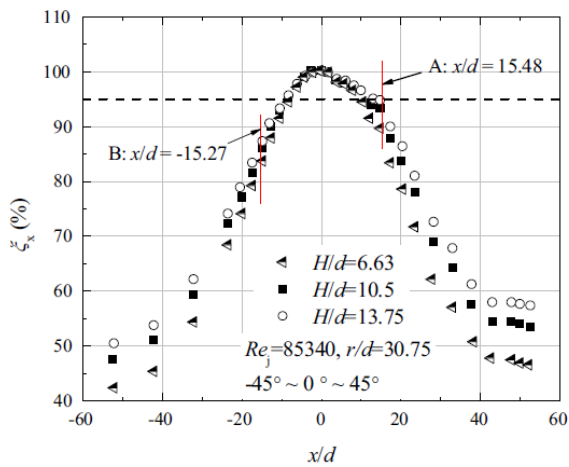


Figure 5.4: Data from experiment

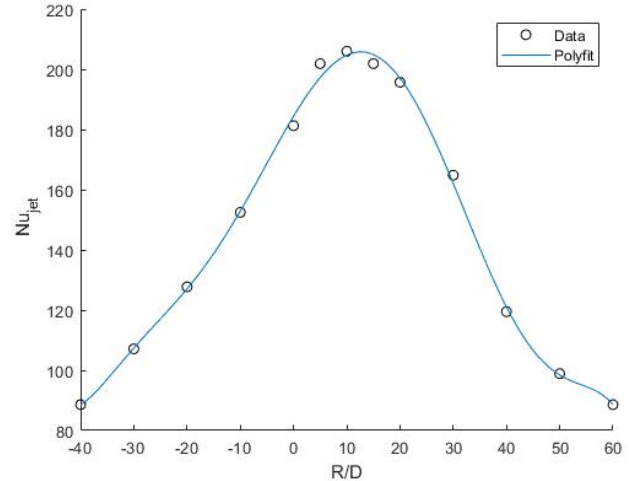


Figure 5.5: Data re-plotted using polyfit

5.2.2 Optimization along y-direction

The plot for Nu_{jet} can be determined from the experimental data in section 5.2.1. What is also needed is the Nu values along the leading edge (Nu_{req}) to achieve the \dot{Q} required to melt the ice. To obtain this, first the distribution of the heat transfer coefficient (h_{req}) is needed. The h_{req} is obtained from 2DFOILICE-ICE and is plotted in Figure 5.6 below, with heat flux in the y-axis and the distance from the distance from stagnation point to any point along the chord on the surface of the wing in the x-axis.

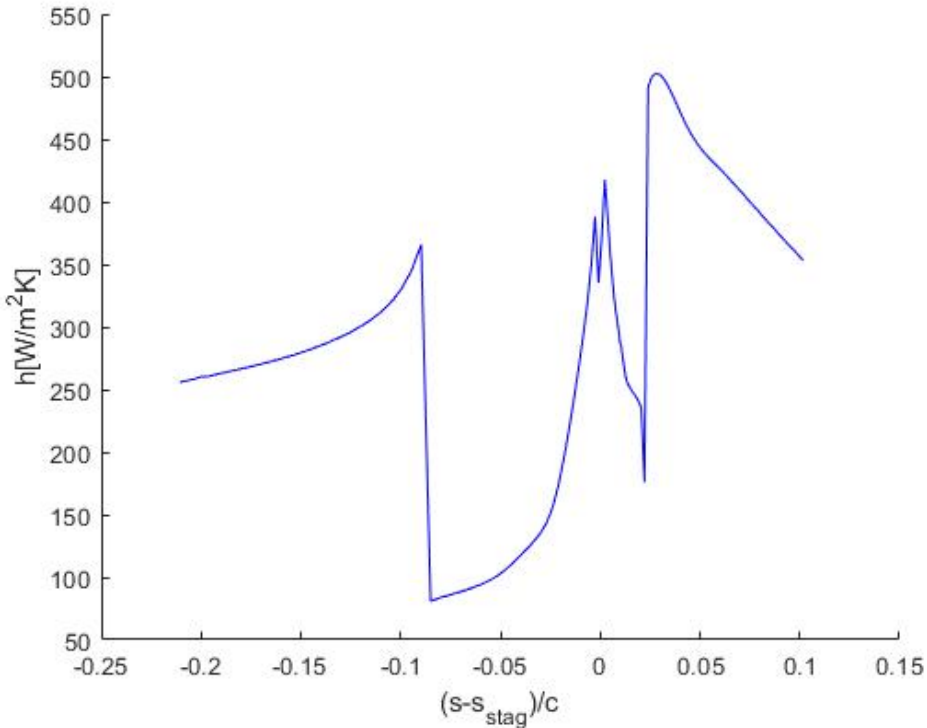


Figure 5.6: Heat transfer coefficient along the leading edge

The h_{req} can be converted to Nu_{req} using the equation below. D and k_{air} are constants here.

$$Nu_{req} = \frac{h_{req}D}{k_{air}} \quad (5.2)$$

Where,

- D is the diameter of the nozzle [m]
- k_{air} is the thermal conductivity of air [W/m K]

The next step is to convert the x-axis from $(s-s_{stag})/c$ into (R/D) . This can be done by multiplying by c/d . [Note: R was defined as the distance from the stagnation point, in other words $R = s-s_{stag}$]. The conversion is shown below:

$$\frac{R}{D} = \frac{s - s_{stag}}{c} * \frac{c}{D} \quad (5.3)$$

With that, all the derivations needed to plot the graph for Nu_{req} versus (R/D) have been found.

The next step is to compare the Nu_{jet} values with the Nu_{req} and choose a suitable value for D in (H/D) , The setting of the D value will be done by trial and error. The goal is to find a D value that causes the Nu_{jet} graph to match the Nu_{req} graph as closely as possible. Several values for D were tested and are shown below in Figure 5.7, 5.8, 5.9.

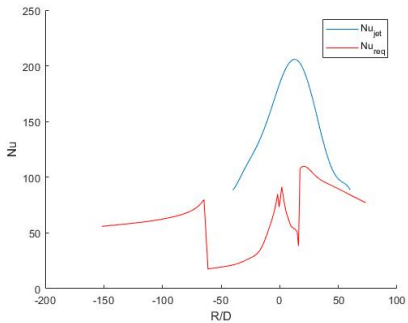


Figure 5.7: $D = 5$ mm

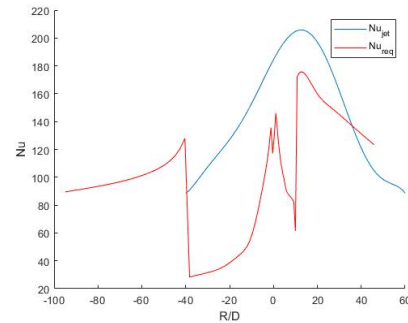


Figure 5.8: $D = 8$ mm

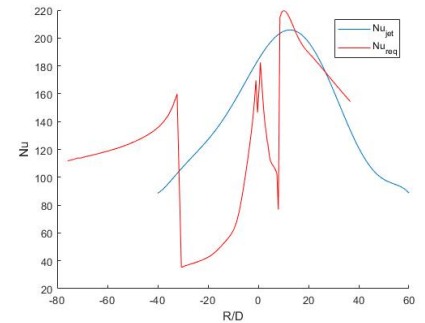


Figure 5.9: $D = 10$ mm

To best fit the the Nu_{req} graph, a double nozzle system along the y-direction was chosen. The 1st nozzle was chosen with $D = 9.2$ mm and the 2nd with $D = 12.5$ mm. The graphs are shown in Figure 5.10 and Figure 5.11. The separation between the 2 nozzles was determined by looking at the separation between the 2 peaks of Figure 5.6.

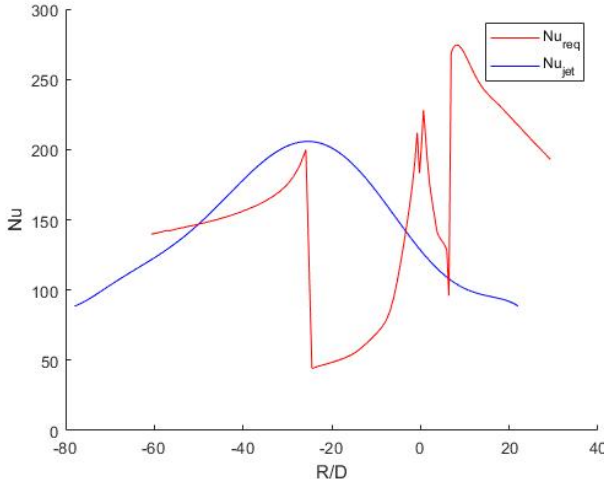


Figure 5.10: $D = 12.5$ mm

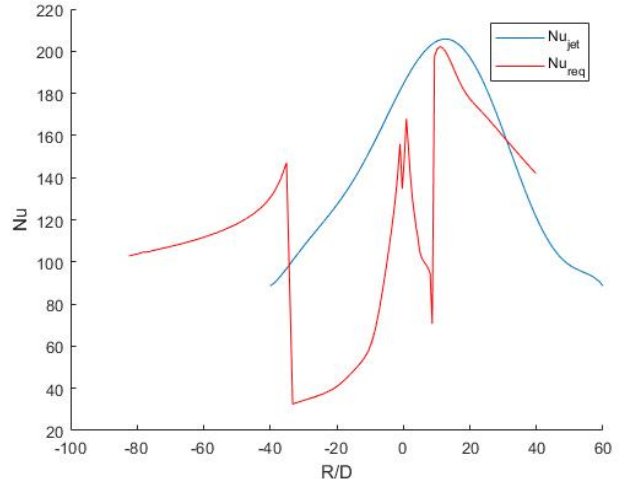


Figure 5.11: $D = 9.2$ mm

5.2.3 Optimization along x-direction

A similar strategy is needed for the optimization along the x-direction. However this time the values of D have already been set from the y-direction. Hence the only thing to check is the separation between the nozzles in the x-direction. The respective peaks of Nu_{req} from Figure 5.10 and Figure 5.11 were taken and set as a constant for Nu_{req} along the x-direction. For $D = 12.5\text{mm}$, a graph for 2 adjacent nozzles along the x-direction was plotted. The graphs were set such that their intersection was still above the horizontal line for Nu_{req} . From there, the distance between the 2 peaks was determined and was taken as the center to center separation of the nozzles in the x-direction. The same was done for $D = 9.2\text{mm}$. The graphs are shown in 5.12 and Figure 5.13.

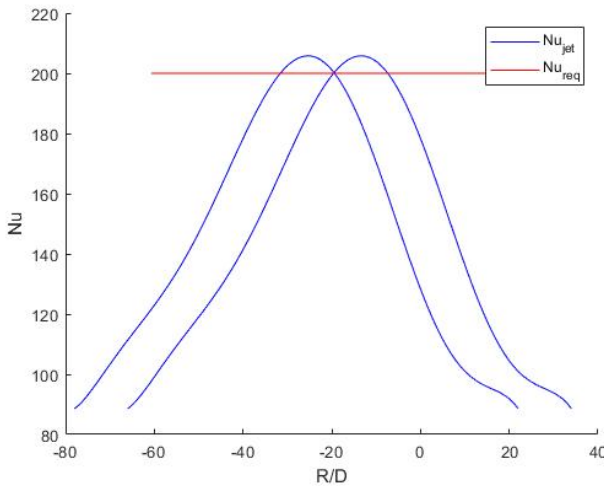


Figure 5.12: $D = 12.5$ mm

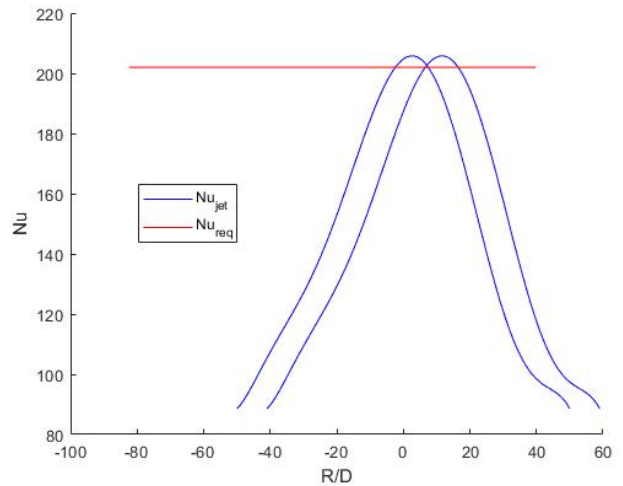


Figure 5.13: $D = 9.2$ mm

5.2.4 Final Layout of Nozzles And Mass Flow

The final layout of the nozzles is shown below in Figure 5.14. [Note: The figure is not to size]

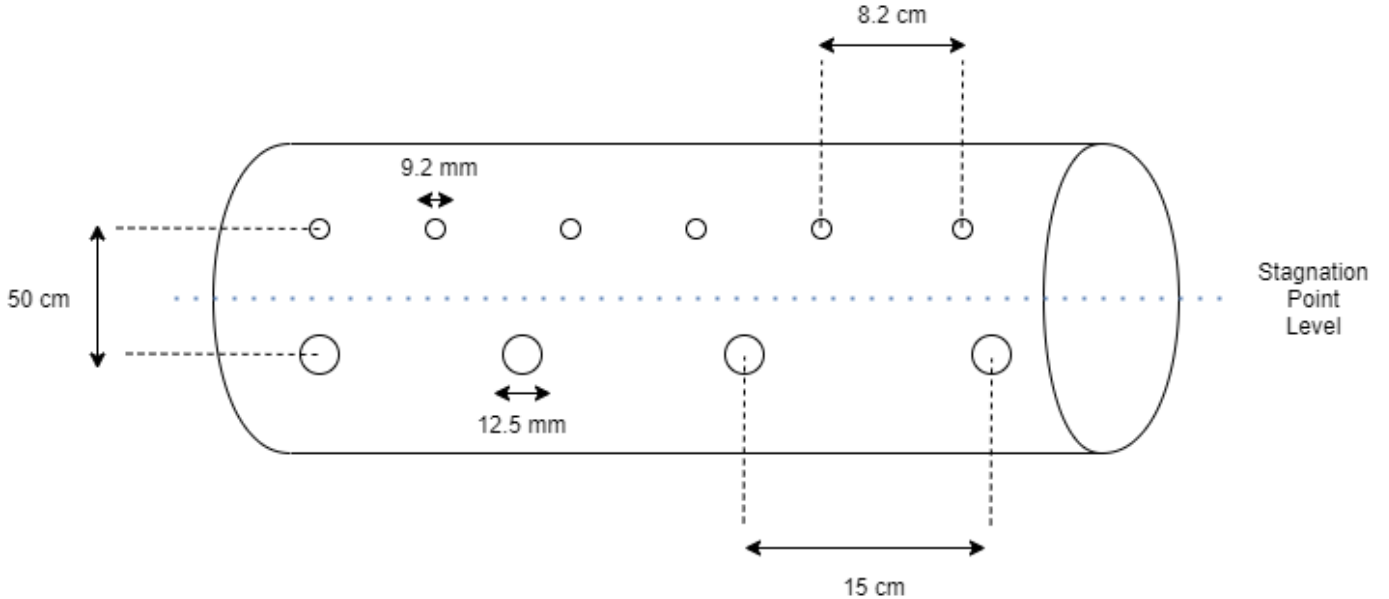


Figure 5.14: Layout of nozzles on piccolo tube

To calculate the mass flow (\dot{m}) the number of nozzles along the x-direction had to be determined. This was done by dividing the length of the wing by the separation between adjacent nozzles. For the upper layer ($D = 9.2\text{mm}$) and lower layer ($D = 12.5\text{mm}$) this calculation is shown below:

$$n_{upper} = \frac{L_{wing}}{\text{Separation}} = \frac{13}{8.2 \cdot 10^{-2}} \approx 157 \quad (5.4)$$

$$n_{lower} = \frac{L_{wing}}{\text{Separation}} = \frac{13}{15 \cdot 10^{-2}} \approx 86 \quad (5.5)$$

Similar steps to section 4.5 were carried out to determine the mass flow for the upper and lower layer using the new D values found. The final mass flow for the upper and lower layers is shown below:

$$\dot{m}_{upper,total} = n_{upper} \cdot \dot{m}_{upper} = 157 \cdot 0.0012 = 0.1884\text{kg/s} \quad (5.6)$$

$$\dot{m}_{lower,total} = n_{lower} \cdot \dot{m}_{lower} = 86 \cdot 0.0027 = 0.2322\text{kg/s} \quad (5.7)$$

Hence the total mass flow is as shown below:

$$\dot{m}_{total} = \dot{m}_{upper,total} + \dot{m}_{lower,total} = 0.1884 + 0.2322 = 0.4206\text{kg/s} \quad (5.8)$$

To have a rough idea of what the value of \dot{m}_{total} means, the mass flow rate of an engine will be estimated. The diameter (D) of the engine is taken as 3.4m [42]. The speed (V) can be taken as the cruising speed of 86 m/s. The ρ at 2000m (cruising altitude) is 0.94 kg/m^3 . Using this, the mass flow rate of the engine (\dot{m}_{engine}) can be calculated using the equation below:

$$\dot{m}_{engine} = \rho \cdot V \cdot (\pi/4)D^2 = 733\text{kg/s} \quad (5.9)$$

Hence the percentage of the mass flow rate required by the jets to the mass flow available from the engine is as follows:

$$\% \dot{m}_{used} = \frac{\dot{m}_{total}}{\dot{m}_{engine}} \times 100\% = 0.0574\% \quad (5.10)$$

5.2.5 Conclusion

Through this optimization process, the ideal pattern and number of nozzles were determined. This meant that the choice of number of nozzles enabled to achieve the heat energy required with as minimal energy wastage as possible. In other words, designing as efficient a system as possible. The number of nozzles found was a very reasonable number as it could be easily spread out within the dimensions of the piccolo tube. The $\% \dot{m}_{used}$ shows that a very small percentage of air from the engines is needed to run this impinging jet system.

5.3 Ice-phobic Anti-icing System

First of all, a linear velocity profile is assumed.

At first the flow is a laminar flow, but the flow transitions to a turbulent flow. The generally Reynolds number at which this happens is:

$$Re_{cr} = \frac{Ux_{cr}}{\nu} \quad (5.11)$$

With this the critical x can be calculated, by setting the value of $Re_{cr} = 5 \cdot 10^5$. Before this value, the flow is laminar, after this value, the flow is turbulent. For laminar flow, a set of equations is derived to calculate the local shear stress. These equations can be derived from the Blasius equiation.

$$\tau_{wall}(x) = \frac{1}{2} C_f \rho U^2 \quad (5.12)$$

$$C_f(x) = \frac{0.664}{\sqrt{Re(x)}} \quad (5.13)$$

From experiments, the friction coefficient is determined for a turbulent flow.[38]

$$C_f(x) = \frac{0.059}{Re(x)^{\frac{1}{5}}} \quad (5.14)$$

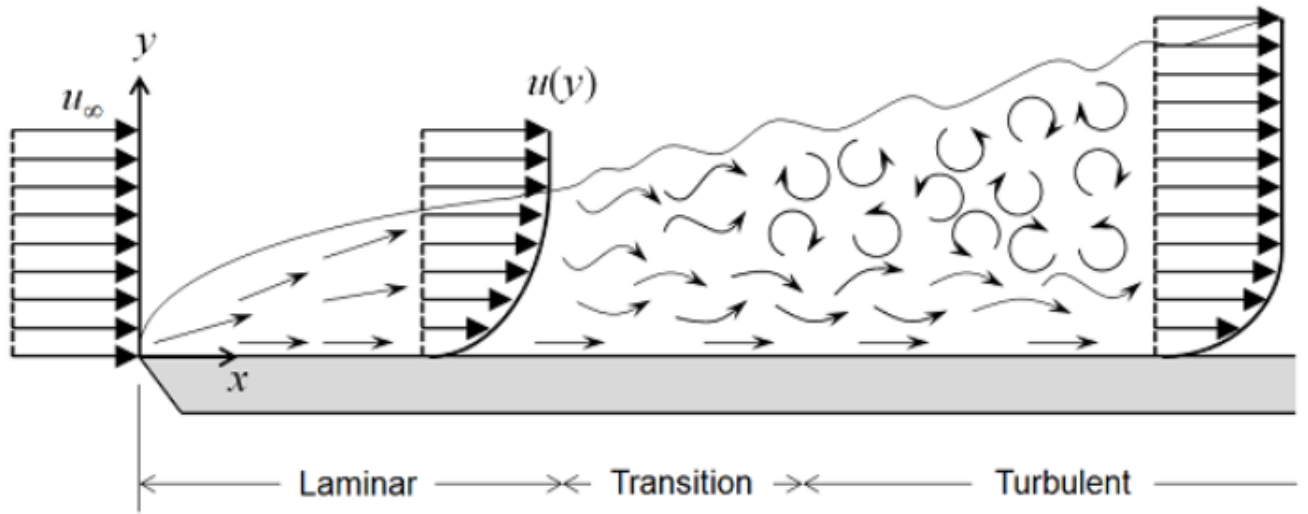


Figure 5.15: Model of the boundary layer profile, assuming a flat plate [43]

Computing the Shear Stresses exerted on the wing

Using these equations the shear stresses along the wings can be computed. Assuming an air velocity of 86 m/s and the properties of air at a height of 1500m along with a wing length of 3.6m. This length is the length in the moving direction. The value of x_{cr} is .0.0957m These results can be found in figure 5.16.

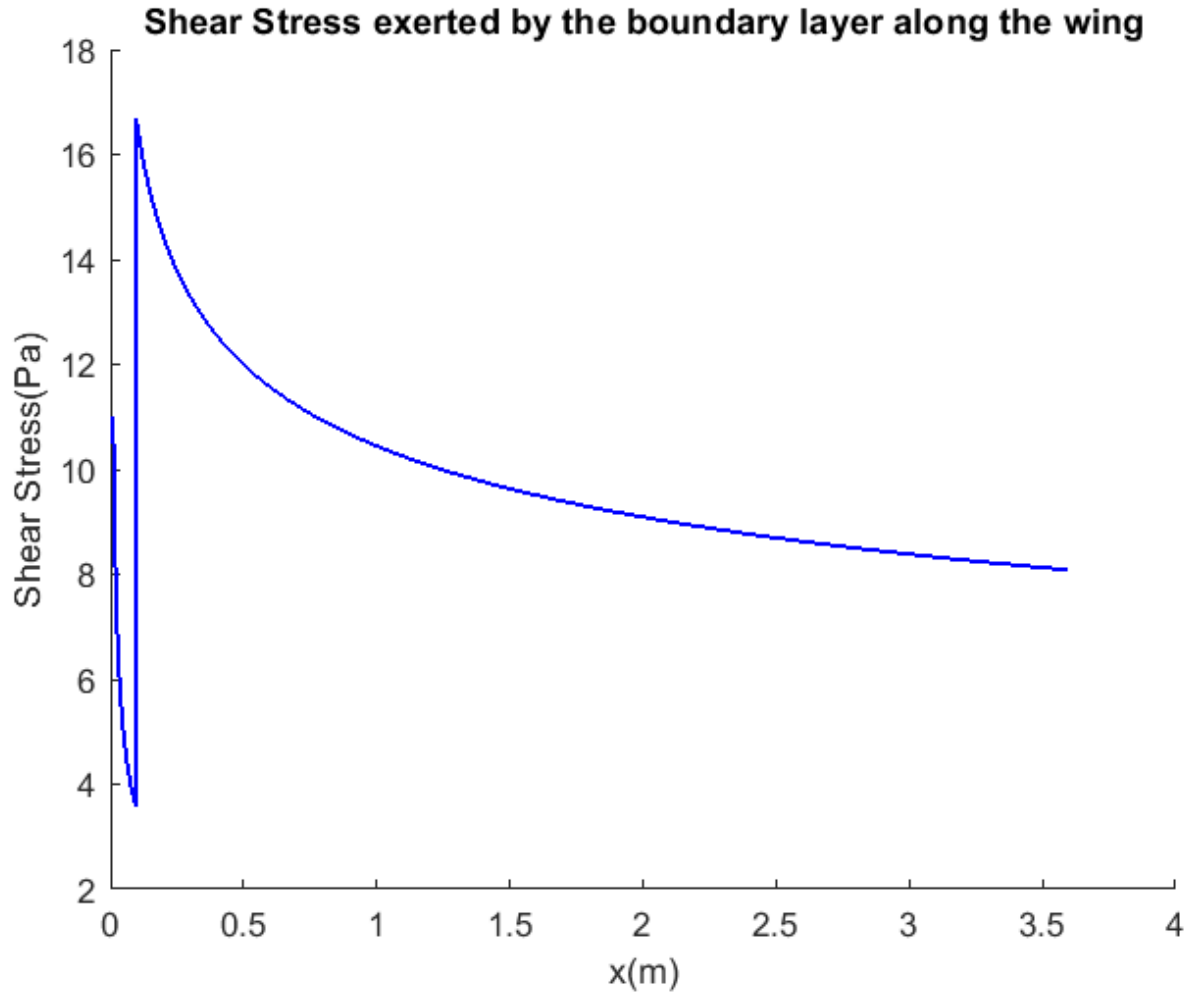


Figure 5.16: Shear Stress exerted by the boundary layer along the wing

5.3.1 Comparison to Ice-adhesion strength

The Ice-adhesion strength on a super-hydrophobic coating is 53.6 ± 6 kPa , taken from [21] As can be seen in figure 5.16, the highest shear stress acting on the wing is at $x = x_{cr}$. This shear stress is calculated to be 16.699 Pa. The lowest shear stress is just before that point, 3.557 Pa. This shows that all values of the shear stress are much smaller than the adhesion strength.

Assumptions

The following assumptions are made:

- The wing is assumed as a flat plate
- p is constant for all x and y across the boundary layer
- The flow is steady
- gravity is neglected, set to be 0 for calculating the shear stress
- μ is constant

- The fluid is incompressible: $\rho = \text{constant}$
- The critical Reynolds number is a generally accepted value, so a transition point is used instead of a transition region.
- The surface is smooth
- U varies slower with x than with y

Recommendation

To have Ice-phobic materials as a possible solution, the shear stress needs to be higher than the adhesion strength. This is not the case. This leads to the conclusion that it is not possible to only apply ice-phobic materials to the wing.

Chapter 6

Ethics in Engineering

6.1 Step 1: Ethical Risk Sweeping

The word "risk" usually refers to an undesirable event, the cause of an unexpected event is a lack of awareness of the unknown in evaluating potential and actual damage. Underinsurance law, risk normally refers to the probability of personal injury, harm, or loss. Risk is defined and measured using numbers, odds, and measurable risk accumulation. Even the severity of the harm factors in as certain practices can pose a high risk of harm but keep a low likelihood of occurrence. The risk of a nuclear plant mishap, for example, is small but the environmental harm may be huge. Certain practices can typically present low hazard risk and low probability of occurrence. Aviation remains the safest mode of flight, due to the low number of accidents and deaths in comparison with other ways of transport. In this step all the possible outcomes for failure cases are analyzed in order to prevent the potential damage toward people or systems that are morally significant. Almost all of the items are hard to detect in specific cases.

- Do not share the moral perspective of other stakeholders
- Fail to anticipate the likely causal interactions that will lead to harm
- Consider only material/economic causes of harm
- Fail to draw the distinction between conventional and moral norms.
- The ethical risks are subtle, complex or significant only in aggregate
- Misclassify ethical risk as legal, economic cultural or PR risk
- Lack explicit, regularized practices of looking for them.

To classify the potential risk, a table of probability vs impact will be done to analyze each case and evaluate it taking into account the harm that it will cause. In the following table, each of the problems will be rated from 1 to 5, with 5 being the highest risk. The rank is the average between probability and impact

	Risk Description	Probability	Impact	Rank
1	Bigger engine for same airframe	4	3	3.5
2	Overweight due to new system	3	3	3
3	Unskilled workers	4	5	4.5
4	Inexperienced Pilots	4	5	4.5
5	Extra lift need for the new weight	3	4	3.5
6	Failing FAA regulations	4.5	4.5	4.5
7	Ignoring sensor warnings	5	4.5	4.75
8	Electrical Problem	3	4	3.5
9	Ice formation in different altitudes	3	4	3.5
10	No enough heat to de-icing the wing	3	5	4
11	Carbon footprint	4	4	4
12	Rushed production	2	4	3
13	Supply chain	3	5	4

Table 6.1: Probability vs Impact

The potential problems have already been classified quantitatively in the table 6.1 according to the impact they could cause in a real situation, they will now be divided into three categories (low, moderate, significant) in order to prevent and monitor them in a constant way to avoid damages that could become catastrophic without proper management. The low impact be called as acceptable risks, which can be carried in a situation, because if they failed they would not cause fatal damage, those with a rank less than 2.5 could enter this category. The moderate impacts are risks that will have to be monitored in a constant way to avoid risks that would cause very serious losses will be those that have a rank between 2.5 and 3.75. And finally the significant problems should be changed or avoided in order to guarantee the best quality of the plane , periodic revision and maintenance.

6.2 Step 2: Ethical Pre-mortems and Post-mortems

6.2.1 Post-Mortems

- Because the most important thing on every flight is to keep passengers safe. No action should be taken that could jeopardize the safety of passengers. Increasing speed or reducing equipment costs that increase the possibility of possible failures.
- Future changes to aircraft systems must be for the good of stakeholders, investors, airlines, but primarily passengers. These new systems require training for pilots, these training must be taken seriously, because in a contingency, pilots must be able to make the best decisions regarding what the pilot considers.
- The pilots are responsible for many human lives during the flights, therefore recommendations or experiences of their flights will be very helpful for the rest of the pilots who are in training, it can even be helpful for the engineers, in the creation of future improvements to these anti-ice systems.

6.2.2 Pre-Mortems

- Many times these new technologies have a delivery date, which can cause calculation failures or skip steps when testing this new technology, this can create many economic losses and affect many stakeholders, if in this case this system is tested on a plane in real time of flight, it could present failures and endanger the crew. Therefore these technologies must be well evaluated and take the necessary time to develop them.
- Ignoring Federal Aviation Regulations for the benefit of third parties could endanger the lives of passengers. Therefore these regulations must be respected during the flight and in the creation of this new technology, meeting the imposed standards.
- There are many competitors in the aviation market, and this competition could jeopardize the safety of the crew. It is extremely important to keep in mind that this competitiveness can be very dangerous. If in such a case the purpose is to create an antifreeze system that is the fastest, many factors must be taken into account, and be careful not to jeopardize other aspects such as the material of the airplane wing and create a catastrophe. An antifreeze system that works without endangering the lives of passengers is preferable.
- Many factors are under consideration, the sale of these systems are also of utmost importance to keep afloat the companies that are responsible for creating this new technology. But the sale values or the profit factor of these products should not affect the safety of people on board the plane, reducing manufacturing costs are often the first dilemma that puts people at risk, the use of low-cost materials cost and low required properties puts many lives at risk. Therefore this technology must be very

6.3 Step 3: Expanding the Ethical Circle

In this part, analysis will be done on the various stakeholders relating to the project: The Design of An Anti-icing System for An Airplane wing. It is important to expand the ethical circle by considering the views of the stakeholders to prevent 'Group Think' (unable to accurately asses alternate perspective other than those currently being operated in), 'Bubble Mentality' (unable to place yourself in the shoes of other stakeholders due to a lack of diversity in demographic and cognition) and 'Friedman Fallacy' (inadvertently prioritising the profits later down in the design process although the reason to start the project in the first place was noble). A list of stakeholders, their interests and the impact of their interests on the project is shown below in Table 6.2.

Stake holders	Interests	Impact
Pilots	Easy to operate	High
	Reliable data	High
	Responsive system	High
Airlines	Improve system	High
	Reliable system	High
	Makretable system	Low
Management Team	Affordable	High
	Innovation	Med
	Achive Targets	Med
Engineering Team	Reliable mechanism	High
	Mantain and develop skill level	Med
	Reputation	Low
Passengers	Safety	High
	Comfortable journey	Med
Investor	Market provider	Low
Competitors	Markets monopolization	Low
Other Engineers	Innovative system	Low

Table 6.2: Stakeholder Overview Table

It can be seen that certain groups have higher impact on the final design than others. The ones which have the most direct impact can be considered the 'primary stakeholders' and the ones which have a more indirect or less of an impact can be categorized as "secondary stakeholders". For this case, the pilots, airlines, management team, engineering team and passengers can be considered as the Primary Stakeholders while the rest can be seen as secondary stakeholders. The primary stakeholders from Table 6.2 were assessed in which interests they are impacted on. The results are shown below in Table 6.3.

Stake holders Group	Finances	Technological	Reliability	Safety
Pilots			x	x
Management Team	x		x	
Engineering Team		x	x	x
Airlines	x	x	x	x
Passenger			x	x

Table 6.3: Stakeholder Interest Table

Finally the various stakeholders were assessed on a graph of their power (or in other words their influence on the final design) versus their interest in the project. The bottom left corner shows the stakeholders that have to be only monitored as they have low power and low interest. This group is of least priority. The passengers fall into this category as they do not directly contribute to the design of the anti-icing system nor is the development of anti-icing system of any particular interest to them (other than their safety of course). The top left corner shows the stakeholders that have to be kept satisfied as they have high power but low interest. Pilots fall in this category as they are the ones who are going to be using the anti-icing system and their input on the design is very valuable.

Their interest in the technological development of an anti-icing system however is not that high as at the end of the day they are only users of the design. The bottom right corner shows the stakeholders that have to be kept informed as they have high interest and low power. Airlines are placed here as the development of a brand new anti-icing system is a good way to further promote their airline as one with state of the art technology. However they have very little say in the final design as they are not involved much in the designing process. Finally, the top right corner shows the group that has high power and high interest which have to be managed closely. The considerations of this group should be the priority when designing the anti-icing system. The management team and engineering team are found here. They are the ones directly involved in the project and have the most interest as it is the field of study they work in day in and day out. Table 6.4 below shows the placement of the primary stakeholders.

High Power	Pilots	Management Team Engineering Team
Low Power	Passengers	Airline
	Low Interest	High Interest

Table 6.4: Power vs Interest Table

6.4 Step 4: Case-based Analysis

In step 4, two cases are analysed to conclude what happened and what should not happen with the anti-icing design. The two cases that are analysed are the Chernobyl accident and the Challenger accident.

6.4.1 Similar cases

The Space Shuttle Challenger disaster in 1986 was caused by the failure of an O-ring. The ring failed to seal the joints in the solid rocket booster (SRB), allowing hot gases to escape. The disaster led to the death of all crew members on board of the orbiter and a halt on the Space Shuttle program for almost three years. The Chernobyl accident in 1986 was caused by a design flaw and miscommunication between engineers. It led to a meltdown and explosion killing thousands and making the area uninhabitable for years to come. A reactor was not working correctly and the engineers were testing to make it work again. But after a new shift came and tested it for the 4th time, the reactor melted.

6.4.2 Parallels and differences

Challenger

An anti-icing system is vital for aircraft to be able to fly under all circumstances, also extreme conditions, something the Space Shuttle was supposed to do as well. However, the O-ring was not designed for the low temperatures that day during the launch. The lack or failure of an anti-icing system can lead to losing lift of an aircraft, as seen in previous crashes. This is similar to the failure of the seal of the SRB. The Space Shuttle program was not meant for the big public, but a Boeing 737Max is. The cases show a similarity in risks (failure of the vehicle) but a difference in people involved (NASA

and the big public).

Chernobyl

The Chernobyl was supposed to be a nuclear power plant to give all people in the area power. The similarities are that the anti-icing system is for public planes just like the nuclear reactor makes energy for all people. The public will be affected if the plane goes down because of a bad anti icing system, and people got affected because of the Chernobyl disaster.

6.4.3 Evaluate choices and outcomes in the cases

Challenger

The manufacturer told NASA they were concerned about the weather conditions that day, and that they did not have test data on the behaviour of the material in such circumstances. They suggested postponing the launch. The engineers were already concerned about the O-rings during the designing process, but these concerns were not properly forwarded to the manufacturer of the SRBs. The failure of the seal could have been prevented if the SRB management did listen to the objections of the engineers. Evidence of O-ring problems was already present in other missions, but these were not reported to the NASA management. It is clear that existing communication was not sufficient. The missions were not paused, despite the problems that were known, clear and acknowledged. The manufacturer did contact NASA to express their worries regarding the operation conditions, but NASA did not want to delay the launch even further.

Chernobyl

First, the engineers should have tested the nuclear power plant thoroughly before building the same model over the whole USSR. All the power plants had the same flaw and it could have happened all over the USSR. Second, the safety tests that the engineers were doing when the reactor melted was the 4th test they did. If the new shift knew that the reactor was tested 3 times before they would have not tested again and not let it melt down. It was because the new shift was inexperienced and they should not have been allowed to test again.

6.4.4 Parallel risks, opportunities, solutions

The risks and technical problems were identified and acknowledged. The problem is that they were not communicated properly so superior staff, or not communicated at all. Here, the problems were ignored, either by the superior staff (management) or by the manufacturer itself. While designing and producing an anti-icing system, all the staff should be able to give their opinion about it and review the design if necessary. Communication is key, and nobody should keep information secret for whatever reason.

The engineering team did not have enough evidence to prove the management a delayed launch was necessary. The seals were not designed for the conditions that day, but it was not tested that it would go wrong. This evidence was maybe the one thing needed to convince superior staff that the launch should be delayed. This same thing can happen for aircraft. The anti-icing system should be able to operate in extreme conditions, but most importantly, the limits of the system should be clear. If the operating conditions fall outside the operating limits, the flight should be delayed or the reactor should not be tested again. The management should trust the engineers on these limits, rather than

focusing on other gains than safety. Code of conduct is something everyone has to follow. Managements can set guidelines, rules or a code that tells employers how to behave. If everyone follows that code, miscommunication errors are less likely to occur.

6.4.5 Concluded

- Communication with other staff, engineers and management teams, about worries and concerns should be normal and practised. Withholding information can lead to fatal failures.
- Management teams should trust the engineers on their observations, warnings and concerns.
- The other way around, engineers should be able to give hard evidence. This also means that testing their products in extreme environments is important. The product has to be used within its limits.
- Safety has to be a priority. This means that the system should not be used in conditions beyond its limits, even though this causes delays or costs money.
- Create a code of conduct for the teams and stick to these codes. This is extremely important to function as one team.
- Every mistake has to be evaluated, significant testing has to be done to ensure it can be handled safely.

6.5 Step 5: Remembering the Ethical Benefits of Creative Work

6.5.1 Why an anti-icing system and for what good ends?

To ensure the aeroplane's performance and safety, an anti-icing system should be present at or in the wings. Keeping the wings clean from ice is important to be able to fly. Ice accretion can lead to crashes since it causes the airfoil's shape to change and disturbs the aerodynamic performance of an aircraft. Implementing the system in the aircraft should not come with other problems, since the system should decrease the number of crashes, rather than increasing this number.

6.5.2 Would society/customers be better off with this technique? Is this product a new thing to sell?

This system is an important piece of an aircraft. Without this system, it is not possible to fly in cold, wet weather. The airlines want to offer passengers the opportunity to fly wherever they want to go. Looking from this perspective, an anti-icing system is just another way to increase profits. This is even more when considering that Boeing competes with other aircraft manufacturers, like Airbus. However, it's not always possible to predict the weather and fly only in the best conditions. In this case, there should be a system present that increases safety, by keeping the wings clean. This is an investment for the airlines as well as the manufacturers, but the passengers will be able to fly more often. They feel better about their safety as well.

If the system works as it should work, society would be better off with the use of this system. It is not only beneficial for the airlines, aircraft manufacturers and passengers, it is also important for everyone who does not fly. If an aircraft crashes, it affects more people than just the ones on board. If the system does not work as planned, it could pose a bigger danger than icing accretion is at this moment for society. It may cause more harm than an aircraft without an anti-icing system.

6.5.3 Is the ethical benefit at the centre of the work and thinking of the company?

Safety is the priority of the anti-icing system, so the ethical benefit is at the centre of this design. The anti-system is designed to keep ice from the plane wings so the plane does not stall and fall out of the sky. So this design will keep all people alive and let them travel in safety. All calculations are checks and the regulations are followed so that no errors will occur. The whole team had participation and the team makes all the choices without pressure from the higher ups. But there is pressure to finish the system on time.

6.5.4 What were they willing to sacrifice to make sure the system worked right?

As little risks as possible are made to assure the system works as promised. But due to pressure to finish the system in time a problem was found and neglected. At the testing phase the timing was wrong for the worst tests but the test that was worst with the right time was chosen. But after consideration it was chosen to take the safe route and to test with the worst possible outcome so the system will be as safe as possible. No risks were taken.

6.6 Step 6: Think About the Terrible People

In this step the ‘terrible people’ need to be thought of. For this, a couple of questions need to be asked at key design stages:

6.6.1 Who will want to abuse, steal, misinterpret, hack, destroy, or weaponize what we built?

At first, terrorist organizations can be placed in this category. These people will want to hack or weaponize or destroy the system we built. They want this to let the planes fly without the anti-icing system, and in the end, let them crash to create fear. Shareholders of airline companies will want to go for the highest profit. Because of this, they will not change to a new system of anti-icing, because this will result in higher costs. This will be less safe, resulting to hurt the image of the company, leading to a decrease in stock if other companies choose to go for the cheaper option. So in this way, they misinterpret the importance of this new system. Aeroplane companies or research teams want to steal information about the anti-icing system, to be able to create the anti-icing system themselves. In this way, it may be cheaper for them to create such a system, which is unfair. Governments and the FAA could misinterpret the importance of the new anti-icing system. They may think the planes are safe as they are now, so set no rules to make sure the planes have decent anti-icing.

6.6.2 Who will use it with alarming stupidity/irrationality?

For pilots, the new system will work in a different way than the system that is used now. They are not well trained and thus do not know how to react in certain situations with it. This could lead to unsafe situations. Aeroplane companies will use it with alarming stupidity too. The new system provides a safer anti-icing system, which is more reliable. In order to save costs when choosing this system, the company could choose to use less sensors or back-up systems , since it is already reliable. But if the system has an error, the sensors will not be accurate in that situation. This leads to unsafe situations. With less back-up systems, it could be that the pilot will not be able to control the plane anymore, since there is no anti-icing. This leads to unsafe situations too.

6.6.3 What rewards/incentives/openings have our design inadvertently created for those people?

Under the new conditions is a feeling of safety a big reward. As well the pilots as the passengers and everyone involved will feel safe with the new system, but this can be a misplaced feeling if the pilots do not know how to act in certain situations. For the terrorists creating fear is an incentive to let the planes crash. For the shareholders' and Aeroplane companies choosing another system which is less safe over the new system, a reward is to maximize profit. Also for lowering the amount of sensors and backup systems, a reward is to maximize profit.

6.6.4 How can we remove those rewards/incentives?

First of all, the pilots will need to get in-depth training to know how to react in certain situations. In this way, the feeling of safety will not be misplaced. This training also needs to be adjusted if new insights come in play to keep it safe. Creation of fear will be removed by strict controls on the software and production for the system to make sure the system will not be hacked. Also, corruption in the factories will need to be controlled to make sure the system will not be weaponized. A way to make sure the best system will be used over the cheaper less working system is by implementing new FAA requirements. According to these requirements, aeroplanes need to have an anti-icing system that clears sufficient ice from the wings. Also a minimum amount of sensors and back-up systems need to be implemented in the FAA requirements, in order to make sure these will not be left out to save costs.

6.7 Step 7: Closing the Loop: Ethical Feedback and Iteration

6.7.1 Remember That Ethical Design/Engineering Is Never a Finished Task

To ensure long term success, the ethical design loop needs to be closed. When incorrectly done this can lead to unethical handling. And situations likewise to those in the past as discussed at step 4. Because of the desire to maximize profits, safety could be neglected by big aircraft producers. To prevent this, such handling needs to be prevented or reverse the damage done to the public trust. To

close the loop, ethical feedback channels are of utmost importance, to keep learning from the current ethical problems with the technology.

6.7.2 Identify Feedback Channels that Will Deliver Reliable Data on Ethical Impact

- Pilots feel the effects of icing occurring on the plane when operating it. Thus they will also get a grip of the true effectiveness of the designed anti-icing system. Having them report these opinions and concerns could greatly benefit an engineering team to ensure a safer solution is implemented in new aircraft.
- Informing passengers about the system and asking them about an opinion about it through a survey. The fear of passengers can be measured in this way.
- Another feedback channel is by monitoring the number of aeroplanes that crash due to the occurrence of icing on the wing of the plane. This sounds a bit harsh but gives a clear overview of the safety of the planes and can give a clear sign ethical change is required.

6.7.3 Integrate the Process w/Quality Management User Support; Make it Standard

- To make the process standard the following processes will be used: Pilots will be obligated to give feedback once a month, in order to get continuous feedback. In this way, it is prevented to get no feedback by them.
- Passengers will get an E-mail after each flight in order to get as much feedback as possible. The feedback e-mail will look like the evasys e-mail for our courses.

6.7.4 Develop Formal Procedures and Chains of Responsibility for Ethical Iteration

Processing this ethical feedback, closing the loop, is a great responsibility. Leaving this in the wrong hands could create big ethical problems that will not be solved. For example, leaving the management of big aircraft companies in charge of the processing will most likely end up in a scenario comparable to the current one, maximizing profit while neglecting safety risks. To ensure the intended use of the ethical feedback an independent company, like an NGO, should be appointed. Processing the data and reporting this to all the groups within the chain of responsibility should be accomplished to make sure that ethical change is effected. This chain of responsibility should consist of, Company management, the engineering team and the pilots. As all of these groups are responsible for reliability of aeroplane operation one after another. First of the pilots are operating the plane and should be able to do so, however the aircraft they operate can also be faulty. This being due to a mistake within the engineering of the design, making the engineering team accountable for ethical impact from this mistake. Lastly, the engineering team is under final orders from the management of the company in question, making them also responsible for the ethical impact caused by safety risks from their aircraft.

Chapter 7

Conclusion

The final design of the anti-icing system is a combination of the use of impinging jets and ice-phobic materials. The impinging jets proved to be very effective in preventing ice formation while making use of a very small percentage of the bleed air available. The ice-phobic surfaces by themselves were insufficient as the shear stress produced was lower than the adhesion strength of the ice molecules. The final choice of the anti-icing system is capable of withstanding the different ice accretions such as rime ice, clear ice and mixed ice as well fly safely in atmospheric conditions such as freezing rain and frizzle drizzle that were explored in section 2. The impact location of different sized droplets were also assessed manually (using the potential flow) and using software (2DFOIL-ICE) in section 3 to determine which parts of the airfoil are most prone to ice accretion, allowing the final design of the anti-icing system to prioritize these areas. Several other anti-icing mechanisms were explored in section 4 ranging from the use of electric heating mats to heating via forced convection. This ensured multiple solutions were thought of before choosing the most optimal solution for the Boeing 737 MAX. Finally, optimization of the chosen solution (impinging jets) was done in section 5 to ensure the best results possible were attained while also checking the viability of the solution of ice-phobic surfaces.

Chapter 8

Appendix

8.1 FAA maximum icing atmospheric conditions.

8.1.1 Continuous Icing Maximum:

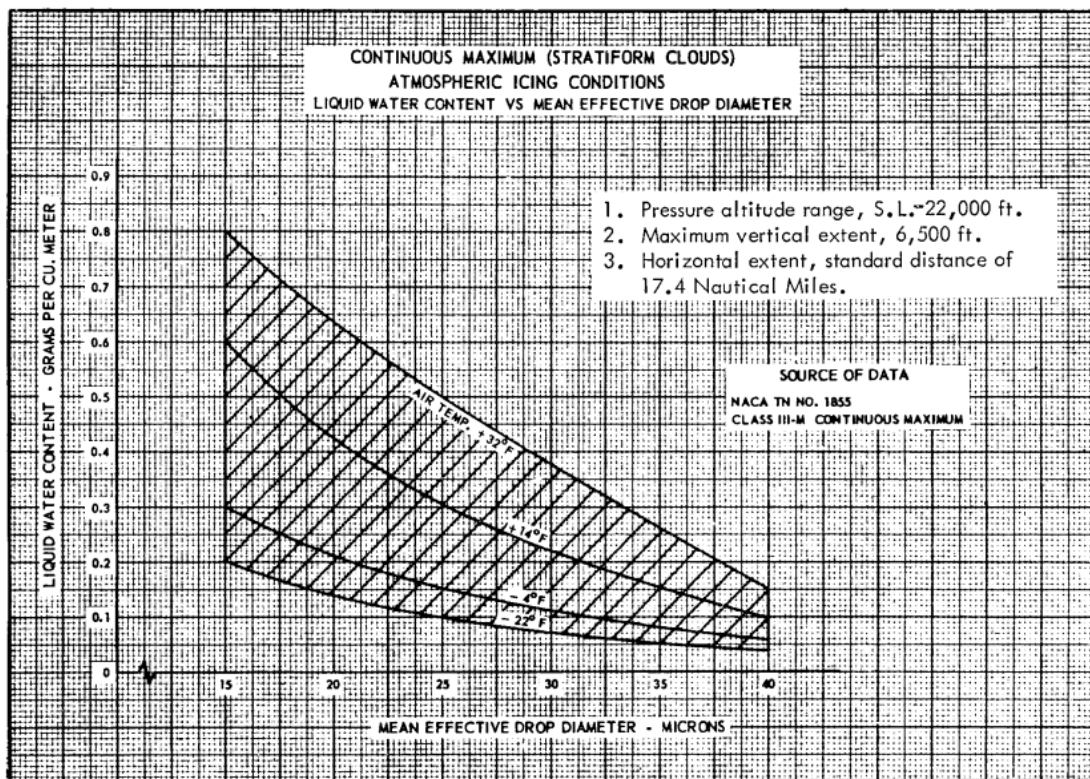


Figure 8.1: Continuous maximum: Liquid water content vs Mean effective diameter, [22]

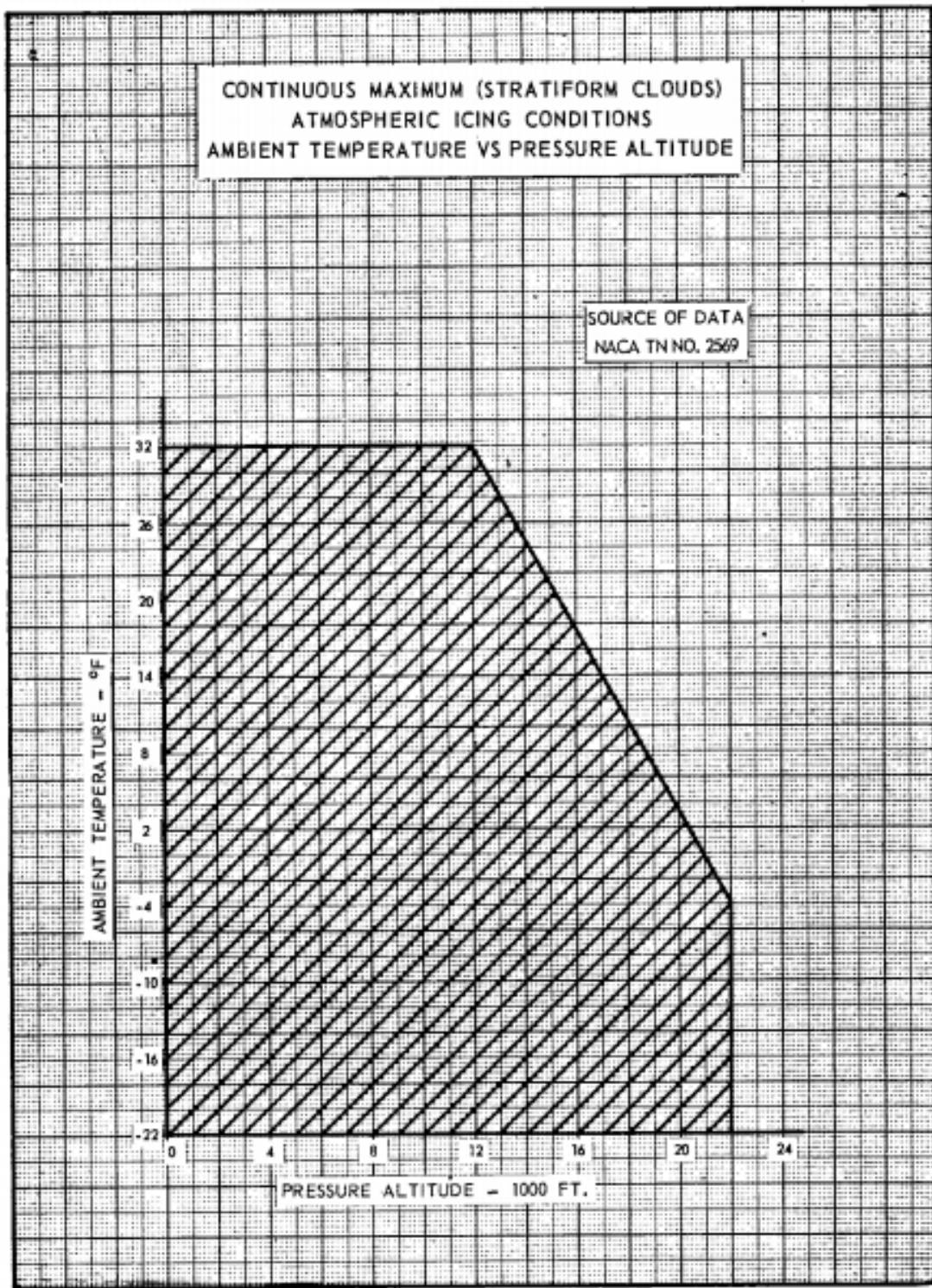


Figure 8.2: Continuous maximum:Temperature vs Pressure, [22]

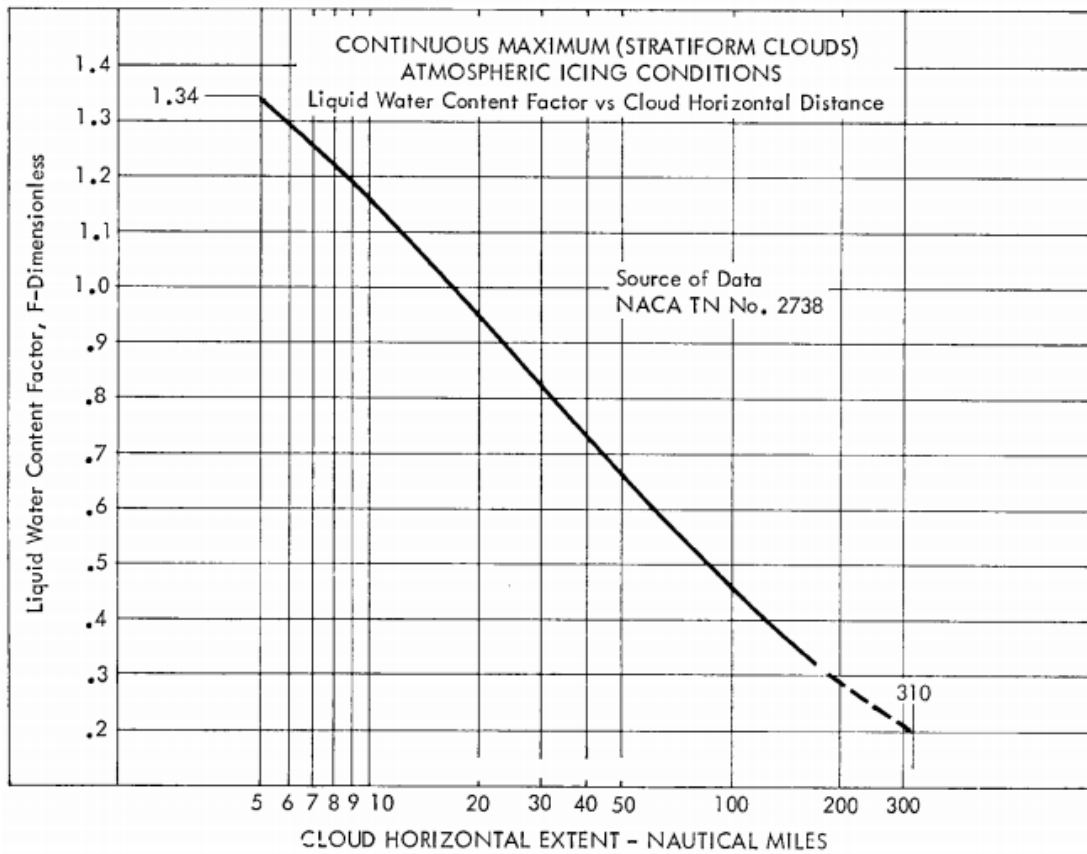


Figure 8.3: Continuous maximum: LWC vs Cloud factor horizontal distance, [22]

8.1.2 Intermittent Icing Maximum:

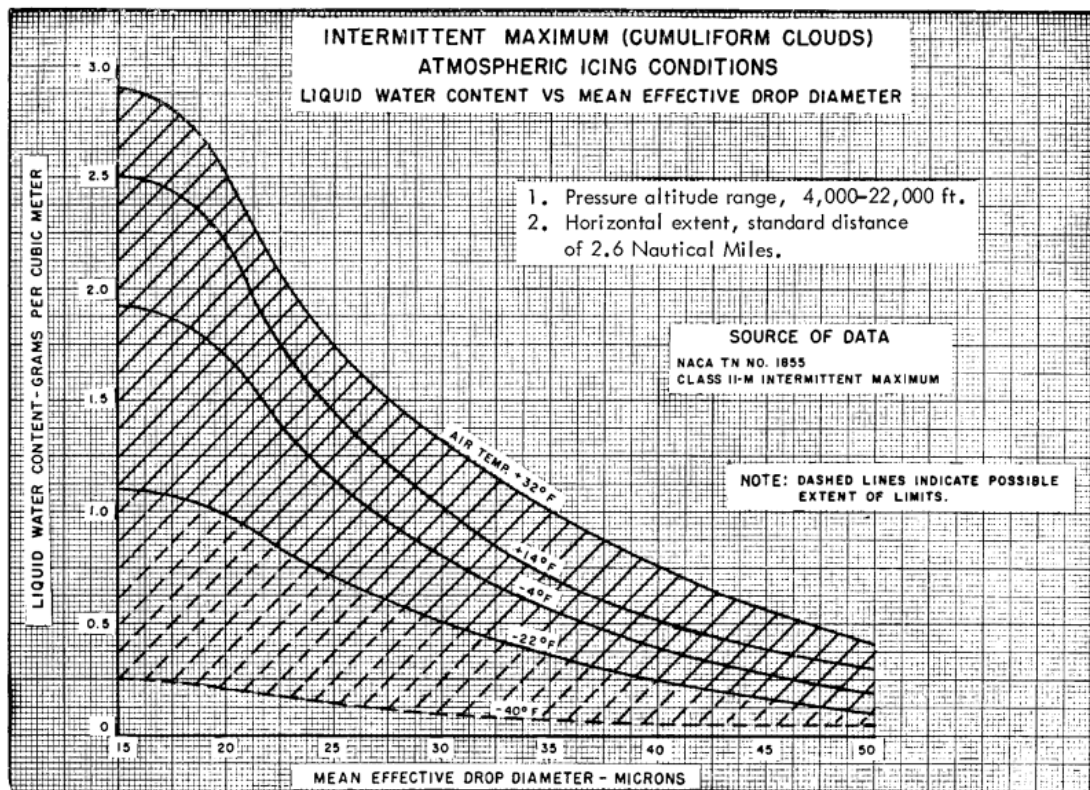


Figure 8.4: Intermittent Icing: Liquid water content vs Mean effective diameter, [22]

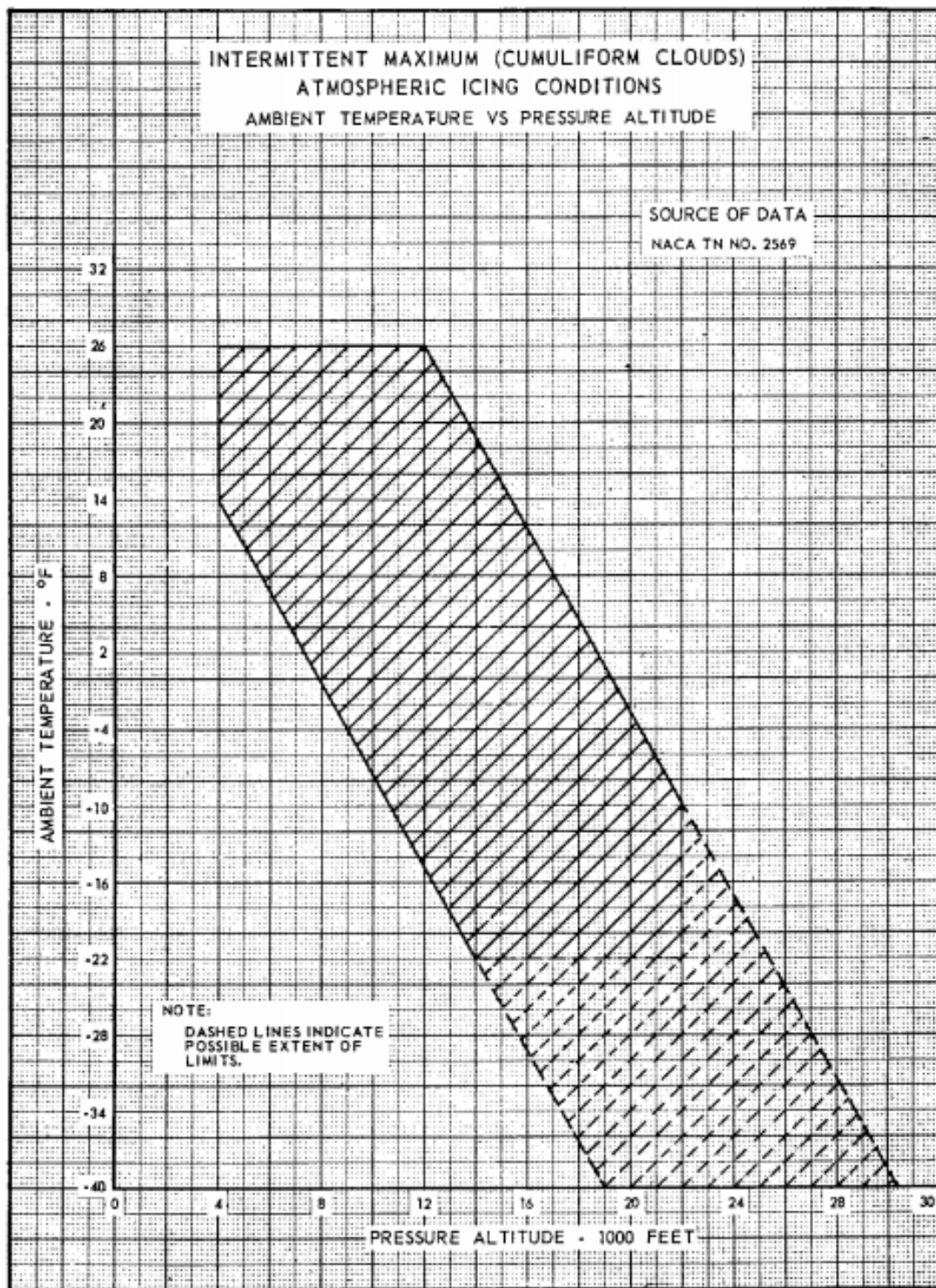


Figure 8.5: Intermittent Icing:Temperature vs Pressure, [22]

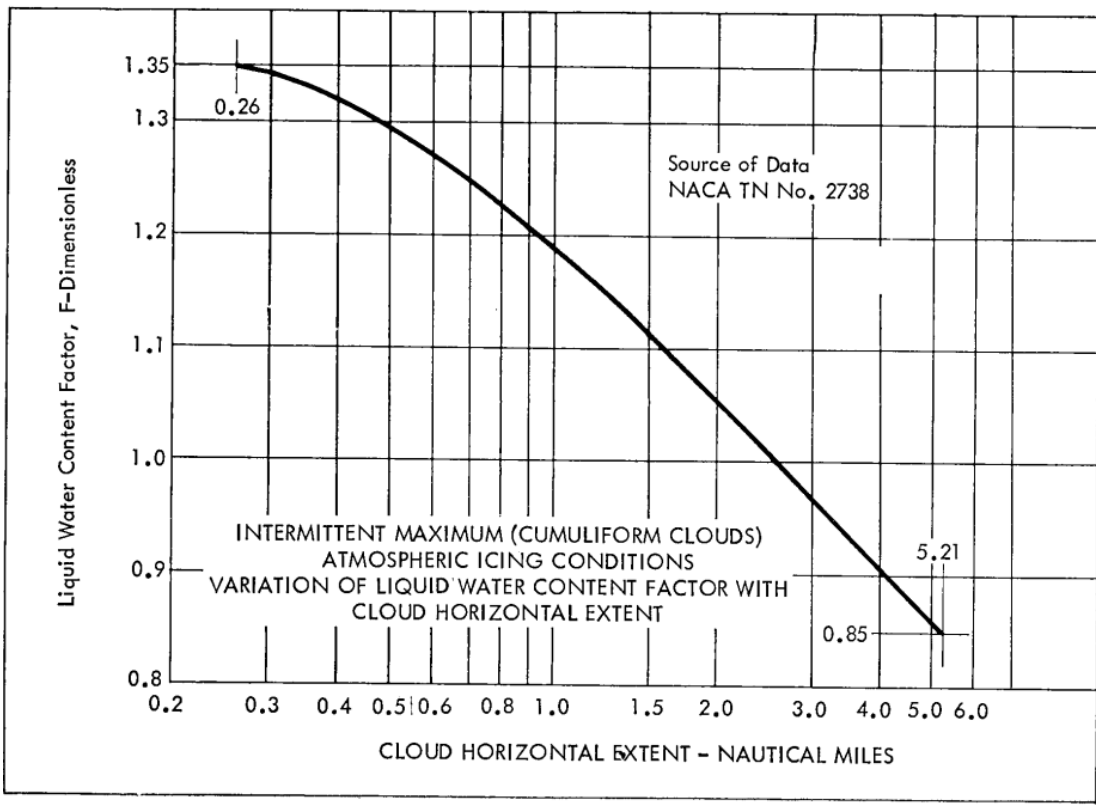


Figure 8.6: Intermittent Icing:Temperature vs Pressure, [22]

8.1.3 Supercooled large drop icing conditions

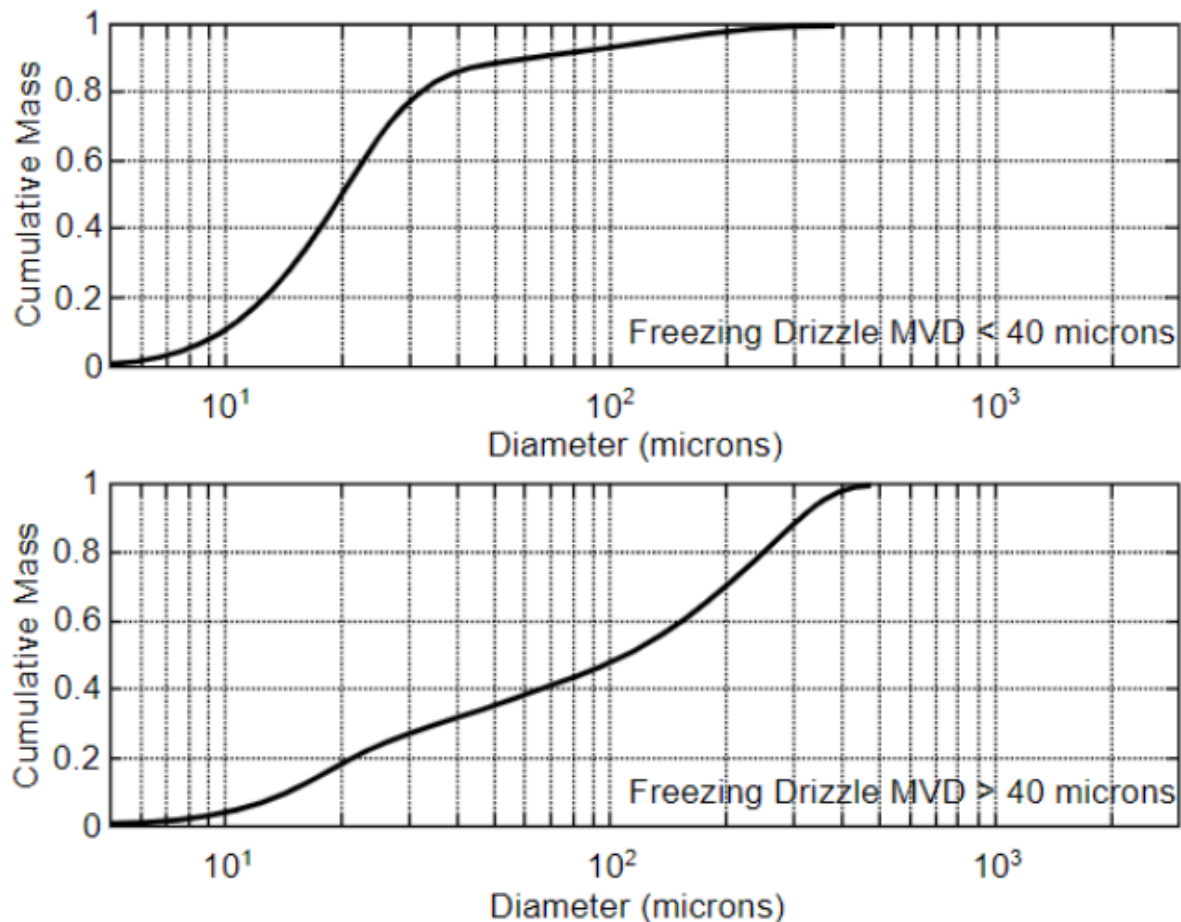


Figure 8.7: Graphs of cumulative mass distribution corresponding to the drop diameters for freezing drizzle. If the median diameter of the drop distribution is less than 40 microns the first graph must be followed and if it is greater than 40 microns the second graph must be followed

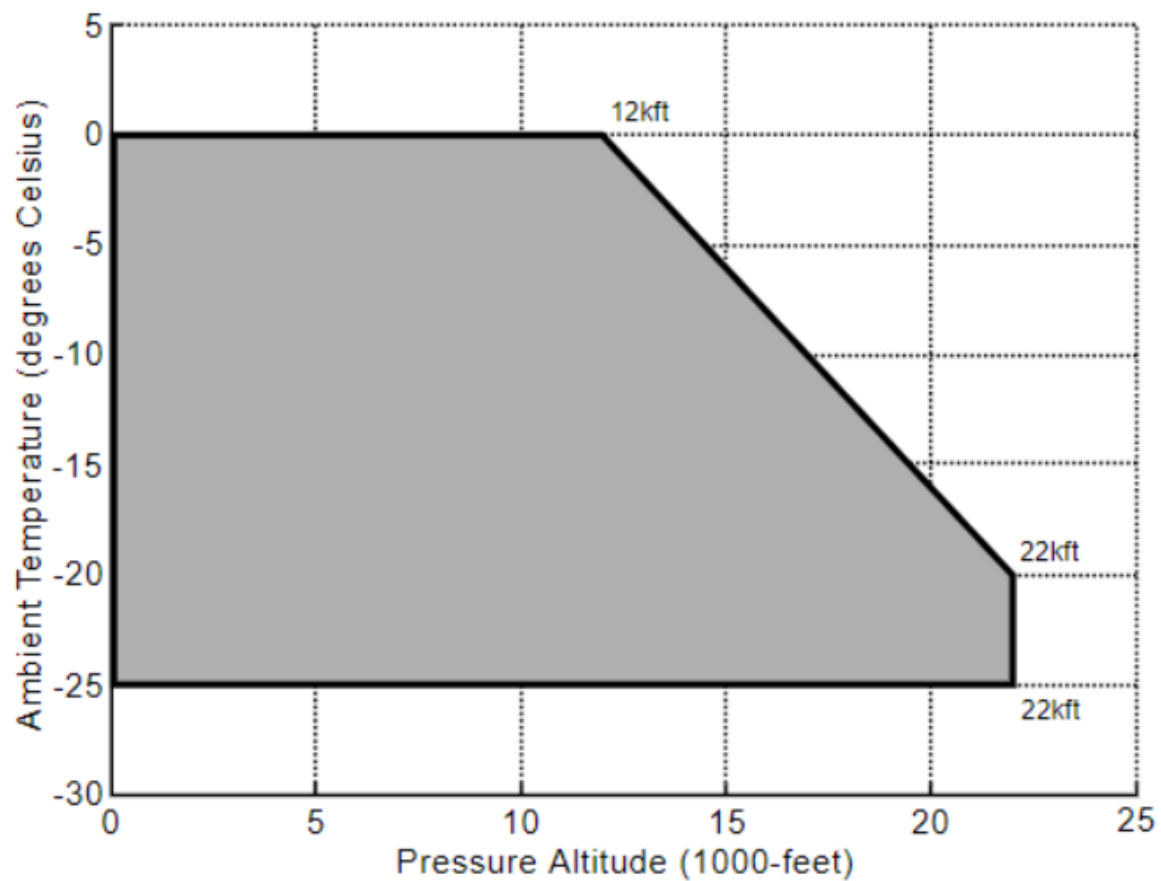


Figure 8.8: Ambient temperature vs altitude for freezing drizzle

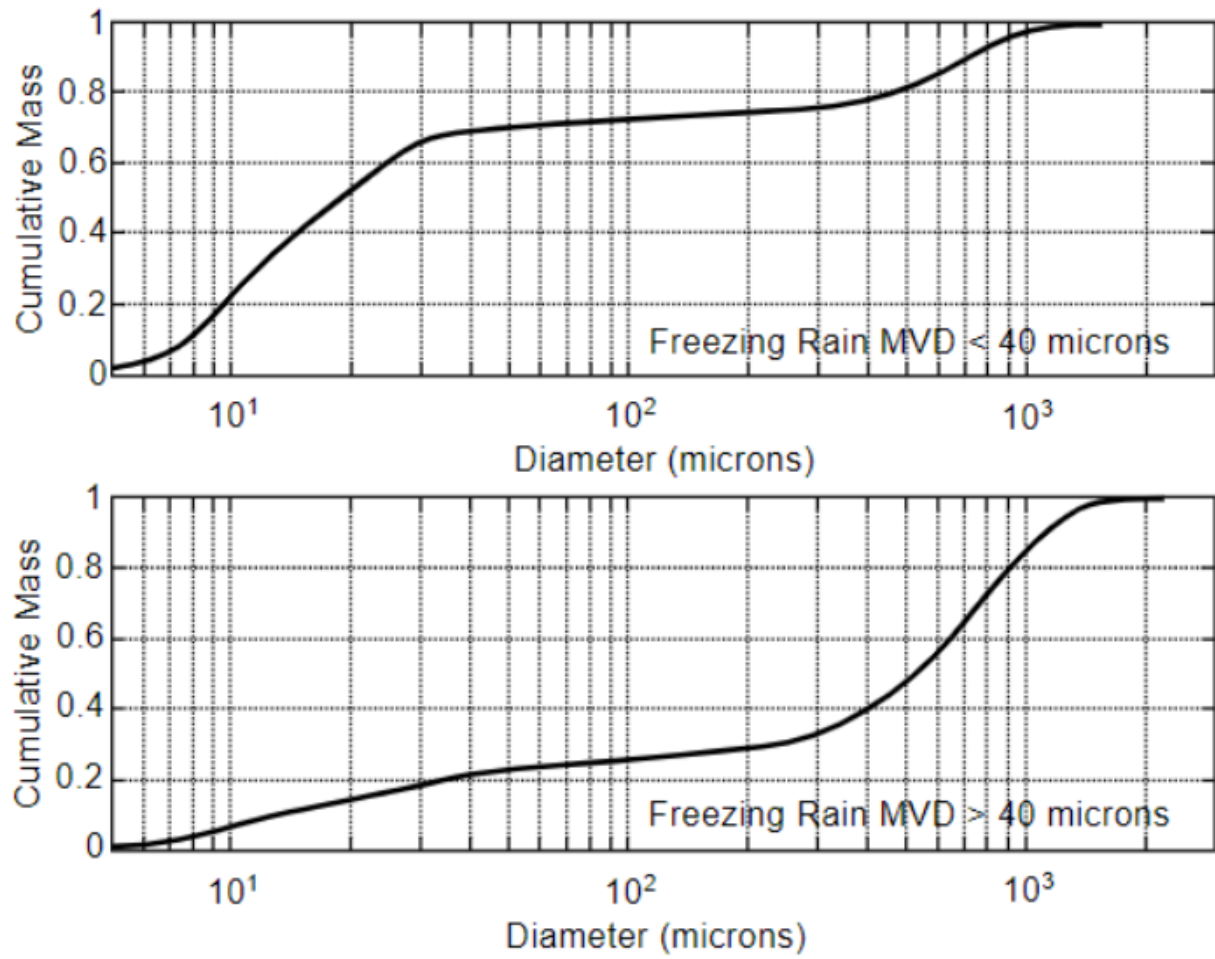


Figure 8.9: Graphs of cumulative mass distribution corresponding to the drop diameters for freezing rain. If the median diameter of the drop distribution is less than 40 microns the first graph must be followed and if it is greater than 40 microns the second graph must be followed

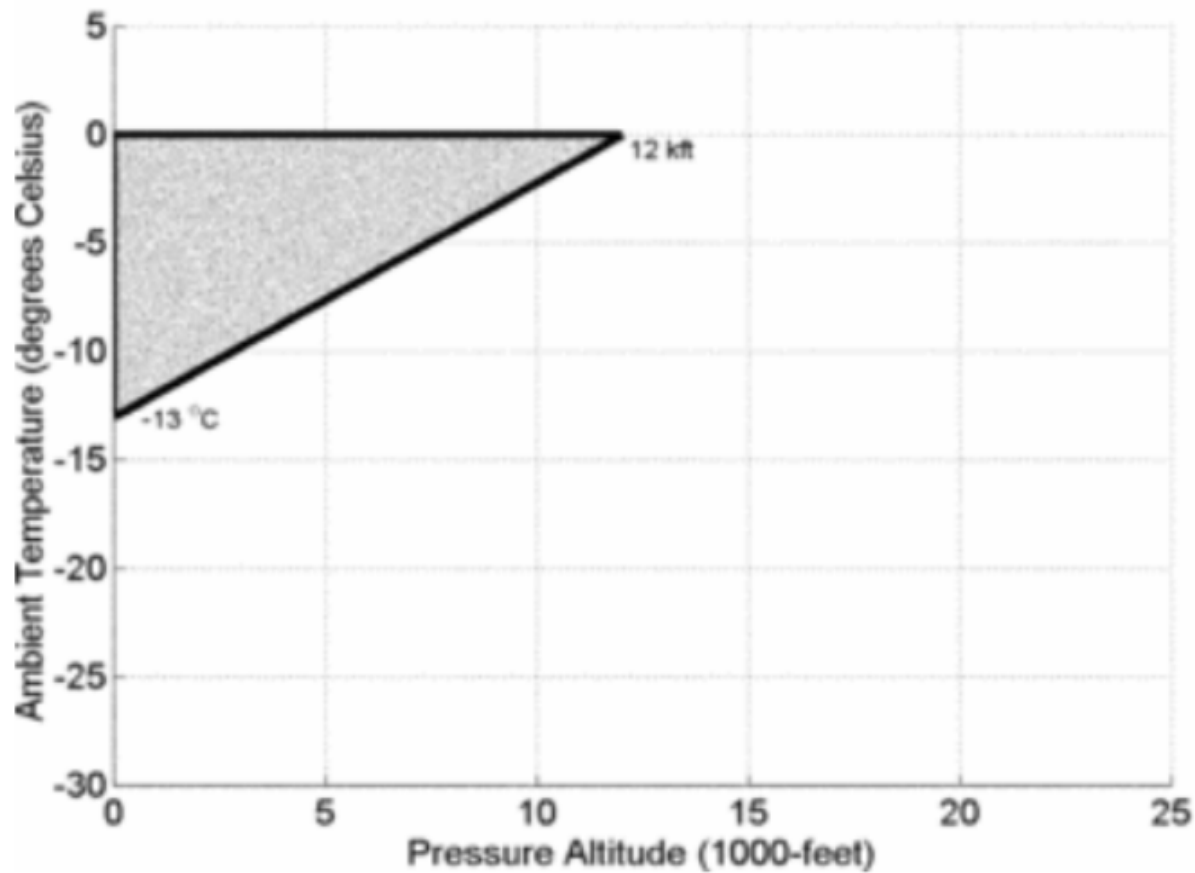


Figure 8.10: Ambient temperature vs altitude for freezing rain

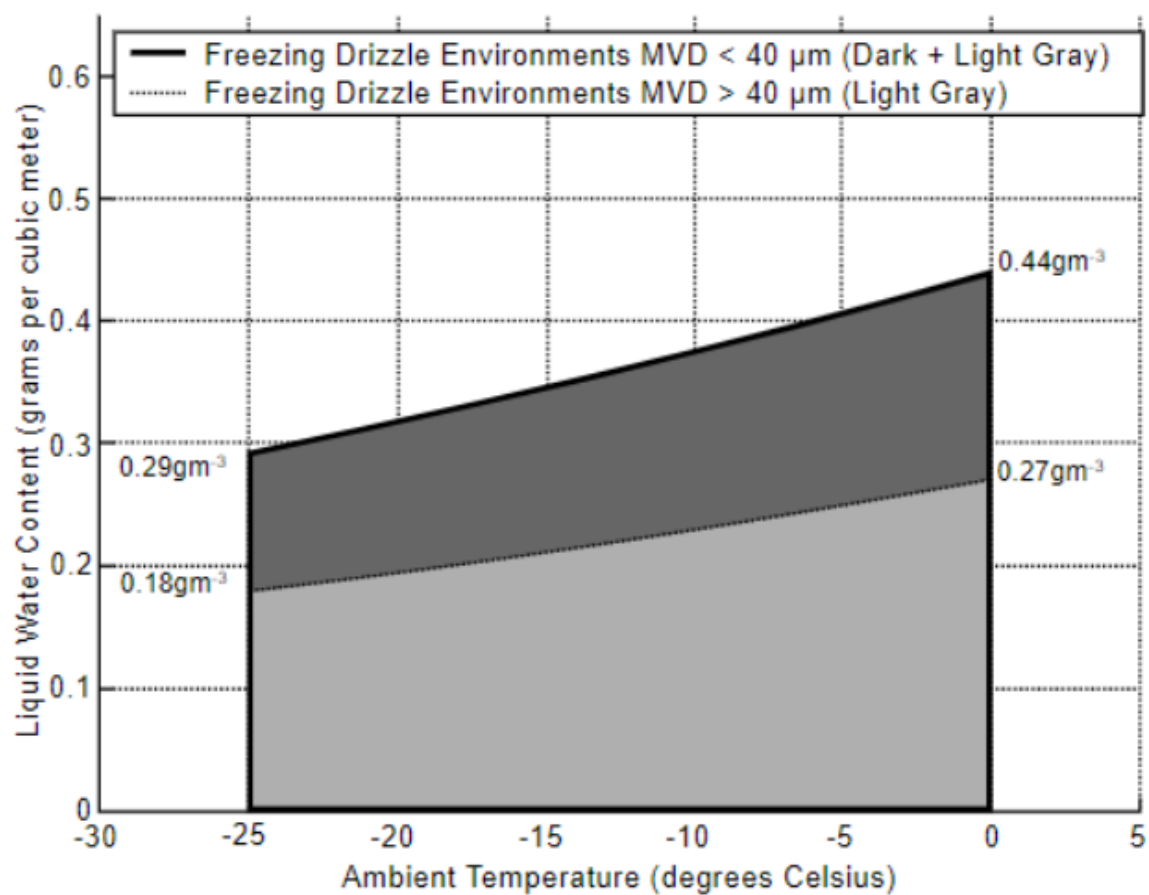


Figure 8.11: Liquid water content for freezing drizzle vs ambient temperature

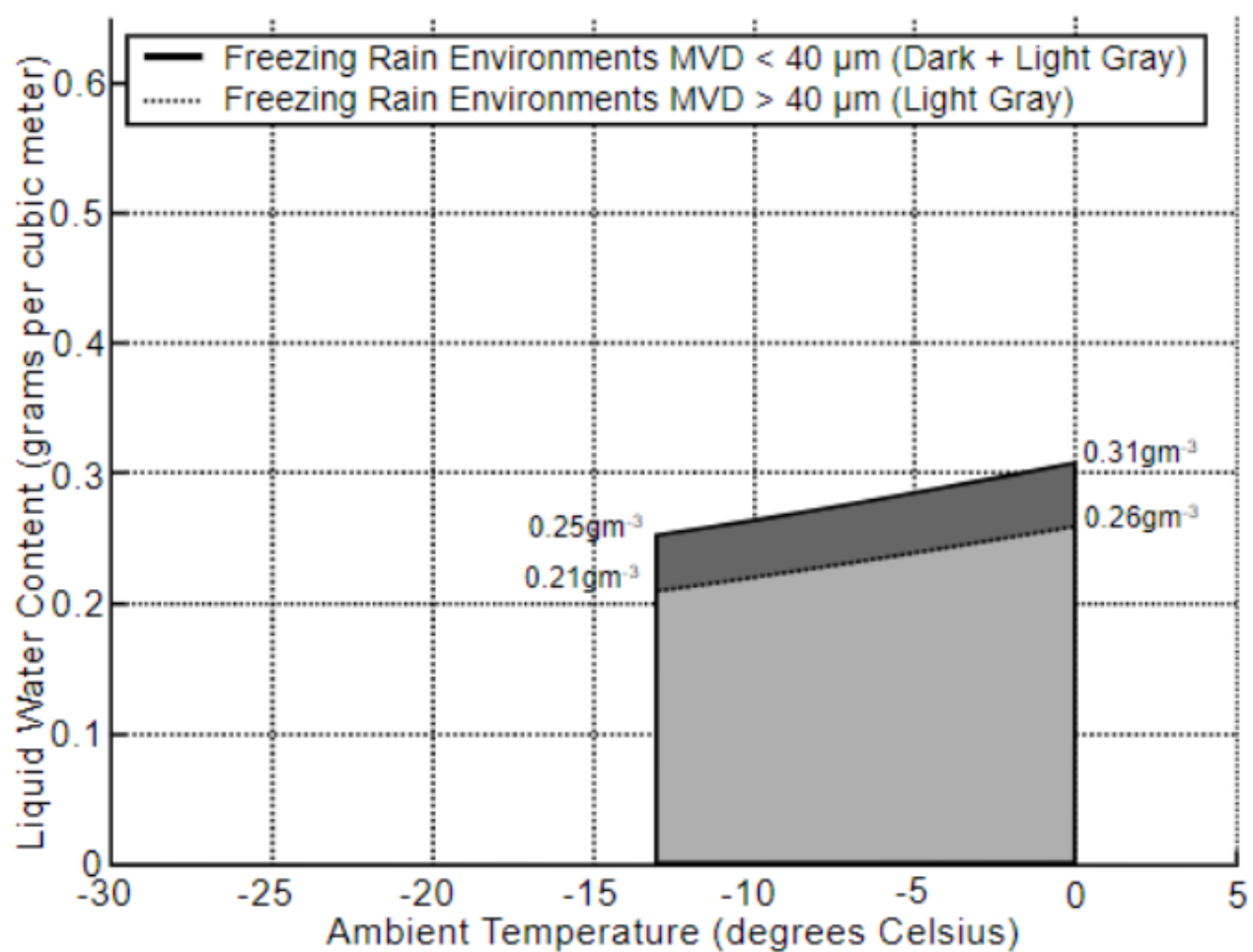


Figure 8.12: Liquid water content for freezing rain vs ambient temperature

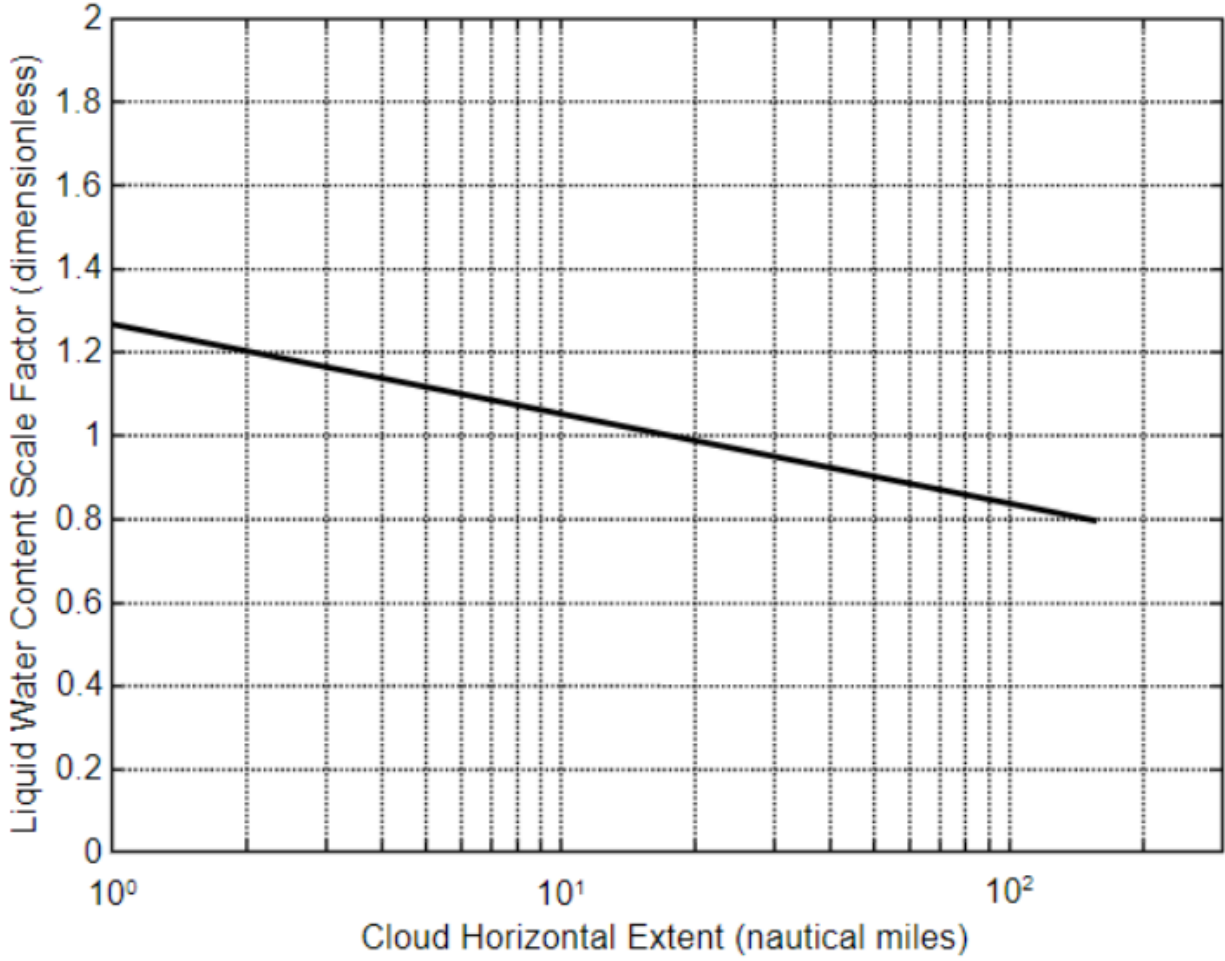


Figure 8.13: Liquid water content scale factor vs cloud horizontal extent

8.2 Derivations to calculate the heat transfer coefficient

Many equations are required to obtain the heat transfer coefficient along the wing of the aircraft

8.2.1 Derivation of the velocity boundary layer

Equations steady state , two dimensional continuity and the momentum conservation.

$$\frac{\partial u}{\partial x} + \frac{\partial v}{\partial y} = 0 \quad (8.1)$$

$$u \frac{\partial u}{\partial x} + v \frac{\partial u}{\partial y} = \nu \frac{\partial^2 u}{\partial y^2} \quad (8.2)$$

The boundaries conditions for those equations are the follow:

$$\begin{aligned} u &= v = 0 & \text{at} & \quad y = 0 & \quad \forall x \\ u &= U & \text{at} & \quad y \rightarrow \infty & \quad \forall x \end{aligned}$$

Making x, y, u and v dimensionless:

$$\begin{aligned}\tilde{x} &= \frac{Ux}{\nu} & \tilde{u} &= \frac{u}{U} \\ \tilde{y} &= \frac{Uy}{\nu} & \tilde{v} &= \frac{v}{U}\end{aligned}$$

The momentum conservation and the inertia equations are inserted :

$$\frac{\partial \tilde{u}}{\partial \tilde{x}} + \frac{\partial \tilde{v}}{\partial \tilde{y}} = 0 \quad (8.3)$$

$$\tilde{u} \frac{\partial \tilde{u}}{\partial \tilde{x}} + \tilde{v} \frac{\partial \tilde{u}}{\partial \tilde{y}} = \frac{\partial^2 \tilde{u}}{\partial \tilde{y}^2} \quad (8.4)$$

Dimensionless boundary conditions :

$$\begin{aligned}\tilde{u} &= \tilde{v} = 0 & \text{at} & \quad y = 0 & \quad \forall x \\ \tilde{u} &= 1 & \text{at} & \quad y \rightarrow \infty & \quad \forall x\end{aligned}$$

Introducing stream function which represent the trajectories of particles in a steady flow.

$$\tilde{\Psi}(\tilde{x}, \tilde{y}) = \int_0^{\tilde{y}} \tilde{u}(\tilde{x}, \tilde{s}) d\tilde{s} \quad (8.5)$$

Differentiating $\tilde{\Psi}$ to find the relation with \tilde{u} and \tilde{v} using the equation 8.3:

$$\frac{\partial \tilde{\Psi}}{\partial \tilde{x}} = \frac{\partial}{\partial \tilde{x}} \int_0^{\tilde{y}} \tilde{u}(\tilde{x}, \tilde{s}) d\tilde{s} = \int_0^{\tilde{y}} \frac{\partial \tilde{u}}{\partial \tilde{x}} d\tilde{s} = - \int_0^{\tilde{y}} \frac{\partial \tilde{v}}{\partial \tilde{x}} d\tilde{s} = \tilde{v}(\tilde{x}, \tilde{s}) \Big|_{\tilde{s}=0}^{\tilde{s}=\tilde{y}} = -\tilde{v}(\tilde{x}, \tilde{y}) \quad (8.6)$$

The following relations are obtained from Equations 8.6:

$$\frac{\partial \tilde{\Psi}}{\partial \tilde{x}} = -\tilde{v} \quad \frac{\partial \tilde{\Psi}}{\partial \tilde{y}} = \tilde{u} \quad (8.7)$$

With the use of the continuity and momentum conservation equations, the following relations are found:

$$\frac{\partial u}{\partial x} + \frac{\partial v}{\partial y} = \frac{\partial^2 \tilde{\Psi}}{\partial \tilde{x} \partial \tilde{y}} - \frac{\partial^2 \tilde{\Psi}}{\partial \tilde{x} \partial \tilde{y}} = 0 \quad (8.8)$$

$$\tilde{\Psi}_{\tilde{y}} \tilde{\Psi}_{\tilde{x}\tilde{y}} - \tilde{\Psi}_{\tilde{x}} \tilde{\Psi}_{\tilde{x}\tilde{y}} = \tilde{\Psi}_{\tilde{y}\tilde{y}\tilde{y}} \quad (8.9)$$

Introducing Blasius solution:

$$\tilde{\Psi} = \sqrt{\tilde{x}} f(\eta) \quad \eta = \frac{\tilde{y}}{\sqrt{\tilde{x}}} \quad (8.10)$$

$$ff'' + 2f''' = 0 \quad \text{with} \quad f'' = \frac{d^2 f}{d\eta^2} \quad \text{and} \quad f' = \tilde{\Psi} = \tilde{u} \quad (8.11)$$

Using the velocity boundary layer :

$$\tilde{\delta}(\tilde{x}) = \eta \sqrt{\tilde{x}} \quad (8.12)$$

Inserting correct value of η for $\tilde{u}(\tilde{\delta}) = 0.99$

$$\tilde{\delta}(\tilde{x}) = 4.91 \sqrt{\tilde{x}} \quad (8.13)$$

Assigning dimensions:

$$\delta(x) = 4.91 \sqrt{\frac{x\nu}{U}} = \frac{4.91x}{\sqrt{Re(x)}} \quad (8.14)$$

Derivation for the friction coefficient

Using the stream function Ψ and η to obtain a realtion for the velocity in x direction u .

$$\Psi = \tilde{\Psi}\nu = \sqrt{\frac{Ux}{\nu}}f\nu = U\sqrt{\frac{\nu x}{U}}f \quad (8.15)$$

$$\eta = \frac{\tilde{y}}{\sqrt{\tilde{x}}} = \frac{\frac{Uy}{\nu}}{\sqrt{\frac{Ux}{\nu}}} = y\sqrt{\frac{U}{\nu x}} \quad (8.16)$$

$$u = \frac{\partial \Psi}{\partial y} = \frac{\partial \Psi}{\partial \eta} \frac{\partial \eta}{\partial y} = U\sqrt{\frac{\nu x}{U}} \frac{df}{d\eta} \sqrt{\frac{U}{\nu x}} = U \frac{df}{d\eta} \quad (8.17)$$

Differentiating u to y :

$$\frac{\partial u}{\partial y} = U \frac{\partial \eta}{\partial y} \frac{d^2 f}{d\eta^2} = \sqrt{\frac{U}{\nu x}} = U \frac{U}{\nu x} \frac{d^2 f}{d\eta^2} \quad (8.18)$$

Inserting the relation of the shear stress at the wall :

$$\tau_{wall} = \mu \frac{\partial u}{\partial y} \Big|_{y=0} = \mu U \frac{U}{\nu x} \frac{d^2 f}{d\eta^2} \Big|_{\eta=0} \quad (8.19)$$

Insert the exact value for $\frac{d^2 f}{d\eta^2}$

$$\tau_{wall} = 0.332\mu U \frac{U}{\nu x} = 0.332U \sqrt{\frac{\mu^2 U}{\frac{\mu}{\rho} x}} = 0.332U \sqrt{\frac{U\mu\rho}{x}} = 0.332U \sqrt{\frac{U\mu\rho}{x} \frac{U\rho}{U\rho}} \quad (8.20)$$

$$= 0.332U \sqrt{U^2 \rho^2 \frac{\mu}{U\rho x}} = 0.332\rho U^2 \frac{1}{\sqrt{Re(x)}} \quad (8.21)$$

Finally the friction coefficient is :

$$C_f(x) = \frac{2\tau_{wall}}{\rho U^2} = \frac{2 \cdot 0.332 \cdot \rho U^2 \cdot \frac{1}{\sqrt{Re(x)}}}{\rho U^2} = \frac{0.664}{\sqrt{Re(x)}} \quad (8.22)$$

8.2.2 Derivation of the local heat transfer coefficient

The local heat transfer coefficient can be found from the energy equation and the dimensionless temperature :

$$\theta(x, y) = \frac{T(x, y) - T_s}{T_\infty - T_s} \quad (8.23)$$

Noting that T_s and T_∞ substitution in the equation energy(equation 8.2) result in :

$$u \frac{\partial \theta}{\partial x} + v \frac{\partial \theta}{\partial y} = \alpha \frac{\partial^2 \theta}{\partial y^2} \quad (8.24)$$

The flow of a fluid over an isothermal flat is comparable with the velocity profiles , and the results will be similar,using the chain rule and some relations the new expression is:

$$2 \frac{d^2 \theta}{d\eta^2} + Pr f \frac{d\theta}{d\eta} = 0 \quad \text{where} \quad Pr = \frac{\nu}{\alpha} \quad (8.25)$$

With the boundary conditions $\theta(0) = 0$ and $\theta(\infty) = 1$ and the use of tables , the thermal boundary layer can be found:

$$\frac{d\theta}{d\eta} \Big|_{\eta=0} = 0.332 Pr^{\frac{1}{3}} \quad (8.26)$$

The temperature gradient at the surface is

$$\begin{aligned} \frac{\partial T}{\partial y} \Big|_{y=0} &= (T_\infty - T_s) \frac{\partial \theta}{\partial y} \Big|_{y=0} = (T_\infty - T_s) \frac{\partial \theta}{\partial \eta} \Big|_{\eta=0} \frac{\partial \eta}{\partial y} \Big|_{y=0} \\ &= 0.332 Pr^{1/3} (T_\infty - T_s) \sqrt{\frac{V}{\nu x}} \end{aligned} \quad (8.27)$$

The local convection coefficient and Nusselt number become:

$$h_x = \frac{q_s}{(T_\infty - T_s)} = \frac{-k \cdot \frac{\partial T}{\partial y} \Big|_{y=0}}{(T_\infty - T_s)} = 0.332 Pr^{1/3} k \sqrt{\frac{V}{\nu x}} \quad (8.28)$$

Finally it can be write as:

$$Nu_x = \frac{h_x x}{k} = 0.332 Pr^{1/3} Re_x^{1/2} \Rightarrow h_x = 0.332 Pr^{1/3} Re_x^{1/2} \frac{k}{x} \quad (8.29)$$

Analogy Reynolds-Chilton-Colburn

Using an analogy the local heat transfer can be found, the analogy related the friction coefficient and the heat transfer. at the final the result will be the same:

$$\frac{C_f}{2} = Nu_x Re_x^{-1} Pr^{-1/3} \quad (8.30)$$

Which can be written as:

$$\frac{C_f}{2} = St_x Pr^{2/3} \quad \text{where} \quad St = \frac{h_x}{\rho U_\infty C_p} \quad (8.31)$$

Inserting the definition of the Nusselt number:

$$\frac{C_f}{2} = \frac{h_x x}{k} Re_x^{-1} Pr^{-1/3} \quad (8.32)$$

Rewriting in terms of heat transfer coefficient and replacing values the final relation is found:

$$h_x = \frac{1}{2} Re_x C_f Pr^{-1/3} \frac{k}{x} = \frac{1}{2} \cdot 0.0664 \frac{Re_x}{\sqrt{Re_x}} Pr^{-1/3} \frac{k}{x} \quad (8.33)$$

Also the thermal boundary layer thickness can be derived from the equation 8.33;

$$\delta_t = \frac{\delta}{Pr^{1/3}} = \frac{4.91x}{Pr^{1/3} \sqrt{Re_x}} \quad (8.34)$$

Finally the local heat transfer coefficient is the same as we calculate using the thermal boundaries.

$$h_x = 0.332 Re^{1/2} Pr^{1/3} \frac{k}{x}$$

8.3 2DFOIL-ICE tests

8.3.1 Test 1: low, cold, wet (fog)

Altitude: 1000

Temperature: 263.15

Droplet diameter: 50 (only at low altitudes)

LWC: 3

Pressure: 90 908

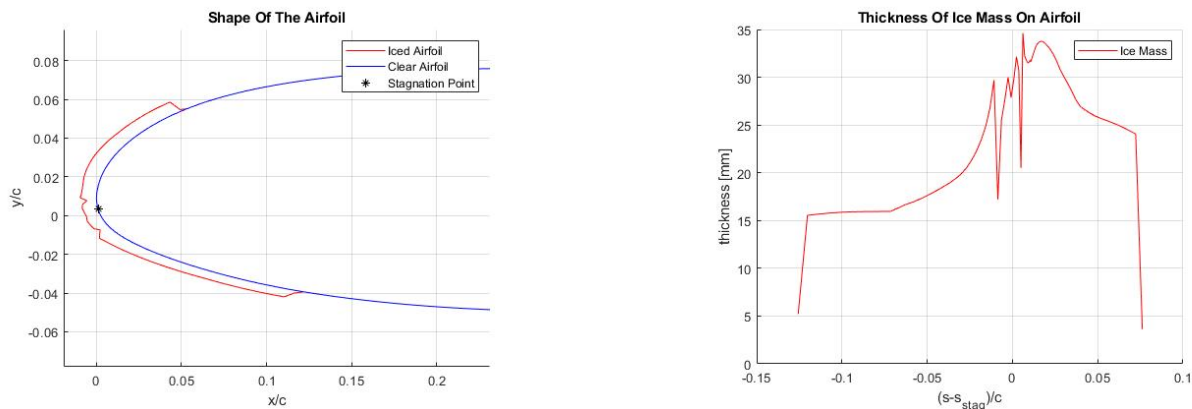


Figure 8.14: Cross section of the ice accretion on Figure 8.15: A graph of the ice thickness against the airfoil
Figure 8.15: A graph of the ice thickness against the distance from the stagnation point

8.3.2 Test 2: slightly higher, cold, wet

Altitude: 1500

Temperature: 263.15

Droplet diameter: 50

LWC: 3

Pressure: 81 917

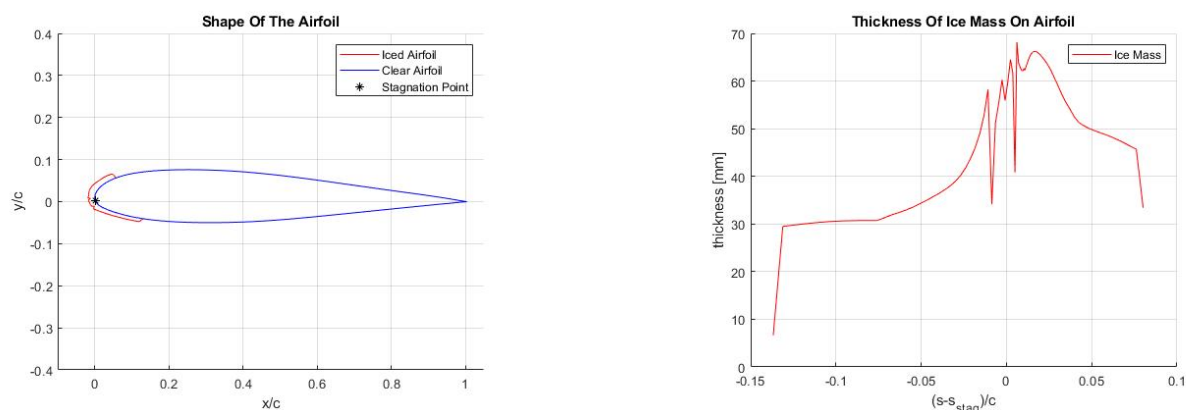


Figure 8.16: Cross section of the ice accretion on Figure 8.17: A graph of the ice thickness against the airfoil
Figure 8.17: A graph of the ice thickness against the distance from the stagnation point

8.3.3 Test 3: low, medium warm, wet

Altitude: 1000
 Temperature: 267.15
 Droplet diameter: 50
 LWC: 3
 Pressure: 87 723

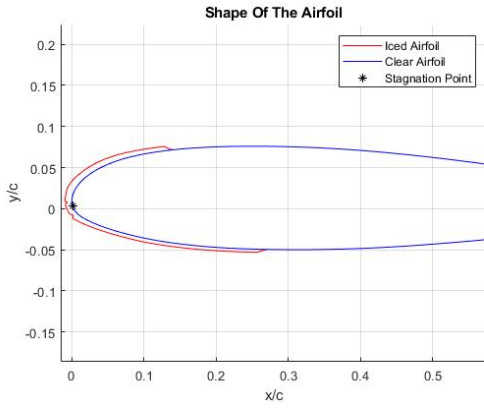


Figure 8.18: Cross section of the ice accretion on the airfoil

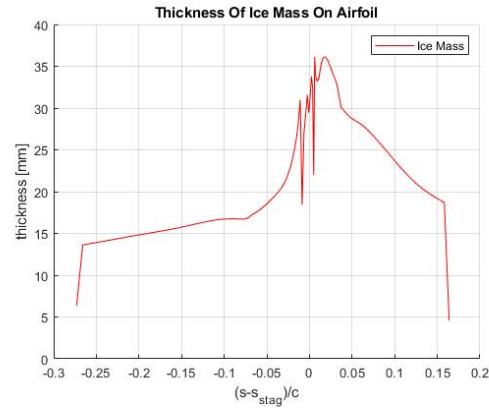


Figure 8.19: A graph of the ice thickness against the distance from the stagnation point

8.3.4 Test 4: high, cold, dry (clouds do not allow rainy weather at this altitude)

Altitude: 5000
 Temperature: 263.15
 Droplet diameter: 15
 LWC: 0.25
 Pressure: 51 434

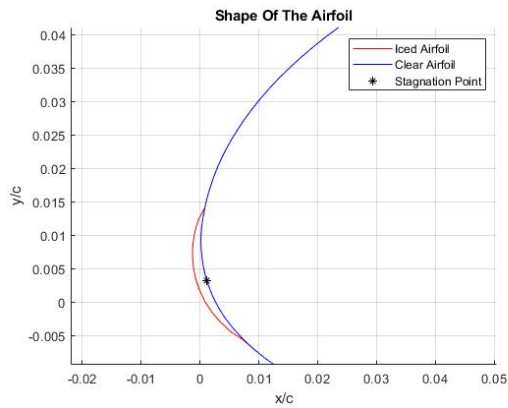
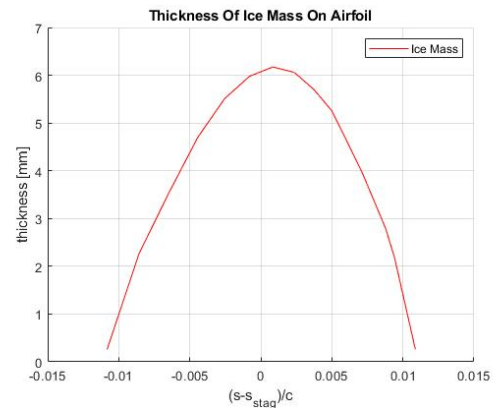


Figure 8.20: Cross section of the ice accretion on the airfoil



8.3.5 Test 5: high, warm, dry

Altitude: 5000
 Temperature: 271.15
 Droplet diameter: 15
 LWC: 0.25
 Pressure: 52 452

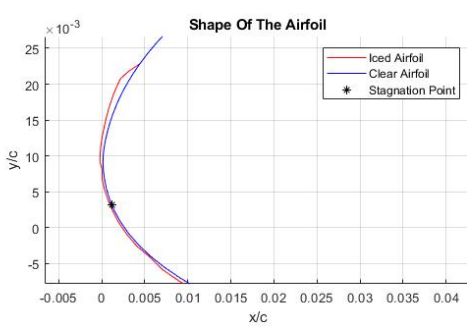


Figure 8.22: Cross section of the ice accretion on the airfoil

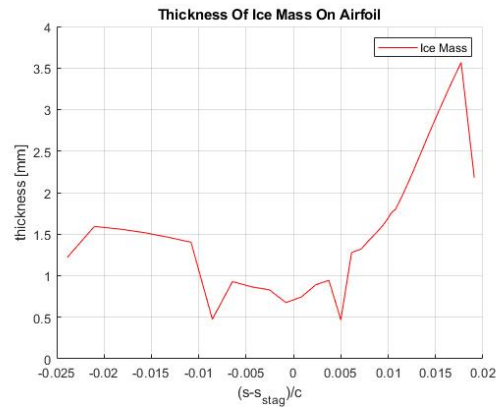


Figure 8.23: A graph of the ice thickness against the distance from the stagnation point

8.3.6 Test 6: low, warm, dry

Altitude: 1000
 Temperature: 271.15
 Droplet diameter: 35 (smallest for these clouds)
 LWC: 1.6
 Pressure: 87 893

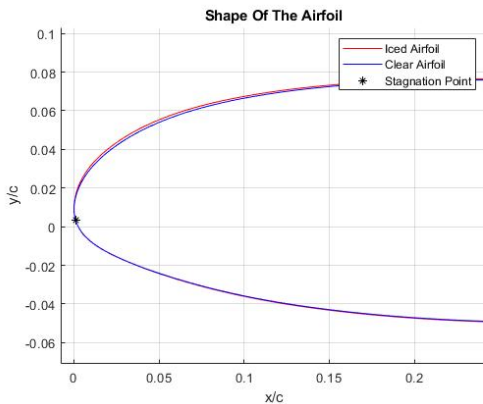


Figure 8.24: Cross section of the ice accretion on the airfoil

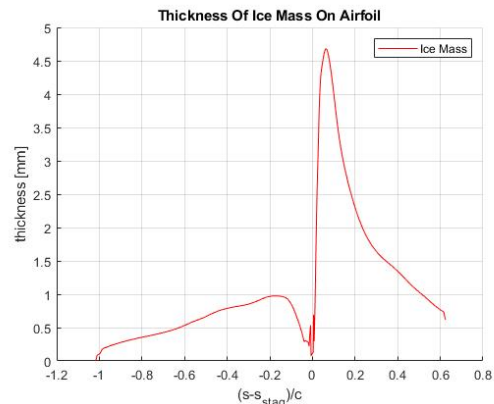


Figure 8.25: A graph of the ice thickness against the distance from the stagnation point

8.3.7 Test 7: low, warm, wet

Altitude: 1000

Temperature: 271.15

Droplet diameter: 50 (smallest for these clouds)

LWC: 3

Pressure: 87 893

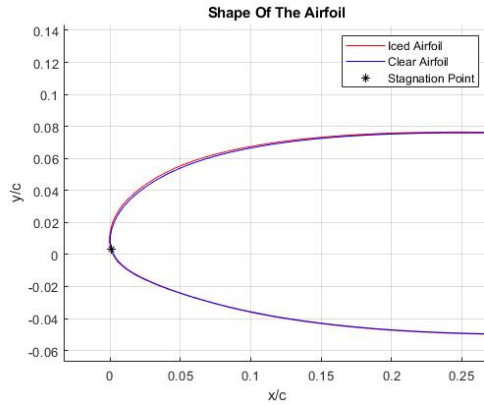
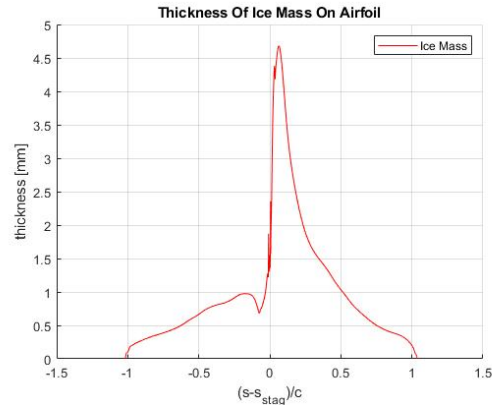


Figure 8.26: Cross section of the ice accretion on Figure 8.27: A graph of the ice thickness against the airfoil



the distance from the stagnation point

8.3.8 Test 8: freezing rain (low, wet, big droplets, cold)

Altitude: 1000

Temperature: 263.15

Droplet diameter: 500 (only at low altitudes, for freezing rain. Worst case scenario assumption)

LWC: 3

Pressure: 90 908

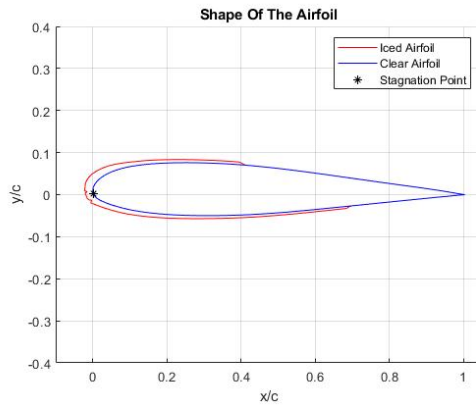
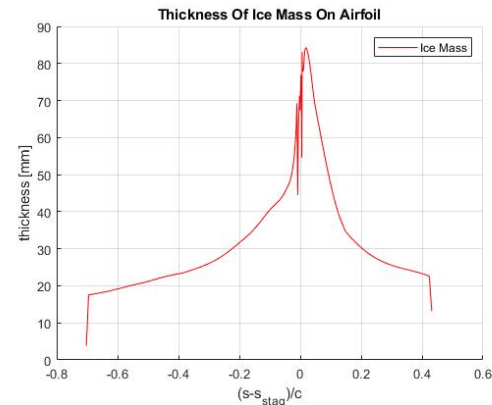


Figure 8.28: Cross section of the ice accretion on Figure 8.29: A graph of the ice thickness against the airfoil



the distance from the stagnation point

8.3.9 Test 9: freezing drizzle (low, wet, still big droplets, cold)

Altitude: 1000

Temperature: 263.15

Droplet diameter: 100 (only at low altitudes, for freezing drizzle. Worst case scenario assumption)

LWC: 3

Pressure: 90 908

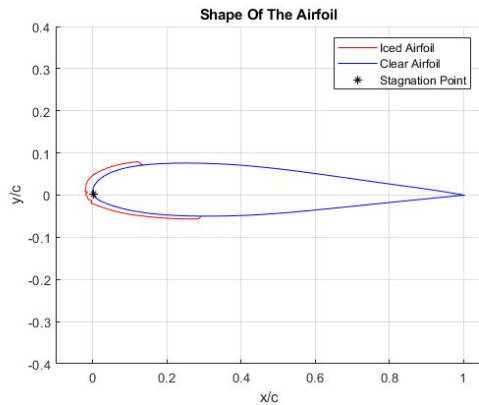


Figure 8.30: Cross section of the ice accretion on the airfoil

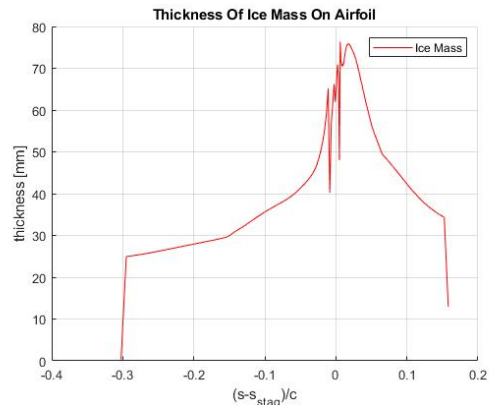


Figure 8.31: A graph of the ice thickness against the distance from the stagnation point

Bibliography

- [1] D. S. Z. Jin, Z. Wang and Z. Yang, “The impact and freezing processes of a water droplet on different inclined cold surfaces,” *International Journal of Heat and Mass Transfer*, 20-Feb-2016.
- [2] X. G. L. L. G. Y. W. D. Du, Y. and X. Yang, “Study of solidification and microstructure characteristics for aircraft icing,” *International Journal of Thermophysics*, vol. 41.
- [3] T. Vukits, “Overview and risk assessment of icing for transport category aircraft and components,” *AIAA Aerospace Sciences Meeting Exhibit*, vol. 40, 2002.
- [4] R. R. A. Heinrich and G. Zumwalt, “Aircraft icing handbook,” vol. 1, 1991.
- [5] A. P. B. M. P. Spencer J. Stebbins, Eric Loth, “Review of computational methods for aerodynamic analysis of iced lifting surfaces,” *Progress in Aerospace Sciences*, vol. 111, 2019.
- [6] W. . W. Z. Cao, Yihua Tan, “Aircraft icing: An ongoing threat to aviation safety,” *Aerospace Science and Technology*, vol. 75, 2018.
- [7] B. A. Bragg, M.B. and L. Blumenthal, “Iced-airfoil aerodynamics,” *Progress in Aerospace Sciences*, vol. 41, 2005.
- [8] N. P. D. R. W. Gent and J. T. Cansdale, “Aircraft icing,” *Philosophical Transactions of the Royal Society of London. Series A: Mathematical, Physical and Engineering Sciences*, 2000.
- [9] Z. Goraj, “An overview of the deicing and antiicing technologies with prospects for the future,” *ICAS*, vol. 24.
- [10] Mediawiki, “Aircraft bleed air system,” 2018.
- [11] *Aviation Maintenance Technician Handbook*. U.S. Department of Transportation, 2012.
- [12] D. Sweet, “Goodrich pneumatic de-icing systems enhance safety in icing conditions,” *Collins Aerospace*, 2019.
- [13] R. C. Scott Thomas and C. MacArthur, “Aircraft anti-icing and de-icing techniques and modeling,” *Journal of aircraft*, vol. 33, 1996.
- [14] A. M. Hossein Ashrafizadeh and P. Mertiny, “Erosive and abrasive wear resistance of polyurethane liners,” 2017.
- [15] TKS[©], “Tks ice proctecyion.” <https://www.cav-systems.com/tks/>, February 2020. ” Accessed on 2020-12-02”.

- [16] C. Cutler, "How a tks system works," February 2020. "Accessed on 2020-18-02".
- [17] W. R. G.W.Zumwalt, R.L.Schrag, "Electro-impulse de-icing testing analysis and design," *Science and Technical Information Division*, 1988.
- [18] G. HEYDARI, "Toward anti-icing and de-icing surfaces: Effects of surface topography and temperature," 2016.
- [19] V. P.-B. M. B. E. B. P. V. L. B. Xiao Huang, Nick Tepylo, "A survey of icephobic coatings and their potential use in a hybrid coating/active ice protection system for aerospace applications," *HAL*, vol. 1, 2019.
- [20] N. I. f. A. T. S. S. N. R. C. A. G. I. G. C. U. M. C. C.-o. C. E. P. d. M. C. P. . W. C. P. C. D. A. C. Technology Partners (European Co-ordinator, Poland), "The phobic2ice project." <http://www.phobic2ice.com/?l=en>, February 2020. "Accessed on 2020-10-02".
- [21] W. Tong, D. Xiong, N. Wang, Z. Wu, and H. Zhou, "Mechanically robust superhydrophobic coating for aeronautical composite against ice accretion and ice adhesion," *Composites Part B: Engineering*, vol. 176, p. 107267, 2019.
- [22] F. A. Administration, "Electronic code of federal regulations." <https://www.ecfr.gov/cgi-bin/retrieveECFR?gp=&SID=52a5ecc87826d91ed0cd78a0b75ed0f1&mc=true&n=pt14.1.25&r=PART&ty=HTML>, February 2020. "Accessed on 2020-10-02".
- [23] Z. Goraj, "An overview of the deicing and anti-icing technologies with prospects for the future," in *24th international congress of the aeronautical sciences*, vol. 29, 2004.
- [24] C. Hacobian, "Here's how high planes actually fly, according to experts," *TIME*, June 2018.
- [25] "737 max," *Boeing. Technical Specs*.
- [26] T. J. Vukits, "Overview and risk of icing for transport category aircraft and components," *40th AIAA Aerospace Sciences Meeting Exhibit*, vol. 1, pp. 3–9, 2003.
- [27] M. Bragg, T. Hutchison, and J. Merret, "Effect of ice accretion on aircraft flight dynamics," in *38th Aerospace Sciences Meeting and Exhibit*, p. 360, 2000.
- [28] Q. Su, S. Chang, Y. Zhao, H. Zheng, and C. Dang, "A review of loop heat pipes for aircraft anti-icing applications," *Applied Thermal Engineering*, vol. 130, pp. 528–540, 2018.
- [29] D. A. Cancilla, A. Holtkamp, L. Matassa, and X. Fang, "Isolation and characterization of microtox®-active components from aircraft de-icing/anti-icing fluids," *Environmental Toxicology and Chemistry: An International Journal*, vol. 16, no. 3, pp. 430–434, 1997.
- [30] J. Martin, "The adverse aerodynamic effects of inflight icing on airplane operation," *Aviation Safety Newsletter*, no. 1, 2007.
- [31] E. Toolbox, "Drag coefficient." https://www.engineeringtoolbox.com/drag-coefficient-d_627.html, 2001. "Accessed on 2020-02-04".
- [32] Pierre Trotin , Glislain Blanchard, Alexandros Kontogiannis,Phillipe Villedieu, "Description and assesment of the new ONERA 2D icing suite IGLOO2D," 2017. Online; accessed 5 March 2020.

- [33] D. R. Hagmeijer, *Fluid Mechanics 1*. University of Twente, 2020.
- [34] C. Brady, “The boeing 737 technical site.” <http://www.b737.org.uk/737max.htm>, March 2020. ”Accessed on 2020-12-03”.
- [35] J. Sloan, “787 integrates new composite wing deicing system,” *CompositesWorld*, December 2008.
- [36] E. Toolbox, “Aluminum - radiation heat emissivity.” https://www.engineeringtoolbox.com/radiation-heat-emissivity-aluminum-d_433.html, 2001. ”Accessed on 2020-12-03”.
- [37] E. Toolbox, “Emissivity coefficients materials.” https://www.engineeringtoolbox.com/emissivity-coefficients-d_447.html, 2001. ”Accessed on 2020-12-03”.
- [38] A. J. C. Yunus A. Cengel, *Heat and mass transfer*. McGraw-Hill Education, 2015.
- [39] Xueqin Bu, Long Peng, Guiping Lin, Lizhan Bai, Dongsheng Wen, “Jet impingement heat transfer on a concave surface in a wing leading edge: Experimental study and correlation development,” *Experimental Thermal and Fluid Science*, June 2016.
- [40] “Bombardier challenger 605 - ice rain protection,” *Smart Cockpit*.
- [41] Carosena Meola, “A new correlation of nusselt number for impinging jets,” *Heat Transfer Engineering Volume 30*, 2009.
- [42] G. Aviation, “The ge90 engine.” <https://www.geaviation.com/commercial/engines/ge90-engine>. ”Accessed on 2020-02-04”.
- [43] W. Frei, “Turbulence modelling.” <https://www.comsol.com/blogs/which-turbulence-model-should-choose-cfd-application/>, Juli 2017. ”Accessed on 2020-02-04”.